WANG, WEI-YEONG

THE HEAT CAPACITY OF COAL CHARS

City University of New York PH.D. 1982

PLEASE NOTE:

In all cases this material has been filmed in the best possible way from the available copy. Problems encountered with this document have been identified here with a check mark __✓__.

1. Glossy photographs or pages _____
2. Colored illustrations, paper or print _____
3. Photographs with dark background _____
4. Illustrations are poor copy __✓__
5. Pages with black marks, not original copy _____
6. Print shows through as there is text on both sides of page _____
7. Indistinct, broken or small print on several pages __✓__
8. Print exceeds margin requirements _____
9. Tightly bound copy with print lost in spine _____
10. Computer printout pages with indistinct print _____
11. Page(s) _____ lacking when material received, and not available from school or author.
12. Page(s) _____ seem to be missing in numbering only as text follows.
13. Two pages numbered _____. Text follows.
14. Curling and wrinkled pages _____
15. Other _____

THE HEAT CAPACITY OF COAL CHARS

by

WEI-YEONG WANG

A dissertation submitted to the
Graduate Faculty in Engineering in partial fulfillment
of the requirement for the degree of Doctor of
Philosophy, The City University of New York

1981

This manuscript has been read and accepted for the Graduate Faculty in Engineering in satisfaction of the dissertation requirement for the degree of Doctor of Philosophy

Oct 1 1981
date

Leslie Isaacs
Chairman of Examing Committee

Oct 1, 1981
date

Paul R Kaminski
Executive Officer

Prof. Leslie L. Isaacs (Chairman)

Prof. Robert A. Graff

Prof. Alberto D. LaCava

Prof. Gabriel I. Tardos

Prof. Myron Levitsky
Supervisory Committee

The City University of New York

Abstract

THE HEAT CAPACITY OF COAL CHARS

by

Wei-yeong Wang

Adviser:Professor Leslie L. Isaacs

During pyrolysis, the solid phase of coal is transformed into a microcrystalline structure with some extent of graphite-like orderliness. It is of interest to determine the thermodynamics of this structure which is believed to be process and coal origin dependent.

This study has been undertaken to elucidate the effect of the various factors on the heat capacity of coal chars. In order to assess the effect of coal rank and impurity content, several coals were obtained from the Pennsylvania State University Coal Bank. These selected starting materials were, a North Dakota lignite, an Illinois No.6 bituminous and a Virginia coking coal. The carbon content of these coals ranged from 59 to 75 wt% (mineral matter included). Half of each of the received coal sample was demineralized using a standard procedure. Chars were prepared from the received and demineralized coals by pyrolysis. Prior to pyrolysis, the coals were ground to less than 250 mesh size in a ball mill. A relatively slow heating rate of 5°C/minute was employed

for the pyrolysis under dry nitrogen gas atmosphere. Both the pyrolysis temperature and the "soak time" (length of time the sample is kept at the pyrolysis temperature) were varied. The pyrolysis temperatures were 700, 900 and 1100°C. The soak times were 0.1, 1 and 24 hours. The char samples were characterized by chemical composition analysis, X-ray diffraction and porosimetry. Heat capacity data were collected over 75 to 300°K temperature range using an adiabatic calorimeter. The experimental specimens were vacuum dried for one hour at 110°C prior to loading into the calorimeter.

The heat capacity of these samples increases, in general, with increasing temperature and moisture content, and its behavior and order of magnitude are very similar to pure carbons when compared on a moisture free basis.

A modified Debye theory is presented to correlate the heat capacity behavior with the pyrolysis temperature T_p and chemical composition for the chars prepared from the selected coals. The correlation indicates that the heat capacity of coal chars is not a function of T_p alone, but it is also dependent on the coal from which it originates. This correlation model has been used to extend the heat capacity data of a gasifier char to lower temperatures. "Equilibrium" constants for methane formation from this char by hydrogenation gives an upper limit about six times higher than equilibrium over graphite in the

temperature range of 1000 to 1200°K.

The mineral matter content also affects the measured heat capacity. The thermally transformed mineral matter (ash) contributes differently to the total heat capacity than the mineral matter in its original form.

The moisture-containing coal seems to have a higher heat capacity than expected by simple additive principle and shows a broad phase transition around ice point.

Due to the uncertainties of the chemical forms of the mineral matter and the water phase below room temperature, all the heat capacity data are analyzed on a dry mineral matter free basis.

ACKNOWLEDGEMENTS

I wish to thank Professor Leslie L. Isaacs for his guidance, continuous encouragement and interest throughout this work. I also wish to thank Professors Robert Pfeffer, Robert A. Graff, Alberto LaCava and Gabriel Tardos for their substantial help in supporting equipment , advice and financial arrangements.

Appreciations are due to Dr. Jerome Hust of the National Bureau of Standards', Boulder Laboratories, for kindly supplying us the POCO AXM-5Q-1 graphite sample.

I am also grateful to my colleagues Albert Feng and Shi-jen Shen for their constant assistance.

Finally, I wish to acknowledge with gratitude the patience and encouragement of my wife, Yin-yin, and my loving parents.

This work was supported by the National Science Foundation under grants ENG 76-22970 and CPE 7915231.

TABLE OF CONTENTS

Table of Contents (cont.)

Table of Contents (cont.)

LIST OF TABLES

LIST OF FIGURES

List of Figures (cont.)

List of Figures (cont.)

List of Figures (cont.)

List of Figures (cont.)

NOMENCLATURE

A	Surface area of calorimeter, surface area of radiation plate; constant
A_i	Constant, cross-sectional area of electrical lead wire i
a	Constant
a_o	Constant
b	Constant
C	Heat capacity
C'	Heat capacity
C_g^a	Heat capacity of ash (Joule/gm°K)
C^{ch}	Heat capacity of a gasifier char
C_g^o	Heat capacity of organic substance in coal or char (Joule/gm°K)
C_{gac}^o	C_g^o normalized to per gram-atom carbon basis (Joule/g-atom carbon°K)
C_g^s	Heat capacity of coal or char (Joule/gm°K)
C_{gac}^s	C_g^s normalized to per gram-atom carbon basis (Joule/g-atom carbon°K)
C_m	Heat capacity of one mole of char atoms on an ash-free basis (Joule/mole°K)
C_p	Heat capacity at constant pressure
CHN	Carbon, hydrogen and nitrogen
c	Molar concentration of the disturbing atoms in the carbon matrix of ash-free char

Nomenclature (cont.)

DM	Demineralization
DMMF	Dried-mineral matter-free basis of coal
DM PSOC-X-Y-Z	Char prepared from demineralized coal PSOC-X under pyrolysis temperature Y (°C) with soak time Z (hr.)
f	Function of T/T_p
H^o	Standard state enthalpy
h	Planck's constant
I	Current, function of T/T_p
I_o	Constant
Ki	"Equilibrium" constant
K_s	Pseudoequilibrium ratio
k	Boltzmann's constant
ℓ_i	Length of electrical lead wire i between calorimeter and thermal anchor
n	Number of atoms per molecule
n_i	Steichiometric coefficient
PSOC-X	Coal sample indexed by the Pennsylvania State University's Coal Research Center of DOE
p	Pressure
p_j	Partial pressure of species j in the equilibrium mixture
q	Heat input to the calorimeter
q_o	Measured electrical energy

Nomenclature (cont.)

$\dot{q}_{cl}$	Rate of conduction heat exchange through the electrical leads between calorimeter system and leads' thermal anchor
$\dot{q}_{c2}$	Rate of gas conduction heat exchange between calorimeter system and surroundings
$\dot{q}_r$	Rate of radiation heat exchange between calorimeter system and surroundings
R	Universal gas constant
R_h	Heater resistance
R_ℓ	Resistance of electrical lead wire
R_{std}	Resistance of standard resistor
S^o	Standard state entropy
S_o	Residual entropy of char
T	Temperature (°K)
T_{calc}	Thermometer temperature calculated by the curve-fitting equation of the calibration points (°K)
T_{exp}	Thermometer calibration points, temperature calculated after dispersion correction on T_{calc}(°K)
T_p	Pyrolysis temperature
T_1	A steady temperature before heating, temperature of radiation surface 1

Nomenclature (cont.)

T_2	A steady temperature after heating, temperature of radiation surface 2
t	Time
t_m	Mid-time of the heating period
t_1	Corresponding time for T_1
t_2	Corresponding time for T_2
UNDM PSOC-X-Y-Z	Char prepared from undemineralized coal PSOC-X under pyrolysis temperature Y (°C) with soak time Z (hr.)
V	Voltage
V_i	Voltage
w_a	Weight fraction of ash in char
w_c	Weight fraction of carbon in char
x	Dimensionless variable defined by $x = h\nu / kT$ in Debye's theory

Greek Symbols

α	Function of T/T_p
α_i	Intrinsic temperature drift at apparent zero temperature difference between adiabatic shield and calorimeter
β	Heat exchange modulus
γ	Ratio of calorimeter thermal conductivity to heat exchange coefficient between calorimeter and surroundings
ΔG°_R	Standard free-energy change of reaction
ΔH°	Standard enthalpy difference of char
ΔH°_c	Standard heat of combustion
ΔH°_f	Standard heat of formation
ΔH°_R	Standard heat of reaction
ΔS°	Standard entropy difference of char
ΔS°_R	Standard entropy change of reaction
ΔT	Temperature variation
ΔT_i	Temperature rise of calorimeter during heating period i
Δt_i	Duration of heating period i
ε_i	Emissivity of radiation surface i
Θ	Effective Debye's characteristic temperature ($^\circ K$)

Greek Symbols (cont.)

θ_D	Debye's characteristic temperature in the Debye's heat capacity theory (°K)
θ_o	Characteristic temperature in the char heat capacity analysis (°K)
θ	Temperature deviation between adiabatic shield and calorimeter
$\bar{\lambda}_i$	Mean thermal conductivity of electrical lead wire i over a range of temperature
ν	Frequency of lattice vibration
ν_j	Stoichiometric coefficient
ν_m	Limiting frequency of lattice vibration
σ	Stefan-Boltzman's constant
τ	Duration of heating interval, reaction temperature

1. INTRODUCTION

The impending shortage of crude oil has resulted in an interest in developing new processes for the conversion of coal into liquid and gaseous fuels. Most of these processes have char as a process intermediate or as a by-product. Thermodynamic calculations for these processes are difficult to perform to any degree of accuracy, due to the lacks of thermodynamic data on chars. The available data on chars [1,2,3] indicate that the thermodynamic properties will depend on the thermal history and the source (Parentage) of the chars.

The kinetics of coal pyrolysis under different reaction conditions have been studied extensively.[4] In gasification of coals, it is generally assumed to be a two-stage process, [5] with the second stage char formation reaction assumed to be of major importance for the final fuel properties. Studies of the reactivities of heat-treated coals in air, carbon dioxide, hydrogen and steam have been reported by various sources.[6] The complicated nature of chemical structure and the physical state of the chars hindered the development of a generalized kinetic model for the pyrolysis of different coals. For a given process, the following kinetic parameters have been considered of major importance: rank of coal, mineral matter composition, pore structure, charring temperature, reaction temperature and pressure, ambient atmosphere. Char re-

activity decreases, in general, with increasing rank of the parent coal (except for the hydrogen reaction). The effects of mineral matter and pore structure are quite specific and reaction dependent.

Thermodynamic data is required for studying the energetics of chemical reactions and for process evaluations. But due to inherent difficulties, very little progress has been made both theoretically and experimentally in establishing a thermodynamic data base for coals and coal derivatives.

In this thesis work, we have tried to develop a systematic program to study the heat capacity behavior of coal chars of known origin and thermal history. Data have been collected above liquid nitrogen temperature and the correlation model based on the modified Debye theory has been developed and proved to be satisfactory for the char species under investigation.

This thesis is organized into nine chapters: Chapter one gives the motivation for the research; Chapter two gives the theoretical and technical background for this study; the details of the experimental arrangement and procedures are laid out in the Chapter three; the results and discussions will be presented in Chapter four; Chapter five gives an illustration of the application of the data; Chapter six gives the conclusions; some directions for the future studies

related to this work are pointed out in Chapter seven; Chapter eight gives the related references and with some supporting informations appended in Chapter nine.

2. LITERATURE REVIEW

2.1 The Debye Theory of Heat Capacity

In the Debye's theory[7] for the heat capacity of a nonconductive crystalline solid, the material is treated as an infinite elastic continuum and the excitation of all the possible modes of standing waves in the material is studied. This concept leads to the parabolic form for the vibrational spectrum up to a limiting frequency ν_m and to the following expression for the lattice heat capacity per mole:

$$C = 3\ n\ R \left[3 \left(\frac{T}{\theta_D}\right)^3 \int_0^{\theta_D/T} \frac{x^4\ e^x}{(e^x - 1)^2} dx\right] \qquad (1)$$

In this expression n is the number of atoms per molecule, R is the universal gas constant per mole, T is the absolute temperature, θ_D is the "Debye Characteristic Temperature", and x is a dimensionless variable defined by the expression $x = h\nu/kT$. In this last expression h is Planck's constant, ν is the frequency of vibration, and k is Boltzmann's constant. This expression is usually abbreviated to

$$C = 3\ n\ R\ D\ (\theta_D/T) \qquad (2)$$

where $D(\theta_D/T)$ stands for the expression in brackets in equation (1), the "Debye Function". The important thing to

notice here is that for a given substance the lattice heat capacity is dependent only on a function of the ratio of the Debye characteristic temperature, θ_D, to the absolute temperature. This function is the same for all materials, and only the Debye temperature differs from material to material. Therefore, θ_D is a physical parameter which is a characteristic of the material.

Debye's neglect of the detailed structure of the frequency spectrum was remedied in later modifications of the theory.[8] The modification consists letting θ_D be a function of temperature. The θ_D is calculated as a function of temperature from the experimentally observed values of the heat capacity in agreement with the Debye equation. In general, the resulting variation of θ_D with temperature is small from temperature above $\theta D/3$ in case of metallic and inorganic materials. The interatomic force constants for polymeric materials are more strongly dependent on temperature, and as a result, θ_D for these materials is expected to vary greatly with temperature. The Debye theory can further be modified by including the effects of impurity atoms on the lattice. The interaction between the majority atoms and the impurity atoms adds Eistein modes to the vibrational spectrum. Since the Debye theory is a continuum theory, θ_D is insensitive to the structural details of the lattice.

2.2 Calorimetry

Gaede [9] was the first to use the discontinuous Joule heating to measure the heat capacity of a solid. Nernst and Eucken, [10] about 1910, developed the techniques of vacuum calorimetry. A simple schematic representation of such a calorimeter is presented in Figure 1.

In calorimetric measurements, the determination of the fraction of input energy lost to the surroundings by incomplete isolation of the sample is the factor which most severely limits the accuracy of the measurement. Therefore, in designing the experimental apparatus, a decision must be made between retaining a significant but calculable heat leak or endeavoring to eliminate the heat leak to the point at which it is almost insignificant but not calculable. If the controlled temperature shield, 4 in Figure 1, is designed so as to remain at a constant temperature during a measurement, the technique is referred to as using an isothermal shield. This technique of operation was first used by Nernst [10] and his collaborators. If, on the other hand, the temperature of the shield is so regulated as to be as nearly identical as possible with that of the calorimeter, the technique is referred to as using an adiabatic shield (or, in practice, a nearly-adiabatic). The introduction of the adiabatic method at low temperatures is due to Southard and Andrews. [11] The

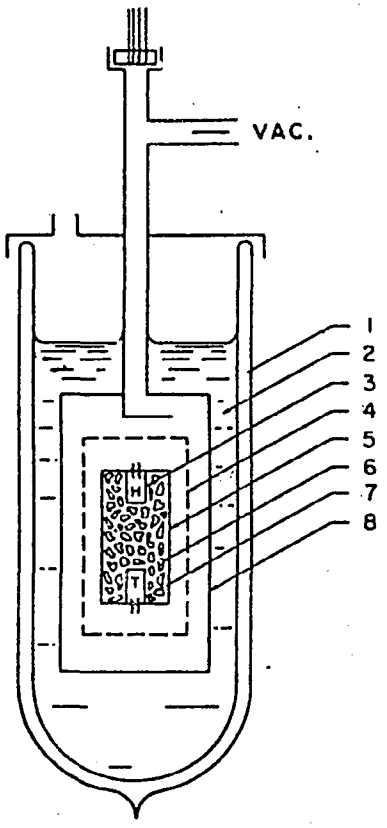

Figure 1. Schematic cryogenic calorimeter with electrical heating.

1. Dewar vessel
2. Liquified gas refrigerant
3. Electrical heater
4. Adiabatic jacket
5. Calorimeter vessel
6. Samples
7. Thermometer
8. Evacuated submarine

adiabatic shield technique is preferred in modern use. This is due to the availability of fast responding, automatic temperature controllers.

The adiabatic technique in the temperature range of 70 to 300°K has been employed by Kasatochkin et al. [1] for the measurement of the heat capacities of anthracite coals and chars.

2.3 Heat Capacity of Carbons

The heat capacity measurements of natural and synthetic graphites have been reported by numerous investigators. The data available covers the entire temperature range of interests and has been reviewed by Kelly and Taylor.[12] The work of De Sorbo [13] is of particular significance.

It has been noted by many of the investigators that the heat capacity of graphite is dependent on the state of the structural perfection of the graphite specimen.[12] Natural crystalline graphite has the lowest heat capacity at any given temperature. Synthetic graphites prepared by carbonization procedures have excess heat capacities relative to natural graphite. The amount of excess is mainly a function of the carbonization temperature. Attempts to eliminate the excess heat capacity of synthetic graphites by annealing above 3000°C were unsuccessful.[3]

Heat capacity data on chars are extremely scarce. An extensive literature search yielded only three sets of data relevant to the task at hand. The Bartlesville and Albany Laboratories [2] of DOE measured the heat capacities, and heats of combustion of Synthane process chars. However, the heat capacities were only measured above 300°K. Data in 50 to 300°K region were reported by Kasatochkin, et al. [1] for chars prepared from a fossil carbon, Schungite (98.1% C), and from anthracite coals (96-98% C). These chars were prepared by "heat treatment" (pyrolysis) ranging from 600 to 2800°C. The third set of data is by Mrozowski et al. [3] on chars from resin C pitch by heat treatment ranging from 600 to 3100°C. They measured heat capacities from 1 to 5°K.

Some generalizations can be deduced from the inspection of these three data sets. First of all, as expected, the heat capacities of the chars behave very similarly to graphite and are of the same order of magnitude as graphite at all experimental temperatures; they also depend on the "heat treatment" temperature and the starting material (parentage).

Figure 2 shows the relative heat capacities of some anthracite coals with reference to the metamorphic carbon content. It indicates that, even for very high rank coals,

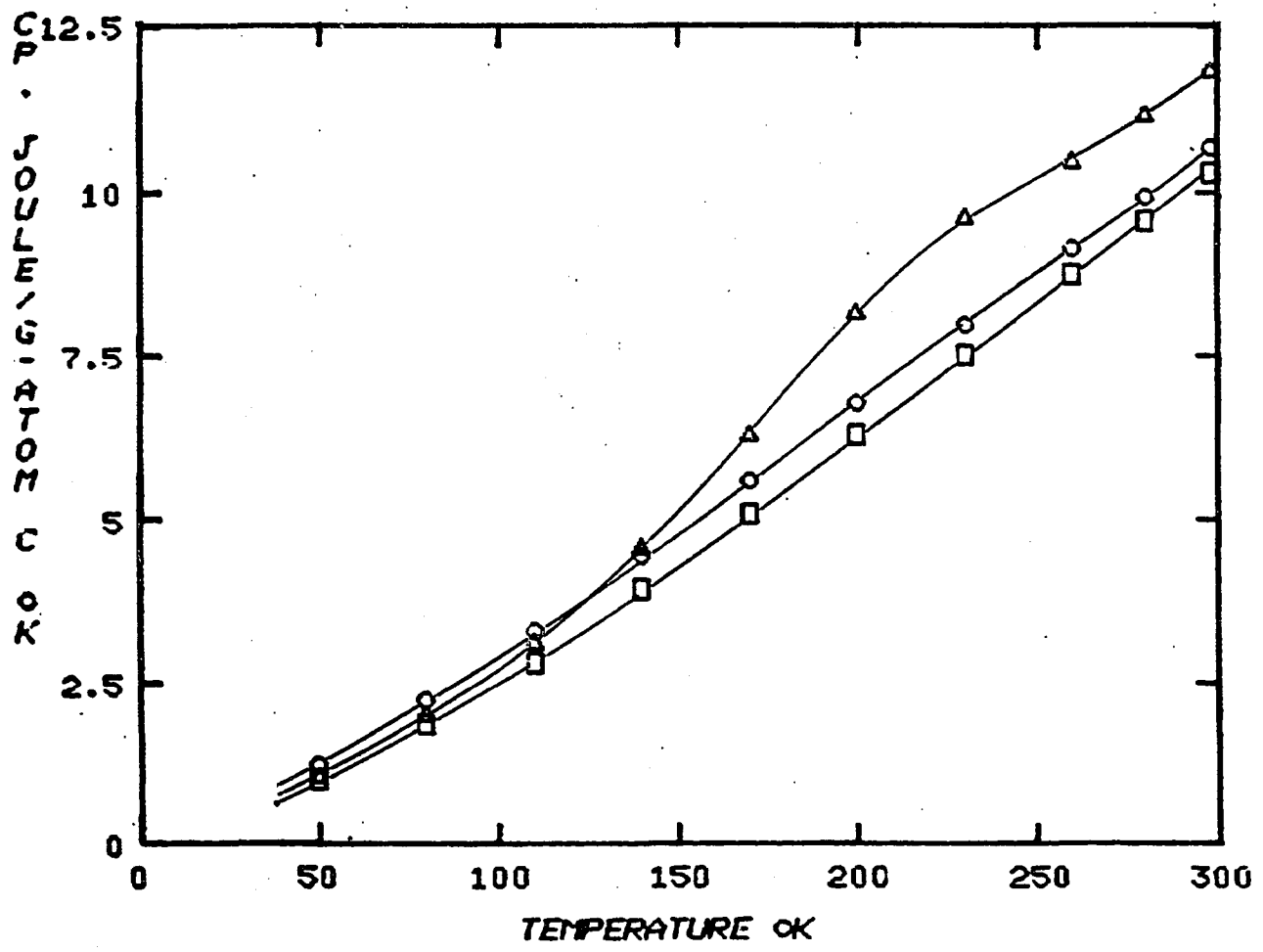

Figure 2-a. Kasatochkin's heat capacity data of 98.1 wt% C Russian Schungite (Δ), 96 wt% C anthracite (o), and 98 wt% C anthracite (□).

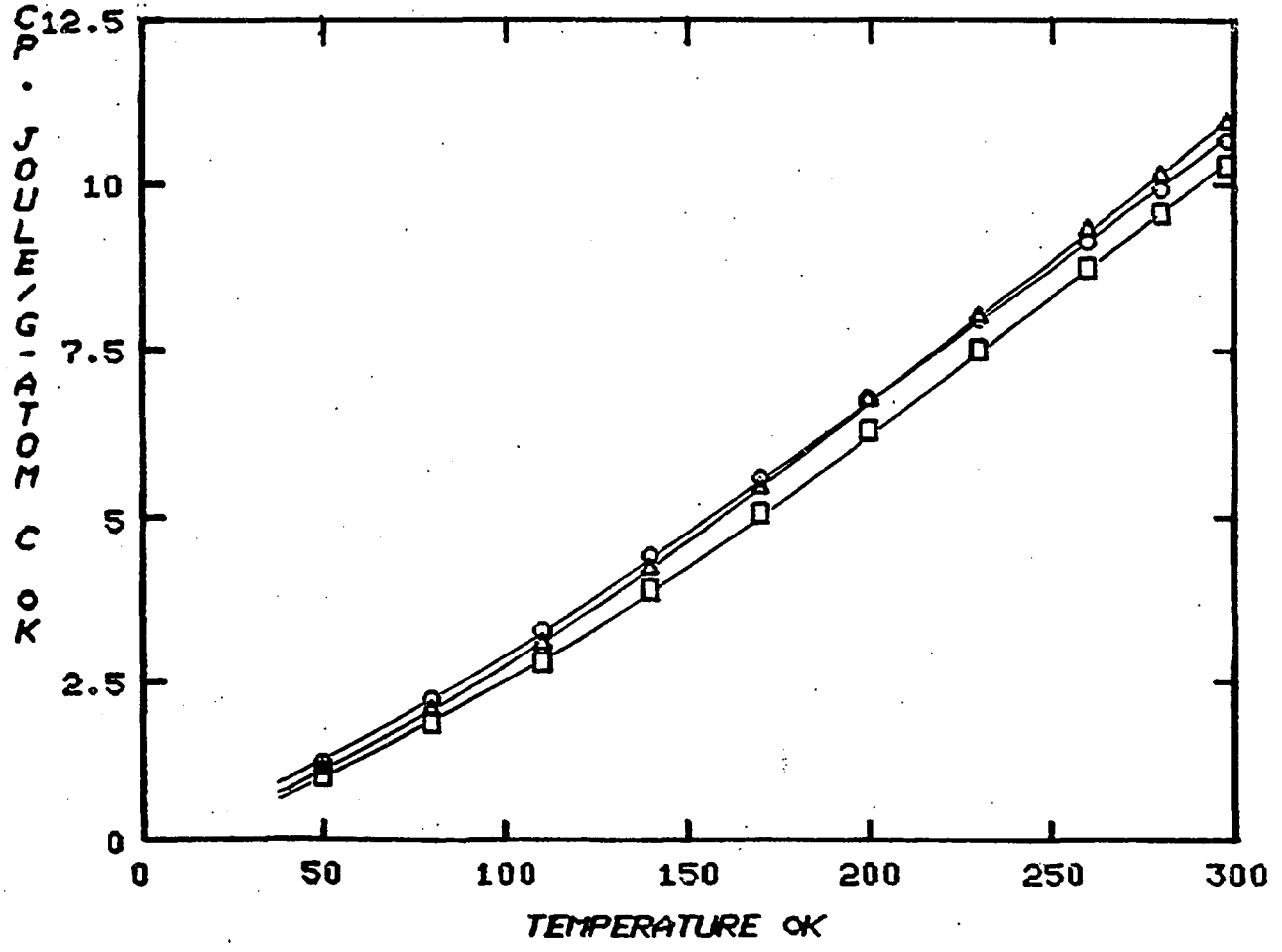

Figure 2-b. Kasatochkin's heat capacity data of 96 wt% C anthracite (o), 96-98 wt% C anthracite (Δ), and 98 wt% C anthracite (□).

heat capacity is not a simple function of the carbon content.

An example of the heat-treatment-temperature dependence of the heat capacity of chars is shown in Figure 3.

The magnitude of the heat capacity of these coal chars is not a function of the heat treatment temperature alone. The 900°C Synthane char has higher heat capacity than the 600°C Schungite char. This difference may be due to the structural difference in the parent coals. Also, it is possible that this difference in heat capacity is related to the composition, and thermal history of the chars.

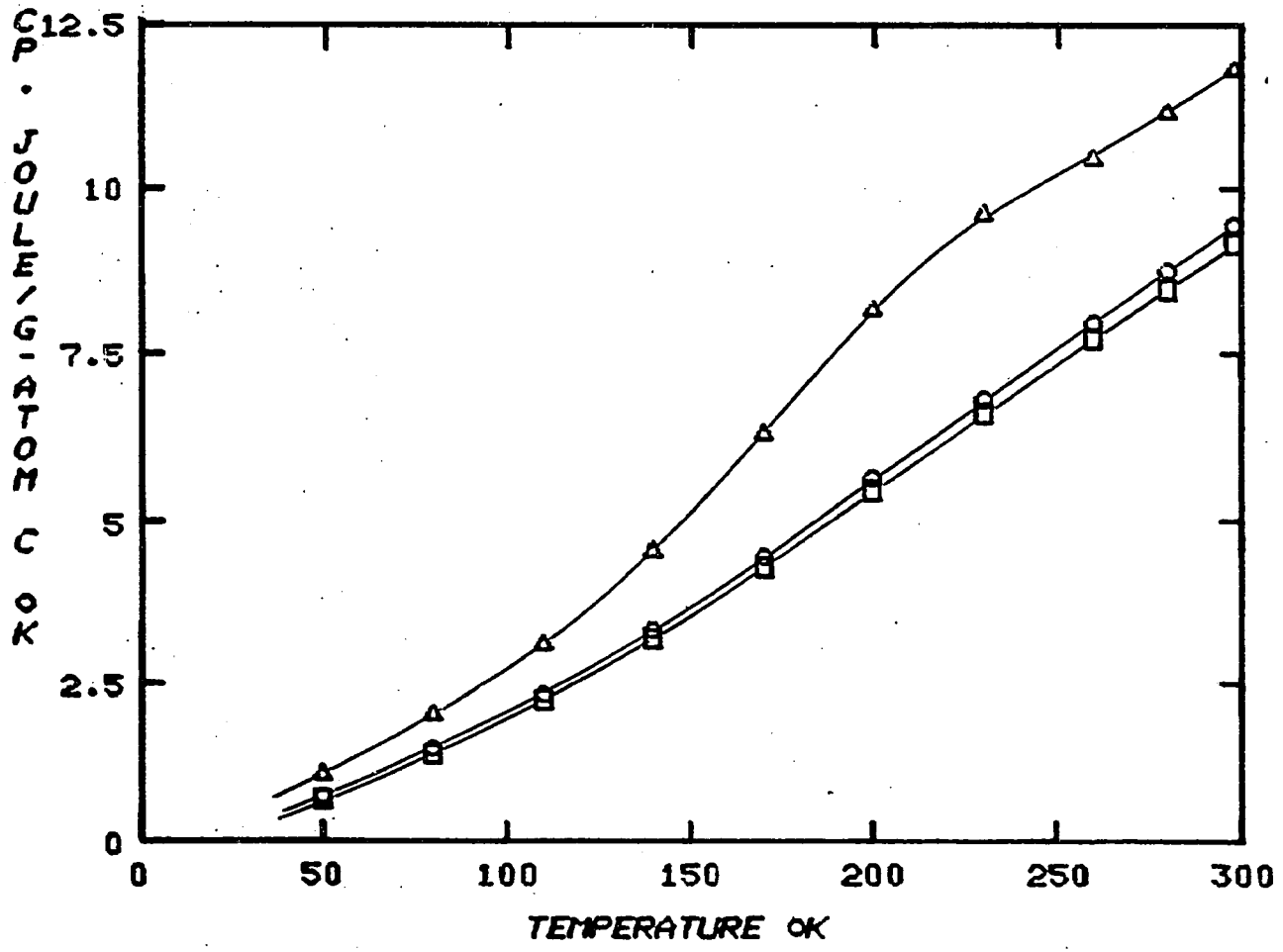

Figure 3. Kasatochkin's heat capacity data of original Schungite (Δ), shungite heat treated at 600°C (o), and at 1000°C (□).

3. EXPERIMENTAL ARRANGEMENT AND PROCEDURE

A flow sheet for the experimental work is shown in Figure 4.

3.1 Sample Preparations

3.1.1 Coal Origins

Samples of chars were prepared by pyrolysis of coals obtained from the Pennsylvania State University's Coal Bank. The coals were, a North Dakota lignite, an Illinois No. 6 bituminous coal, and a highly fluid Virginia coking coal. A detailed description of these coals is available from Pennsylvania State University's Coal Research Center of DOE and they are indexed as PSOC-246, PSOC-22 and PSOC-265 in their data bank (see Table 1).

3.1.2 Size Reduction

The samples originally available in a -20 mesh size were ground in a ball mill then Rotap sieved to -250 mesh size for appropriate analyses without loss of information from the parent coals.

3.1.3 Demineralization Procedure

In order to generate the DMMF (dried mineral matter free) samples, the direct demineralization process devised by

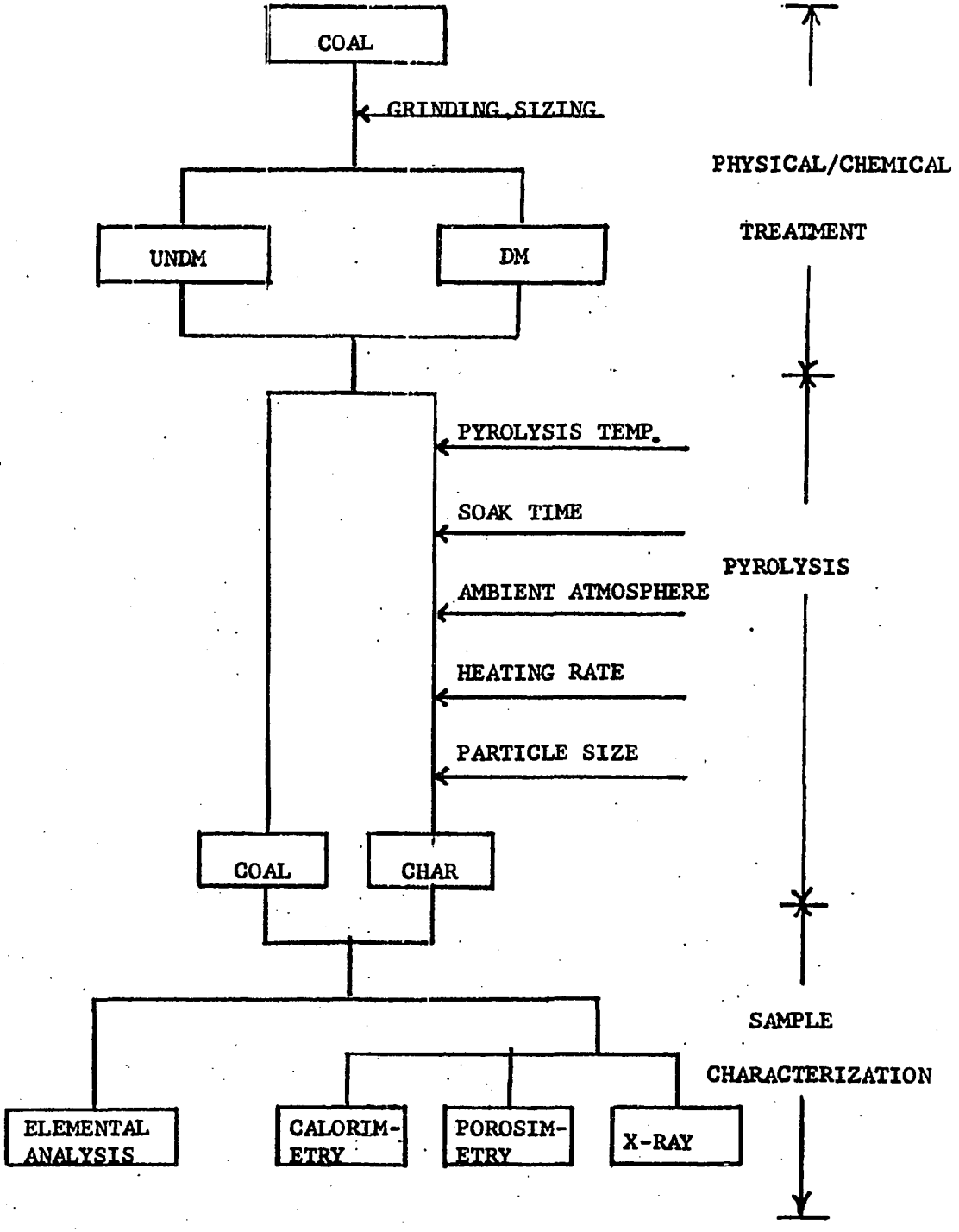

Figure 4. Schematic research program.

Table 1. Chemical Analysis of Coal Samples Reported by Pennsylvania State University's Coal Bank.

Sample			Proximate Analysis (Dry)			Elementary Analysis (Dry)					
Number	ASTM Rank	State	Volatile Matter	Fixed Carbon	Ash	H	C	O	N	S	MM
PSOC-265	HVA	VA	31.66	52.79	15.54	4.44	71.47	3.92	2.03	0.56	17.58
PSOC-282	HVB	IL	36.34	53.51	10.15	4.98	73.19	7.26	2.09	0.71	11.78
PSOC-22	HVC	IL	38.46	51.39	10.14	5.12	70.53	9.46	1.39	1.63	11.88
PSOC-241	Sub.B	WY	40.92	52.09	6.99	4.83	67.89	17.45	1.33	0.37	8.13
PSOC-246	Lignite	ND	44.73	45.57	9.70	4.29	63.67	19.09	1.40	0.56	10.99

Radmacher and Mohrhauer [14] was employed. This method is based on removal of the major part of the mineral matter from the coal by extraction with strong hydrofluoric and hydrochloric acids. Minor modifications of the original method have been made as suggested by Bishop and Ward,[15] and Raj.[16] Following is the description of the procedure:

(1) Treat coal (-250 mesh) with 10% HCl at 50°C for 24 hours, then wash thoroughly with distilled water until the washing water tested neutral (Figure 5).

(2) Treat coal filtrate with 2N HF at 50°C for 7 hours, then wash again with distilled water.

(3) The coal thus treated is dried in oven at 105°C for 12 hours and then kept in desicator.

In the present study the acid treatment was carried out in air (As it has been concluded by Bishop and Ward that no significant coal oxidation had occurred during their treatment.).

3.1.4 Pyrolysis Procedure

Chars were prepared in a Linberg's Model 59972(C2) furnace equipped with programmable temperature controller. A schematic of the experimental apparatus is shown in Figure 6. Following is the description of the procedure:

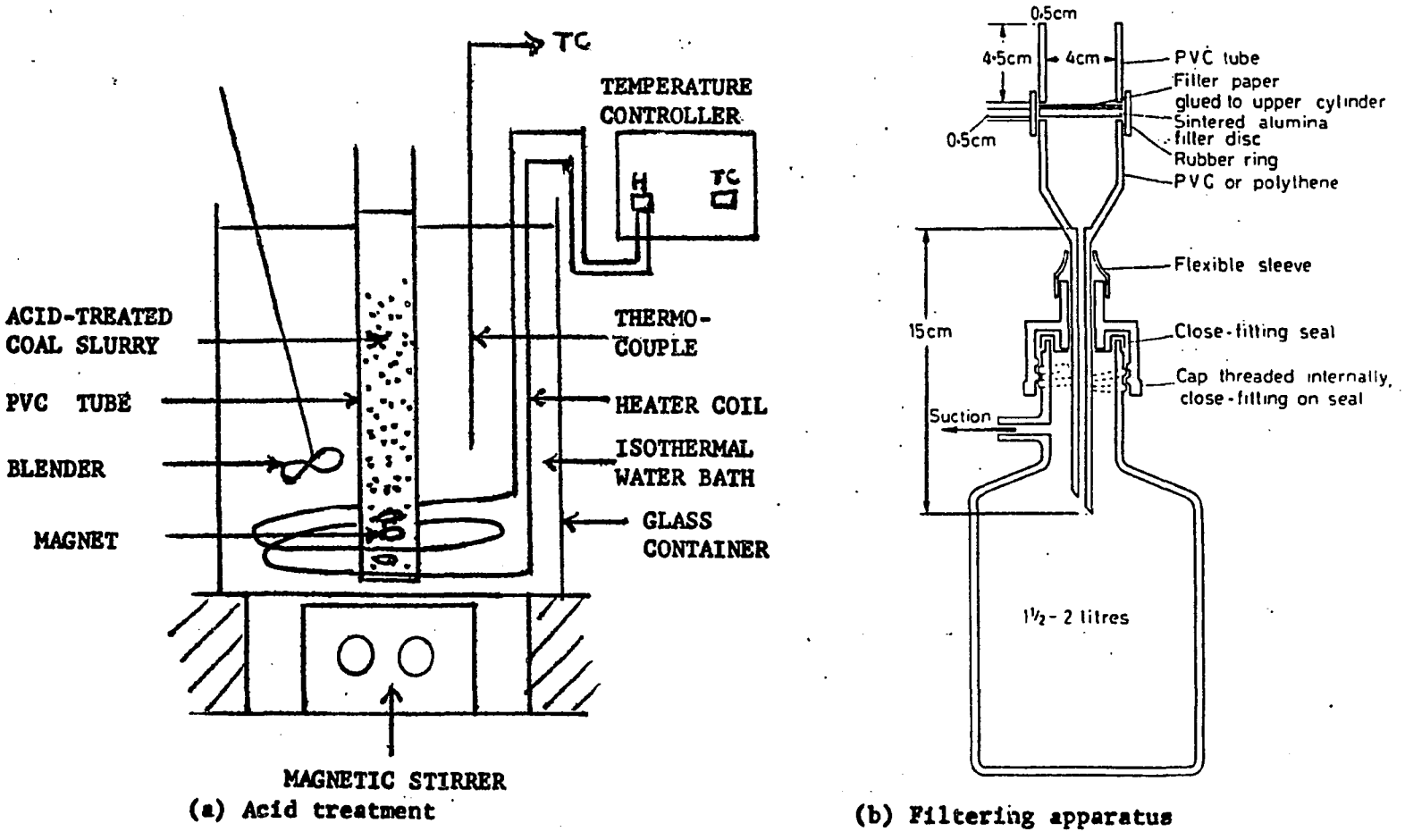

Figure 5. Demineralization process.

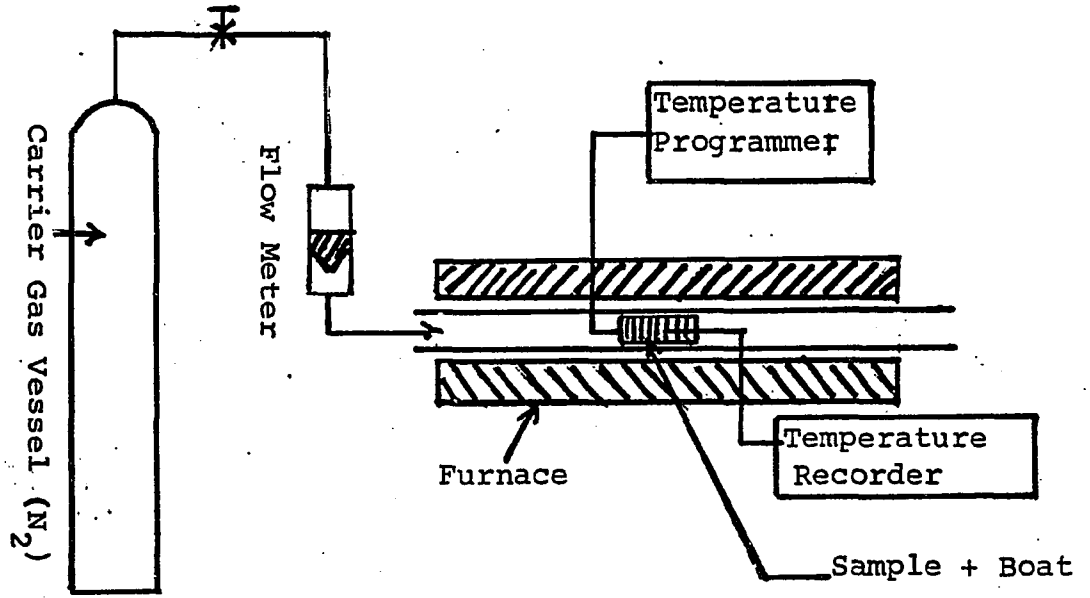

Figure 6. Flow diagram for pyrolysis process.

(1) The furnace is preheated to 200°C and nitrogen gas flow with a flow rate of 1 SCF/hr is started.

(2) The ground coal in an alundum boat is inserted into the furnace.

(3) Once the sample temperature stabilized at 200°C, the furnace temperature is ramped at 5°C/min rate to the desired pyrolysis temperature (700, 900 or 1100°C).

(4) Once the pyrolysis temperature is achieved, the sample is held at this temperature for the selected length of "soak time" (0.1, 1 or 24 hours).

(5) At the end of the soak time, the char is moved from the heat zone of the furnace to a room temperature section of the furnace tube for cooling down.

The stability of this furnace is $\pm$ 0.4°C change in the set temperature, and 0.01°C/min slope discontinuity with $\pm$10% line fluctuation in the temperature ramping.

Owing to the nature of this investigation, which focused on the solid residue, no attempt was made to recover the liquid and gaseous products of pyrolysis. The tar vapor and outgoing gases were discharged through an exhaust system.

3.1.5 Miscellaneous

(1) Samples prepared from above were dried and degassed

in vacuum oven at 110°C for 1 hour before heat capacity measurement, and chemical analysis.

(2) Coke prepared from PSOC-265 Virginia coking coal was reground before drying and degassing process.

3.2 Adiabatic Low Temperature Calorimetry

3.2.1 Introduction

Heat capacity data are of fundamental significance in physics, chemistry and engineering thermodynamics. Because of the difficulty of interpreting and analyzing the contributions of the several degrees of freedom to the thermal properties, heat capacity studies at temperatures above 10 or 20°K are of less interest to the physicist than are those at lower temperatures. On the other hand, the entire temperature range is of significance to chemical thermodynamicist concerned with thermodynamic properties at 300°K and higher. In most instances, the major contribution to these properties originates above 10°K. But, since, in many instances, significant and important contributions come from lower temperatures or are associated with the residual properties, the data below 20°K is also relevant to the chemical thermodynamicists.

The heat capacity of coal chars is similar to that of graphite, therefore, the investigation over the whole temperature range below room temperature will be important.

This chapter is especially concerned with the application of the adiabatic shield technique (or, as it is usually referred to-adiabatic calorimetry) over the temperature range between 77 and 300°K.

The basic steps which are involved in calorimetry are (1) cooling of the sample to the desired temperature, (2) isolation of the sample from the surroundings, (3) addition of energy to the sample, (4) maintenance of nearly adiabatic conditions, and (5) accurate thermometry. Detailed information on the techniques of achieving these steps will be given in the subsequent sections of this chapter.

3.2.2 Apparatus

3.2.2.1 Adiabatic Cryostat

A recirculating mode He-3 cryostat was modified for adiabatic operation up to 300°K. Figure 7 shows the schematic details of the original cryostat. The design and construction of this cryostat was described by Isaacs. [17]

The entire cryostat assembly is suspended from the top plate as shown in the Figure 7. The calorimeter (sample container with or without sample) is suspended from the mechanical heat switch by a harness made of silk threads so that the cooling of the calorimeter can be achieved through

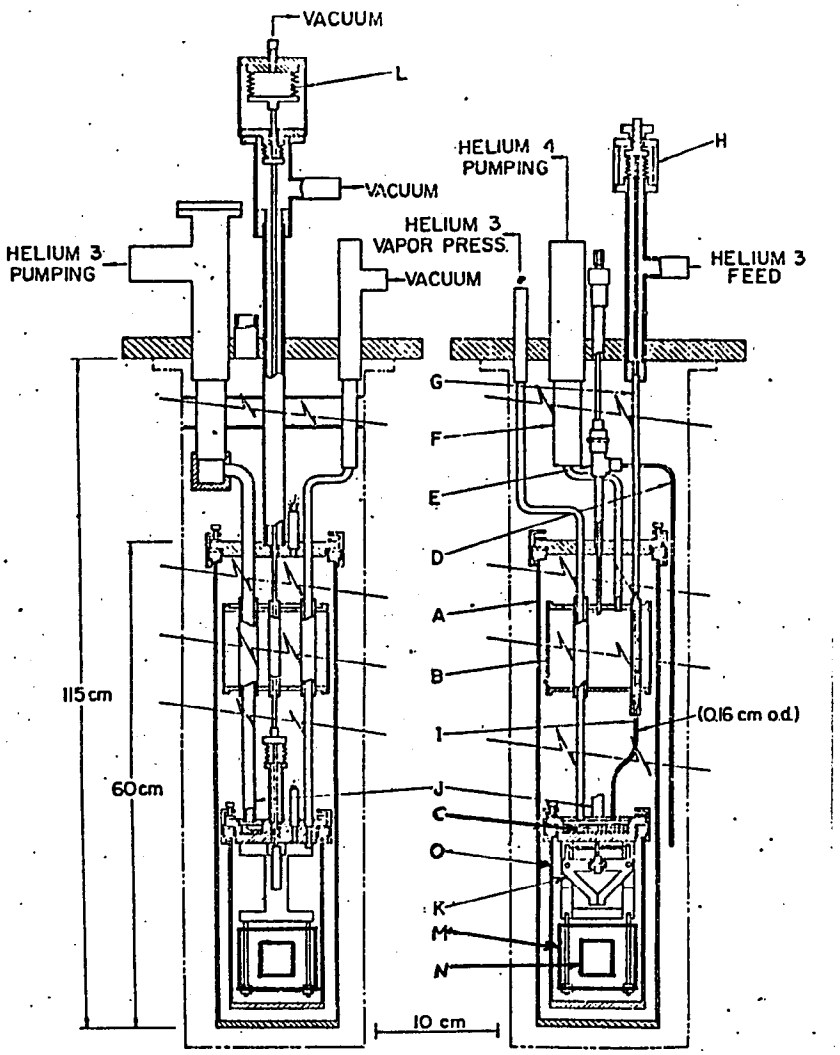

Figure 7. Cryostat for calorimetry.

A. Demountable vacuum jacket
B. He-3 condenser unit
C. He-3 evaporator unit
D. Siphon tube, He-4 feed to B
E. He-4 feed valve
F. He-4 evaporation line
G. He-3 gas feed to condenser
H. Throttle valve
I. He-3 feed to C
J. Sample space evacuation line
K. Mechanical heat switch
L. Bellow control for K
M. Adiabatic shield
N. Calorimeter
O. Demountable vacuum jacket

the following two modes of operation:

(1) Fast cooling: The mechanical heat switch is used here to establish direct thermal contact between calorimeter, adiabatic shield, and the refrigerant.

(2) Slow cooling: The calorimeter is disengaged from the refrigerant. Heat exchange gas is admitted into the vacuum space between jackets A and O, and radiation cooling cools the sample to 77°K in approximately 15 hours.

Adiabatic conditions are established at any operating temperature by careful control of all the factors that lead to heat exchange between the calorimeter and its environment. Gas conduction is minimized by maintaining a high vacuum (10^{-3} Pa) within the sample chamber. The suspension of calorimeter by the silk harness and the use of special low thermal conductivity electrical signal leads minimize conduction heat transfer via solid contacts. The signal leads enter the cryostat through plastic seals as described by Anderson, [18] and were thermally anchored at the appropriate positions in the cryostat. Before contacting the calorimeter, they were attached to a copper ring which is part of the adiabatic shield.

Upon establishment of adiabatic conditions, the temperature evolution of the sample is measured by a Silicon-Diode thermometer mounted in the center of the calorimeter vessel.

Electrical energy is then supplied to the calorimeter and sample by the heating element installed on the calorimeter vessel.

3.2.2.2 The Calorimeter Vessel

(A) General Requirements

The calorimeter vessel must be strong enough to withstand the pressure gradient used for compacting the samples. It must be chemically inert toward the sample. It must provide good thermal contact between the sample and the heater, and between the sample and the thermometer. In addition, it is desirable that the calorimeter (addenda) heat capacity be relatively small compared to that of the sample. Simultaneous satisfaction of all these requirements usually requires a certain amount of compromise in the design, and fabrication of the calorimeter.

Although the requirements are somewhat overlapping, they will be discussed in terms primarily of the thermal diffusivity, and the addenda heat capacity:

(1) Thermal Diffusivity and Heat Distribution:

After several trials of selecting the proper material, aluminum was chosen for the fabrication of the calorimeter.

(2) Heat Capacity of the Empty Vessel:

Aluminum heat capacity changes by a factor of three between 70 and 300°K. As the relative accuracy in the net heat capacity is considered, it is still favorable due to other advantages for constructing the calorimeter.

(B) Typical Design

Figure 8 is the diagram of the calorimeter employed in this study. Main features of this calorimeter are:

(1) To avoid the complication of applying heat exchange media in the calorimeter, the mechanically packed powder sample is allowed under vacuum through the fine holes on the cover plate by slowly decreasing the pressure in operation. The samples were placed under vacuum overnight and the weight loss after 24 hours pumping were found to be negligible (about 0.08 wt%).

(2) As compared to the coal char samples, the heat capacity of this calorimeter was found to be reasonably small in the temperature range of measurement (about 30% of the total for the fully-loaded calorimeter).

3.2.2.3 Measurement Techniques and Adjuvant Circuitry

Adiabatic calorimetry involves a number of electrical measurement and control features. The measurements include regulating the electrical power input to the calorimeter and

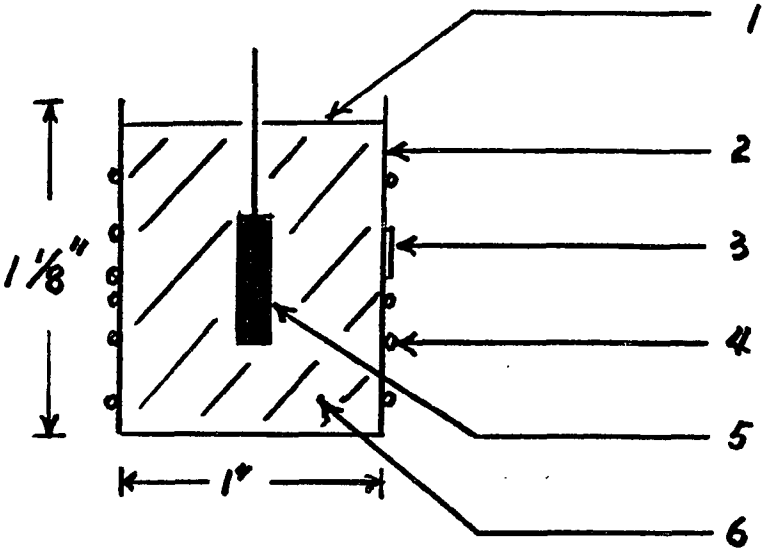

Figure 8. Cross-sectional diagram of the calorimeter.

1, Aluminum cap with fine holes on it

2, Thin-wall Aluminum cylindrical cup

3, Differential thermocouple sleeve

4, 0.003i" enameled manganin wire heater glued on the surface by a thin layer of GE7031

5, Si-Diode thermometer

6, Mechanically packed fine-powder sample

determining the energy input and the resultant temperature increments under adiabatic or nearly-adiabatic conditions by Si-Diode thermometry. The temperatures of the adiabatic shield surfaces and of the electrical lead wires relative to the temperature of the surface of the calorimeter are controlled by heaters which operate in conjunction with thermocouples.

For the determination of the heat capacity of coal chars, the discontinuous heating method was used. In the discontinuous method, measurements are made of the power and duration of the energy input and the calorimeter temperature is monitored continuously as a function of time.

(A) Cryogenic Thermometry

(A-1) Thermometer and Temperature Scale

Silicon-Diode thermometer (SI-400 GG) was used as the temperature sensor over the temperature range of this study. Figures 9 and 10 show the physical configuration and the typical response curve of a Silicon-Diode thermometer. This thermometer was calibrated against reference standards (SI Nos. 2 and 8) by the manufacturer, Scientific Instruments Inc., at 10 microamperes excitation current.

A temperature table was generated by least-square fit on the calibration points (see Table 2). The following

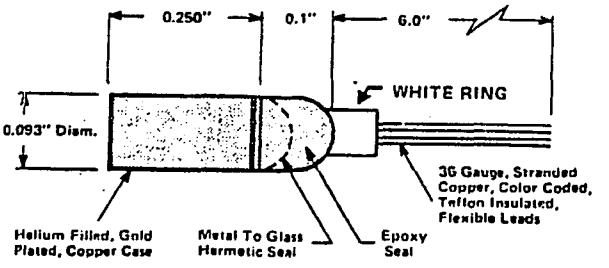

MODEL Si-400 CRYOGENIC TEMPERATURE SENSOR SILICON DIODE THERMOMETER

Figure 9. Physical configuration of the Silicon-Diode thermometer.

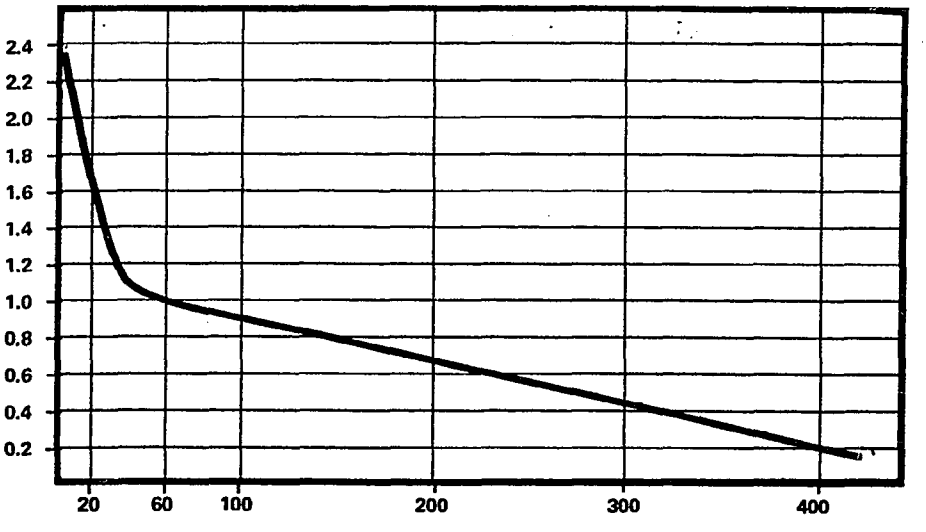

TYPICAL RESPONSE CURVE

Reference Standards for Temperature Measurement: 1K — 100K - Germanium - NBS Calibrated
100K — 400K - Platinum - NBS Calibrated

Figure 10. Typical response curve of the Silicon-Diode thermometer.

Table 2. Silicon-Diode Thermometer Calibration Points.

Model No.: Si-400GG Calibration Current: 10 Microamperes

Serial No.: 10074 Reference Standard: SI Nos. 2 and 8

Temp. -°Kelvin	Output-Volts	Temp. -°Kelvin	Output-Volts
4.00	1.90153	36.00	1.09254
4.50	1.89069	38.00	1.08231
5.00	1.87685	40.00	1.07209
5.50	1.86301	45.00	1.05753
6.00	1.84917	50.00	1.04478
6.50	1.83306	55.00	1.03395
7.00	1.81696	60.00	1.02315
7.50	1.80086	65.00	1.01163
8.00	1.78475	70.00	1.00010
8.50	1.76890	75.00	0.98858
9.00	1.75304	80.00	0.97660
9.50	1.73719	85.00	0.96462
10.00	1.72134	90.00	0.95264
11.00	1.69571	95.00	0.93956
12.00	1.67008	100.00	0.92649
13.00	1.64446	110.00	0.90207
14.00	1.61883	120.00	0.87754
15.00	1.59320	130.00	0.85246
16.00	1.56350	140.00	0.82737
17.00	1.53380	150.00	0.80203
18.00	1.50410	160.00	0.77659
19.00	1.47440	170.00	0.75115
20.00	1.44470	180.00	0.72571
22.00	1.37912	190.00	0.69966
24.00	1.31354	200.00	0.67354
26.00	1.26227	220.00	0.62133
28.00	1.21099	240.00	0.56896
30.00	1.15972	260.00	0.51706
32.00	1.13124	280.00	0.46539
34.00	1.10277	300.00	0.41353

Date: 19 April 1978 Calibrated by: _____

Anthony Bittner

fitting procedure was used:

(1) Least-square polynomial curve fit for the provided calibration points was made by the following equation:

$$T_{calc} = \sum_{i=o}^{4} A_i V^i \qquad (3)$$

The dispersion (ΔT) of the calibration points T_{exp} with respect to the fitting equation is shown in Figure 11.

(2) Each segment of ΔT on the dispersion curve was polynomial curve fitted again, then the measured voltage can be converted to the corresponding temperature for desired accuracy by the following equation:

$$T_{exp} = T_{calc} + \Delta T \qquad (4)$$

Where T_{calc} is calculated by equation 3, and ΔT by the fitting equations of the dispersion curve.

(A-2) Measurement of Thermometer Voltage

Four-lead potentiometric method was used to measure the voltage signal from the Silicon-Diode thermometer. Figure 12 shows the instrumentation schematic diagram. Scientific Instruments' Model 4000 constant current generator was used as the 10-microampere constant current source with the current stability found to be better than 0.1% during 10-hour run.

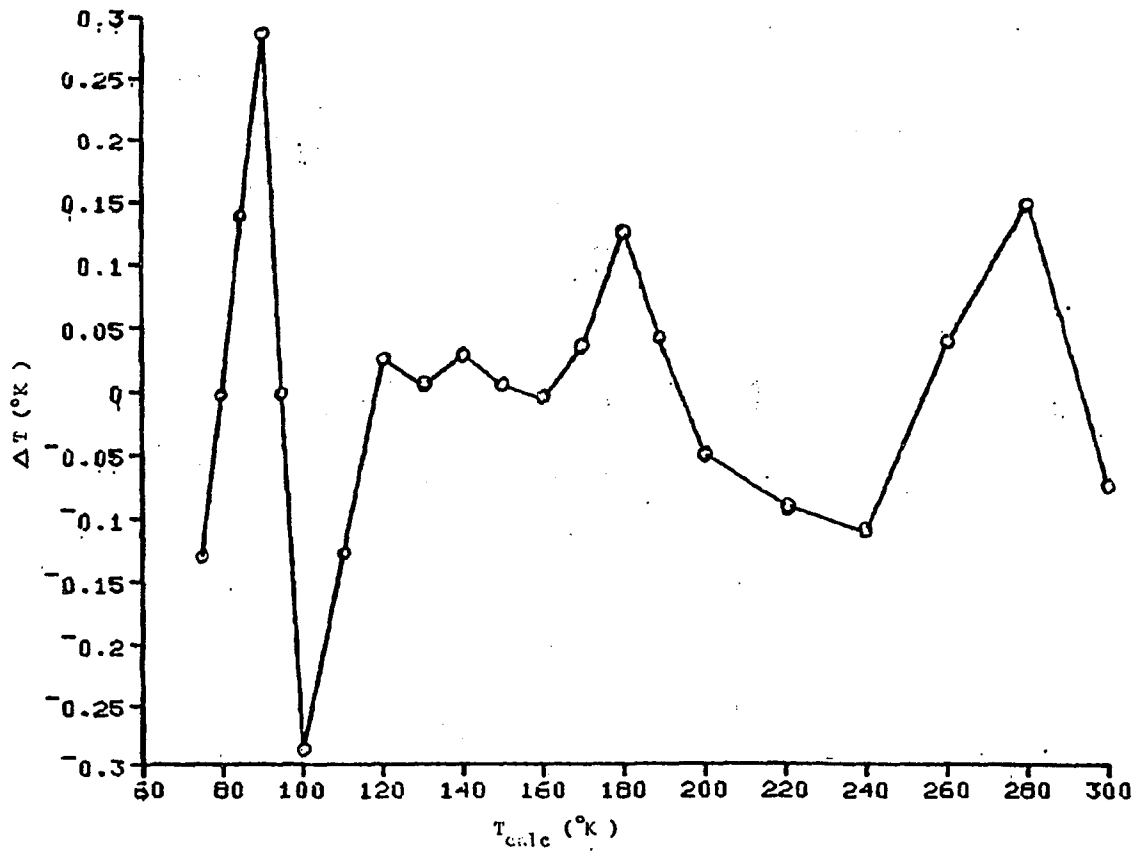

Figure 11. Dispersion curve of the calibration points of the Silicon-Diode thermometer vs the fitting equation T_{calc}.

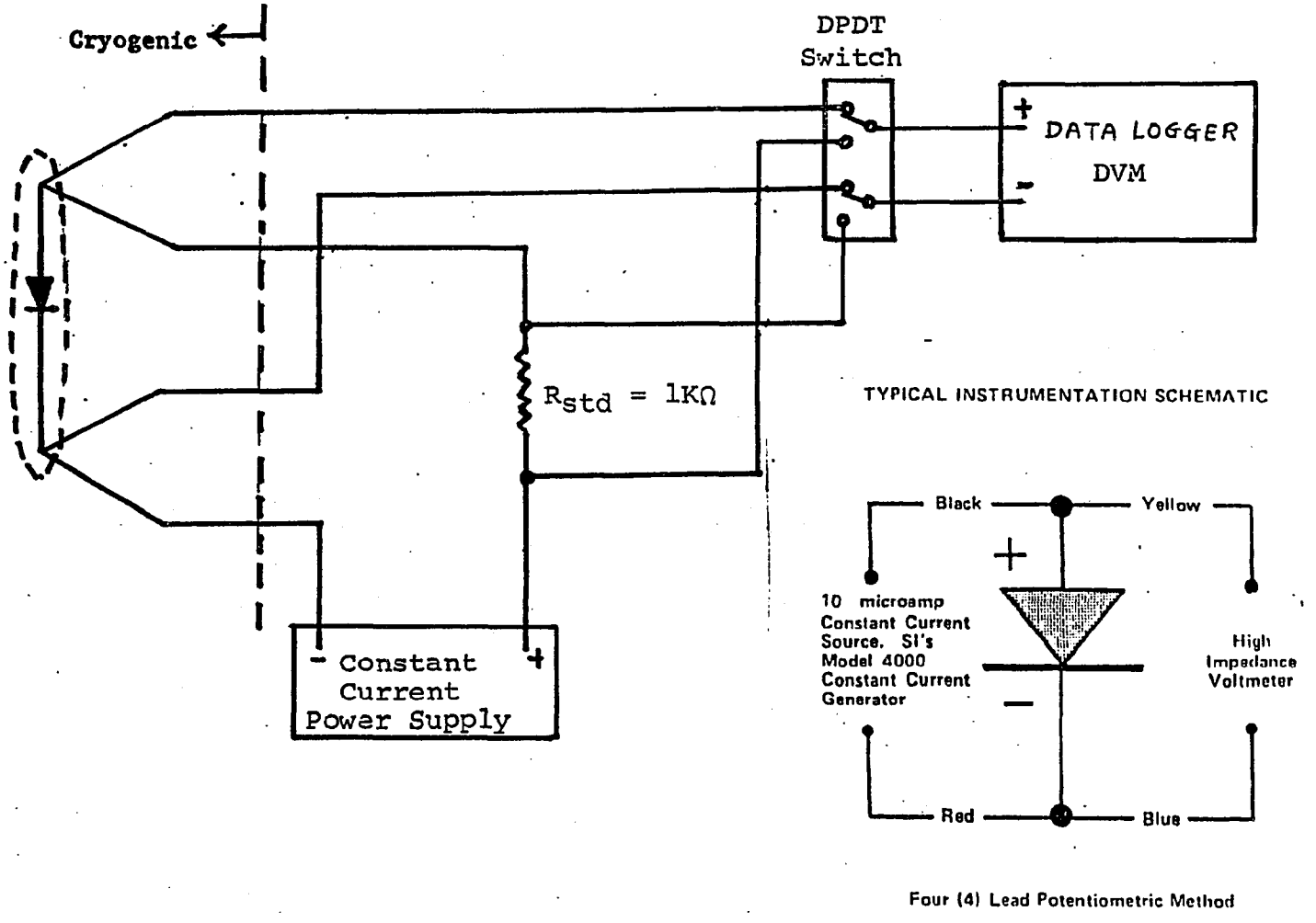

Figure 12. Instrumentation schematic diagram for Silicon-Diode thermometry and the temperature sensing flow diagram.

Hewlett Packard's Model 3467A logging multimeter was used as the high impedance voltmeter with accuracy of 0.1 mV (or the corresponding temperature of 0.04°K).

(A-3) Thermal Effect of the Si-Diode Thermometer

(1) 10 microamperes current flowing through the thermometer with 10^5 ohms internal resistance introduces 10^{-5} watts of power, which corresponds to a change in temperature of less than 10^{-4} °K/sec for a calorimetric system of 10 Joules/°K heat capacity. If the time duration of a complete measuring cycle is 30 minutes, the temperature increase from this source of energy is still very small (about 0.2°K).

(2) Conduction heat loss along long thin lead wire was minimized by anchoring the leads at the adiabatic shield.

(B) Energy Input and Measurement

The energy supplied by the calorimeter heater is given by the time integral of the power: $q = \int_0^\tau VI\, dt$, in which V and I are the instantaneous voltage across and current through the heater, and the duration of the heating interval is denoted by τ.

(B-1) Calorimeter Heater

The heater assembly is designed to distribute the generated heat as rapidly as possible to the calorimeter vessel,

which is, in turn, designed to distribute the heat to the sample. The heater was constructed by winding and gluing 0.0031" enameled manganin wire around the thin wall aluminum calorimeter. The resistance of the heater was chosen to be 100 ohms. Comparison of actual temperature verses time profiles to model calculations (see later Section 3.2.5 and Figure 21) indicates that the internal thermal conductivity of the loaded calorimeter is at least 100 times greater than the heat exchange coefficient between the calorimeter and adiabatic shield.

(B-2) Electrical Energy Measurement

The circuit for the supply and measurement of electrical power to the calorimeter is shown in Figure 13, and Figure 14. Electronic Measurements' Model C630 constant current power supply was used as the energy source. The stability of this power supply is better than 0.02% during the heating period over two minutes, and the effect of the initial thermal transient just after the heater switch is turned on is negligible (transient response time for most models are well below 10^{-3} seconds). The heater switch is controlled by a solid state timer (Figure 15) with adjustable on-off periods (Figure 16).

With the precision voltmeter (Auto Data's Vidar 521C model) operated in the voltage-time-integration mode and the power supplied by the precision constant current power supply,

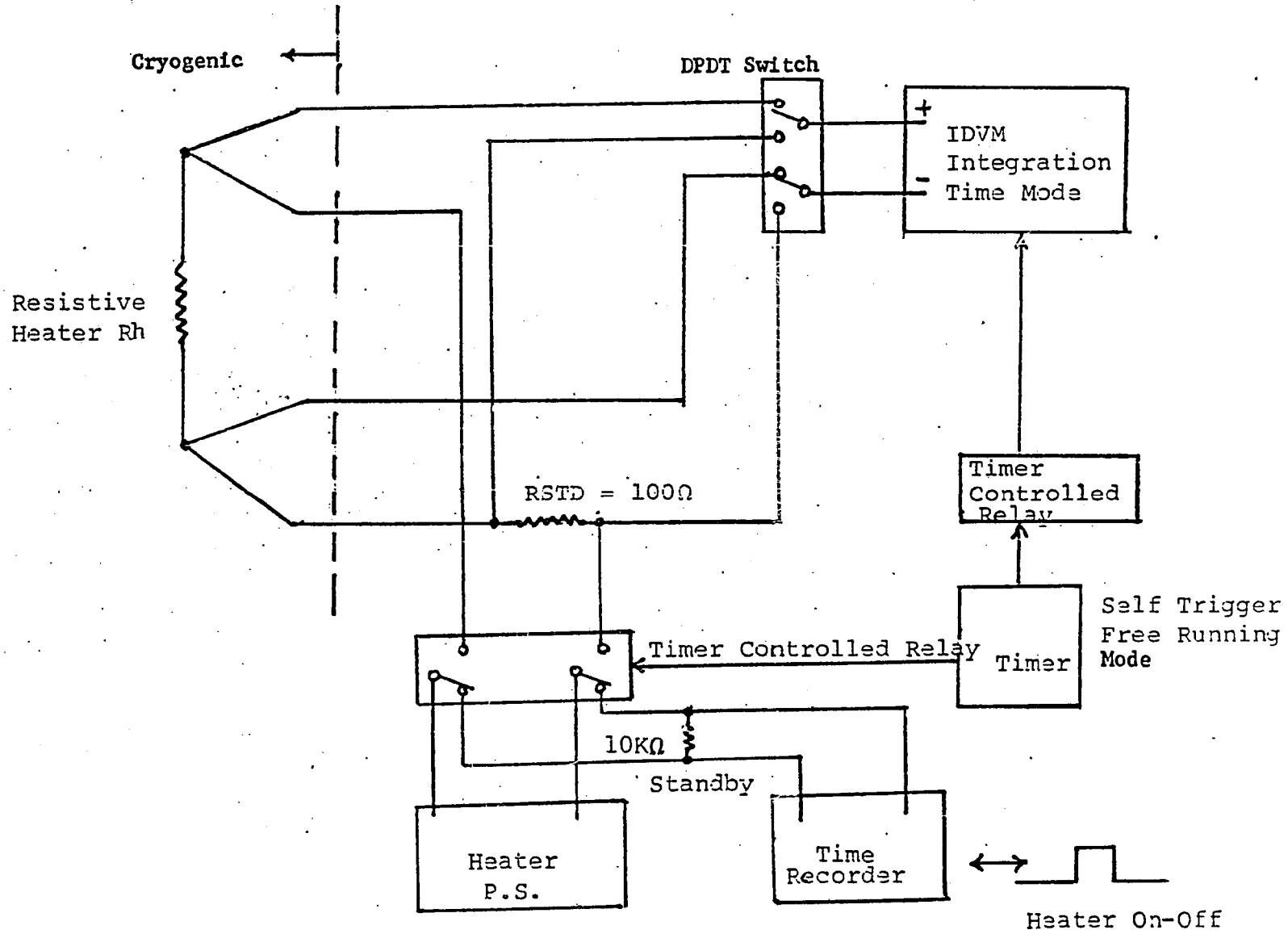

Figure 13. Heater sensing circuit.

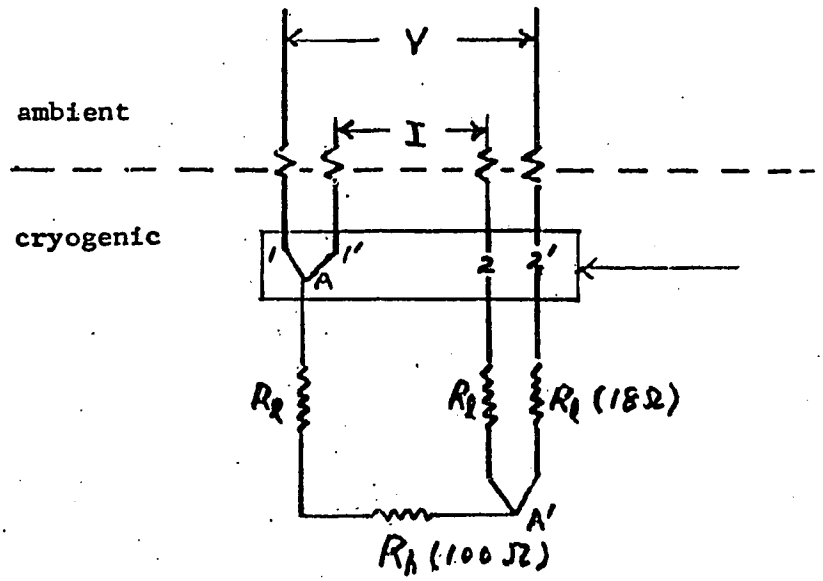

Figure 14. Simplified calorimeter heater circuit.

1, 1'-2 forms part of the current loop

2, The actual resistance to heat the calorimeter is considered as $R_h + R_l$ (A-A')

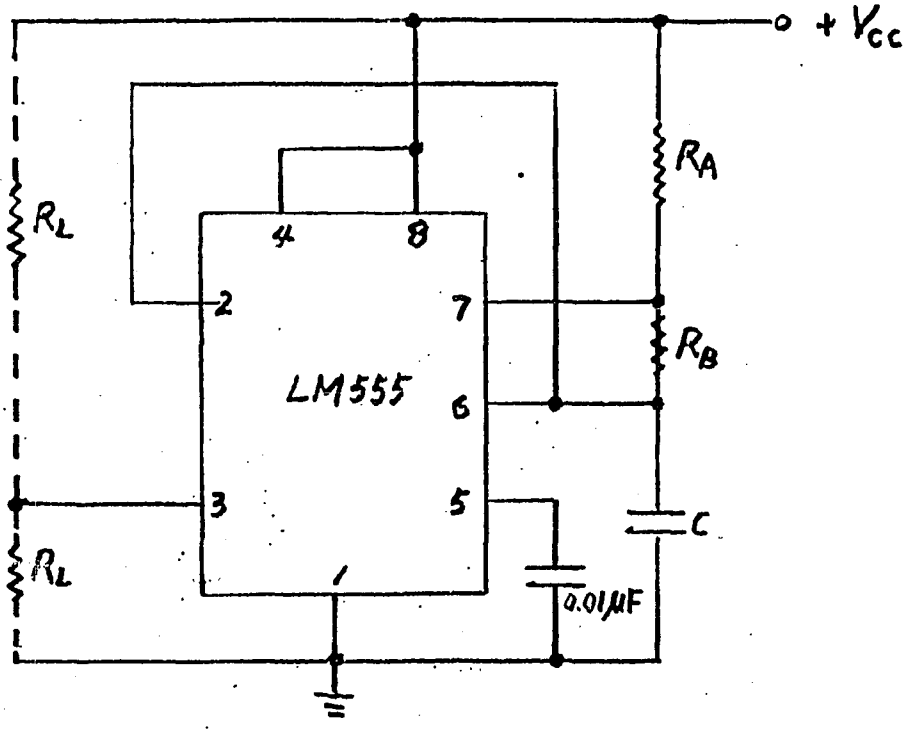

Figure 15. Schematic diagram for the free-running mode solid state timer LM555.

The charging time (output high) is given by:

$t_1 = 0.693 (R_A + R_B) C$

and the discharging time (output low) by:

$t_2 = 0.693 (R_B) C$

The total period is:

$T = t_1 + t_2 = 0.693 (R_A + 2 R_B) C$

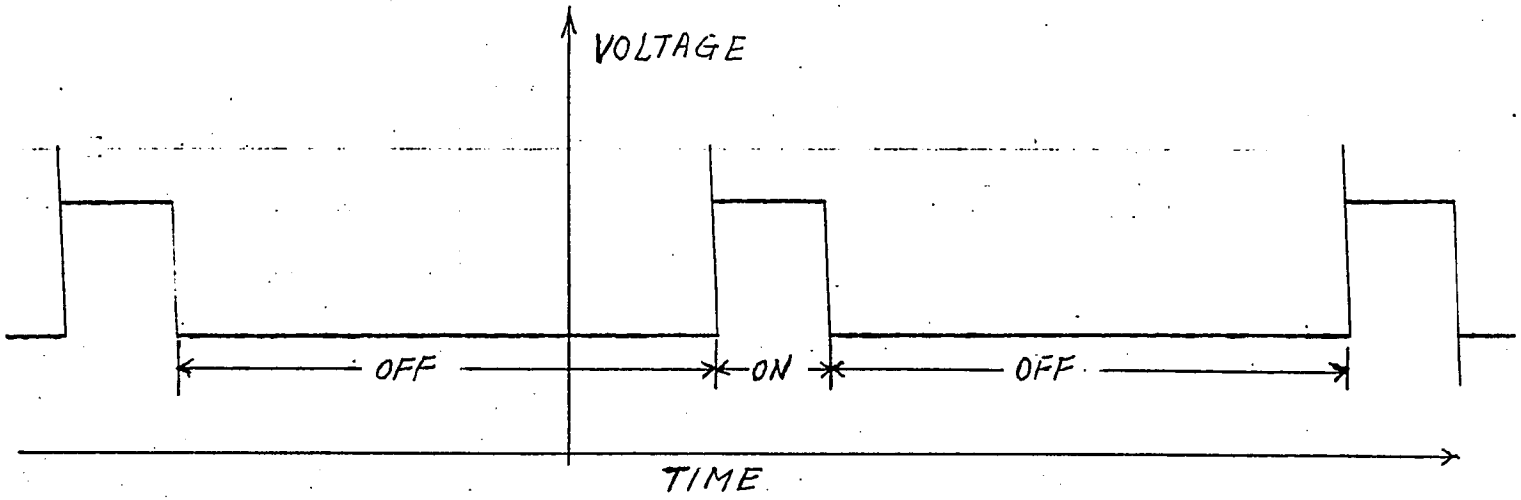

Figure 16. Heater ON-OFF performance check.

the electric energy input to the calorimeter can be calculated by the following equation:

$$q_o = \int_o^T I^2 R\, dt = I \int_o^T I R\, dt = I \int_o^T V dt \quad (5)$$

where, $\int_o^T V dt$ is recorded by Vidar 521C and I is calculated by the voltage drop across a standard resistor (of accuracy 10^{-4}%) recorded by the logging multimeter.

The advantage of this operation is that we don't have to measure the exact duration of heating to calculate the integral of the discretely sampled voltage information.

(C) Shield Control

(1) Temperature of the first vacuum shield with the attached leads' thermal anchor was controlled by the Scientific Instruments' Model 3700 temperature indicator/controller in the manual mode of operation. Chromel-Gold (with 0.07 atomic % Iron) thermocouple was used as the control indicator.

(2) Temperature of the adiabatic shield was controlled by the Scientific Instruments' Model 3700(S) automatic controller. The dual thermocouple used is shown in the Figure 17, with the junction 1 and 2 anchored on the outside surface of the calorimeter and the shield. The manganin wire heater was bifilarly wound around the adiabatic shield surface to avoid reactance effect during heating.

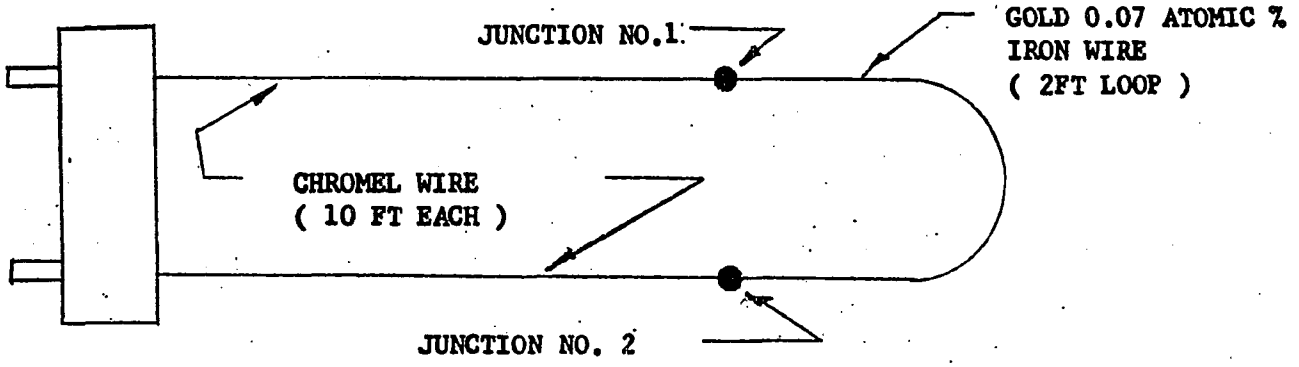

Figure 17. Dual thermocouple for the adiabatic shield temperature control.

3.2.3 Procedure

3.2.3.1 Loading and Cooling of Calorimeter

(1) Before mechanically compacting into the calorimeter, the sample was transferred from vacuum storage and weighed to 0.1 miligram accuracy. The amount of the sample used was approximately 3.5 grams per filling.

(2) The prepared calorimeter and its content was installed in the adiabatic shield with the thermometer and heater wires connected through tiny gold pin connectors.

(3) After the two vacuum shields were assembled, the system was evacuated with the inner vacuum space pumped by the diffusion pump for over 15 hours.

(4) The starting temperature of the calorimeter was reached by using liquid nitrogen in the external dewar (manufactured by the Cryogenic Associates) either through the fast or the slow cooling mode of operation (see Section 3.2.2.1). For both kinds of operation, hydrogen was used as the heat exchange gas in the space between the two vacuum jackets of the cryostat. The exchange gas was evacuated after the lowest temperature was reached.

3.2.3.2 Measurement Procedure

(1) Once the calorimeter stabilized at the desired

temperature, it was thermally isolated from the cryostat, and measurement could commence.

The temperature of the calorimeter was measured every thirty seconds during the measuring cycle. During the heating period, the heater current was also measured at thirty second intervals. Both informations were recorded using the four-channel logging multimeter. The heater voltage-time-integration information was recorded manually.

A measurement cycle consisted of a heating period of 150 seconds and off-heating period of 20 minutes.

(2) A heater current was selected between 30 and 75 mA to give the desired temperature increment of about 5 to 10°K in the 77 to 150°K temperature range and a temperature increment of 10 to 20°K at higher temperatures.

(3) The power outputs of both temperature controllers were regulated during the run with the set point of the manual controller adjusted with reference to the calorimeter temperature to avoid the development of large temperature gradients.

(4) Heat capacity of the empty calorimeter (including heater wires, anchor sleeves, thermometer, GE7031 glue) was measured in a separate experiment. The addenda heat capacity is shown in Figure 18, and is also tabulated in Table 3.

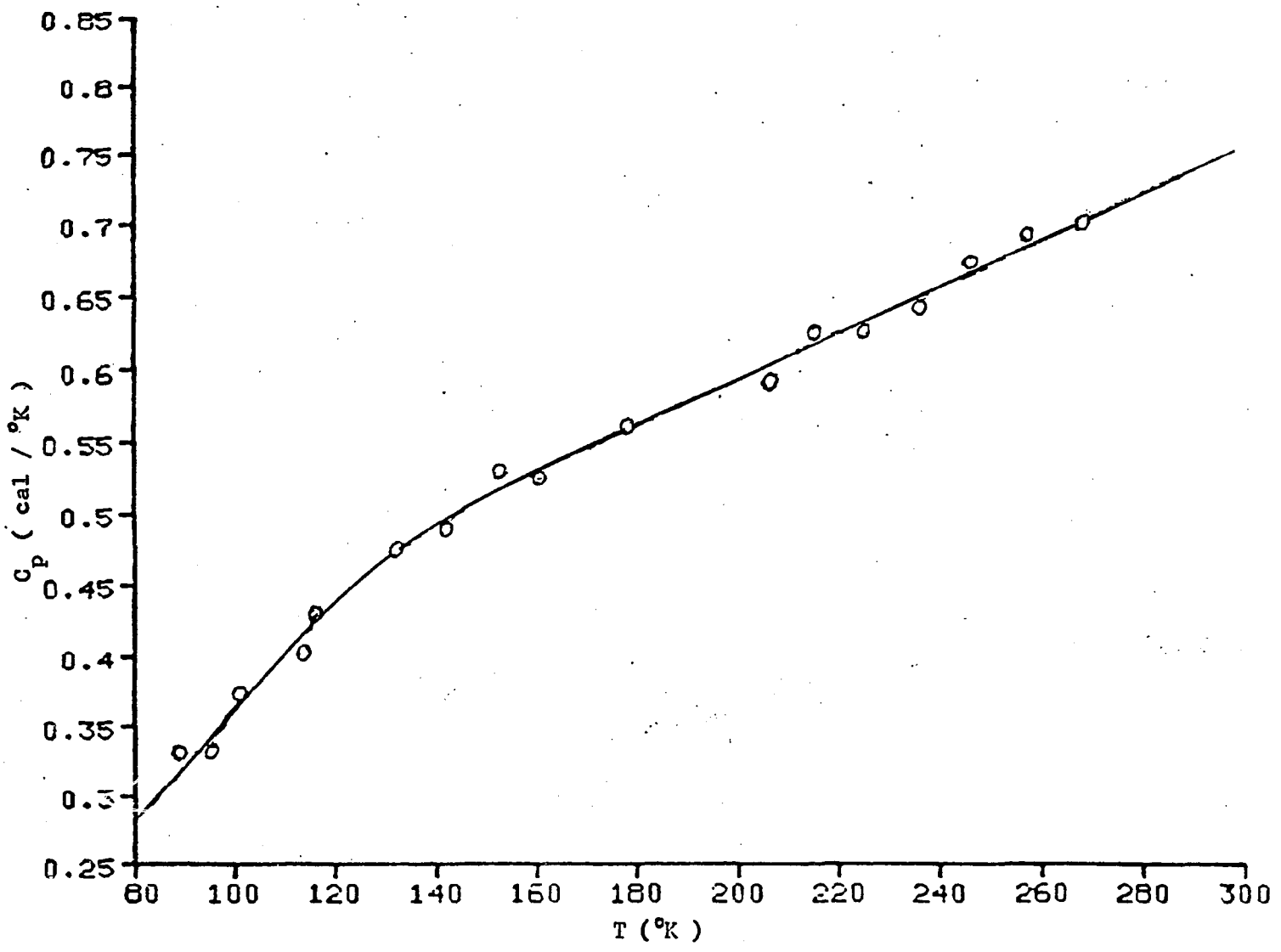

Figure 18. Heat capacity of addenda.

Table 3. Heat Capacity Data of Addenda.

T (°K)	C_p (Joule/°K)	T	C_p
78.03	1.176	178.12	2.351
82.1	1.247	183.67	2.351
87.65	1.389	189.28	2.385
95.2	1.397	193.43	2.402
101.26	1.556	199.87	2.431
104.27	1.594	206.15	2.477
110.58	1.678	215.46	2.615
116.44	1.786	220.58	2.611
123.25	1.874	226.02	2.623
129.67	1.958	236.42	2.868
132.5	1.992	246.17	2.807
136.35	2.012	249.76	2.766
142.22	2.054	256.88	2.887
150.47	2.142	267.54	2.925
153.12	2.213	270.37	2.941
156.76	2.18	277.6	2.933
160.05	2.209	282.13	3.1
164.13	2.259	284.52	3.109
169.07	2.272	288.94	3.146
173.24	2.335	294.37	3.13

3.2.4 Evaluation of the Heat Capacity

Because Newton's law of cooling is applicable to the operating conditions of an adiabatic calorimeter, the mean heat capacity, $q/\Delta T$, may be expressed by the relation: (19)

$$q/\Delta T = \frac{q_o + \int_{t_1}^{t_m} \alpha_1 C' dt + \int_{t_m}^{t_2} \alpha_2 C' dt + \int_{t_1}^{t_2} \beta C' \theta dt}{T_2 - T_1} \qquad (6)$$

In this expression, q_o is the measured electrical energy, α_i is intrinsic temperature drift (dT/dt) at apparent zero temperature difference between the adiabatic shield and the calorimeter, β is a heat exchange modulus, $d^2T/dtd\theta$, (in terms of the difference, θ, between the temperatures of the adiabatic shield and the calorimeter); C' is the heat capacity of the calorimeter system (including the sample), t_m is the mid-time of the heating period, and t_1 and t_2 are the times at which T_1, a steady temperature before heating, and T_2, a corresponding temperature after heating, are observed. The automatic shield temperature controller's performance was observed and it is reliable as the first approximation to assume $q = q_o$ in the heat capacity analysis. The determination of the temperature difference $(T_2 - T_1)$ and q_o will be explained separately.

3.2.4.1 Graphical Determination of Temperature Rise From The Temperature Profile

In conventional adiabatic calorimetry, heat capacities are determined from the temperature rise associated with a measured heat input. Since, in practice, the calorimeter is not in perfect thermal isolation, it is necessary to make a correction to the observed temperature rise to take account of the heat transfer between calorimeter and surroundings.

In the temperature range of this study, reasonable thermal isolation was expected and observed, and the temperature-time curves before and after a heating period (the so-called drift curves) follows Newton's law of cooling (Figures 19 and 20). Under these conditions the corrected temperature rise was found by assuming that the rate of increase of temperature of the calorimeter due to heat transfer during the heating period is equal to the mean of the rates before and after that period. This is equivalent to extrapolating the drift curves to the middle of the heating period and taking the temperature difference there to be the corrected temperature rise. This process is illustrated in the Figure 19 which also indicates how the "after" drift curve for one heating period may be used as the "before" drift curve of the next heating period.

3.2.4.2 Determination of The Electric Energy

q ($=q_o$) was calculated by the following equations:

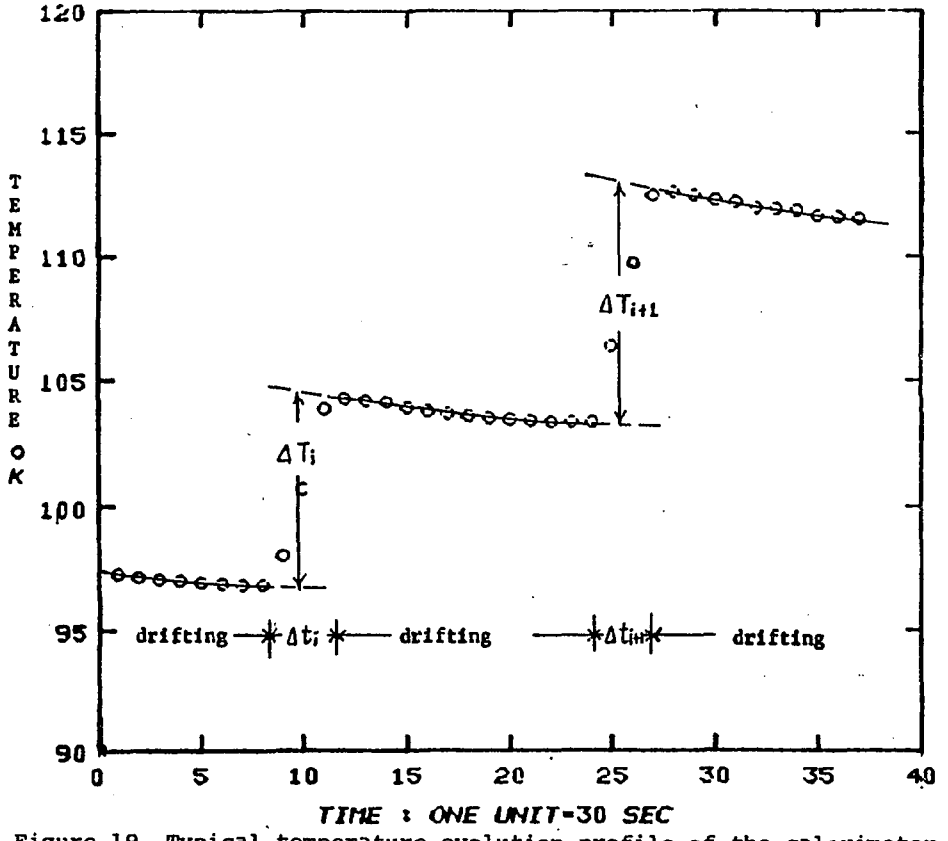

Figure 19. Typical temperature evolution profile of the calorimeter as recorded for a sample char around 100°K.

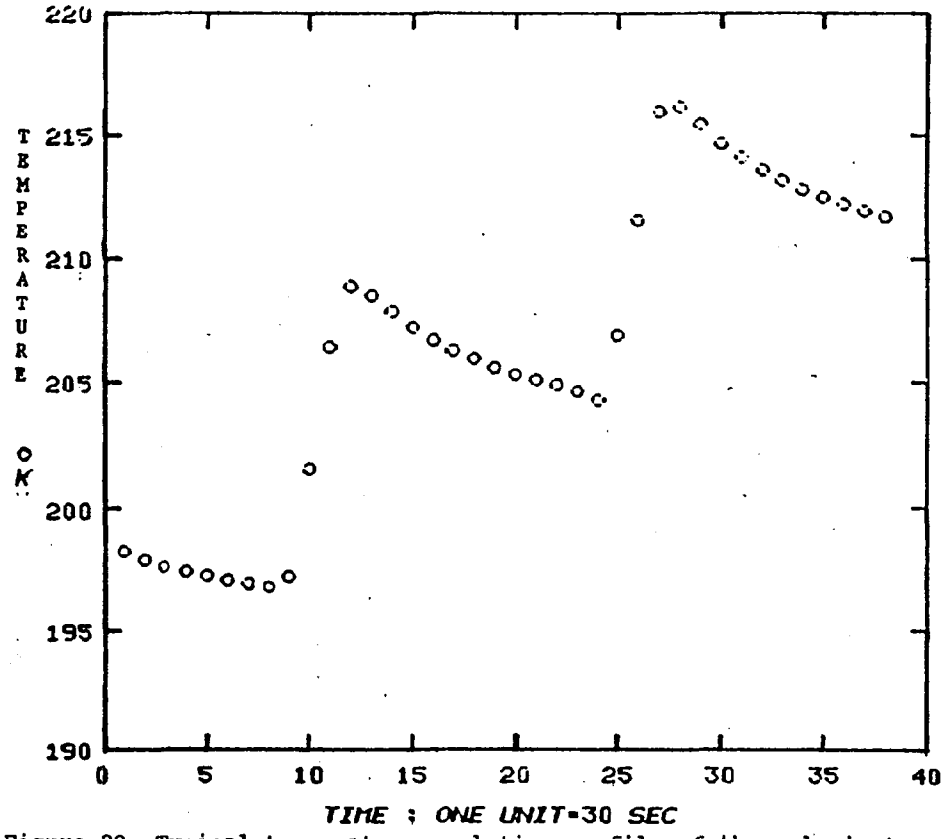

Figure 20. Typical temperature evolution profile of the calorimeter as recorded for a sample char around 200°K.

$$q = I \int_0^\tau V \, dt \qquad (7)$$

where

$$I = \frac{V \text{ (Voltage drop across resistor in series with heater)}}{R_{std} \text{ (Standard resistor)}}$$

$$\int_0^\tau Vdt = \frac{\text{(Vidar 521C Reading)} \cdot \text{(521C Range)}}{(6 \times 10^5)}$$

3.2.5 Heat Exchange Estimation and Experimental Error Analysis

Even when all the precautions are taken in the design of the instrument, the performance of the calorimeter has to be verified experimentally. The limiting factor, that determines the accuracy of the experimental data, is that the heat input to the calorimeter must indeed go into the calorimeter and only very small fraction of energy input are lost to the surroundings.

There is no literature data on thermal conductivities of coal chars in the temperature range of this study. Rather than installing an extra thermometer to monitor the development of the temperature profile inside the calorimeter, separate measurements were made to check the characteristics of the temperature profile (shape and thermal lag after the heat input) and its effect on the subsequent data analysis by

locating the thermometer at different positions along the geometric axis. The heat capacity data thus obtained was found to be scattered randomly around a smooth curve. This indicated that the heat distribution in the calorimeter was rapid compared to the exchange of heat between the calorimeter and the adiabatic shield. However, we still have to estimate the various contributions to the heat exchange between the calorimeter and the surroundings to ensure that the magnitude of this heat exchange is only a small fraction of the energy input to the calorimeter. The possible heat exchange effects were estimated as follows:

(1) Convective heat exchange is eliminated by the evacuation of gas in the sample chamber to less than 10^{-3} Pa.

(2) Heat conducted along the electrical leads between the calorimeter system and the thermal anchor was estimated by the following equation:[20]

$$\dot{q}_{cl} = \sum_i \left(\bar{\lambda}_i \frac{A_i}{\ell_i} \Delta T \right) \qquad (8)$$

where

$\dot{q}_{cl}$ = Rate of conduction heat exchange through the electrical leads

$\bar{\lambda}_i$ = Mean heat conductivity of lead wire i

A_i = Cross-sectional area of lead wire i

ℓ_i = Length of lead wire i between calorimeter and thermal anchor

ΔT = Temperature difference between calorimeter and thermal anchor

The total contribution of $\dot{q}_{c1}$ was calculated by considering seven manganin leads of 0.003 in diameter and 10 cm length, one chromel lead of 0.01 in diameter and 10 cm length, and one gold lead of 0.01 in diameter and 61 cm length. Assuming that in the worst case temperature difference of 15°K exists between the calorimeter and the thermal anchor, the calculated $\dot{q}_{c1}$ accounts for less than 0.015% heat input.

(3) Low pressure gas conduction:

The following equation was used to estimate the gas conduction effect:[20]

$$\dot{q}_{c2} = \text{constant} \cdot a_0 \cdot p\ (T_2 - T_1) \cdot A \qquad (9)$$

where

$\dot{q}_{c2}$ = Rate of gas conduction heat exchange

constant = 1.2 for air

a_0 = Accommodation coefficient (with upper limit $a_0 = 1$)

p = Pressure of the sample chamber as observed at room temperature

A = Surface area of calorimeter

Again, for $\Delta T = 15^{\circ}K$, $\dot{q}_{c2}$ was estimated to be of 0.001%

of the heat input.

(4) Radiation heat exchange between adiabatic shield and calorimeter:

During the heating period of the measurement, the maximum deviation of the temperature difference between adiabatic shield and the calorimeter was observed to be less than 10°K. This large temperature difference persisted only for a short period (10-30 seconds). The radiation heat exchange equation between two parallel plates can be used to estimate the rate of radiation heat exchange between adiabatic shield and calorimeter:[20]

$$\dot{q}_r = \sigma A(T_1^4 - T_2^4) \quad \left(\frac{\varepsilon_1 \ \varepsilon_2}{\varepsilon_1 + \varepsilon_2 - \varepsilon_1 \ \varepsilon_2} \right) \tag{10}$$

where

$\dot{q}_r$ = Rate of radiation heat exchange

σ = Stefan-Boltzman's constant

A = Surface area of radiation plate

T_1, T_2 = Temperature of radiation surface

ε_1, ε_2 = Emissivity of radiation surface

For $\Delta T = 10^\circ K$, $\dot{q}_r$ was estimated to be 0.15% for heat input to the sample at 260°K and 0.004% at 70°K.

The results of the above estimations of the magnitude of the above mentioned heat exchange effects indicate that

the recorded temperature profile is characteristic of the sample.

It is of interest to simulate the dynamic temperature profile for a model of our calorimeter system. For this purpose, the Vasileff's analytical solution [21] of the cooling curve for a cylindrical calorimeter was simulated for various ratios of the calorimeter thermal conductivity to the heat exchange coefficient between calorimeter and surroundings. Figure 21 gives the results of the calculation for several values of this ratio. It is interesting to note that when we back extrapolate these simulated cooling curves to the mid-heating period, the temperatures obtained are nearly the same.

In order to estimate the total error involved in the heat capacity, we have to include the error introduced in the graphical determination of the temperature rise after the heat input to the sample, and the error in the addenda heat capacity. The back-extrapolation method was estimated to introduce less than 3.5% error for the temperature rise. The error of 0.2% was estimated when we subtracted the addenda heat capacity from the total heat capacity. Therefore, the total error in the sample heat capacity is less than 4%.

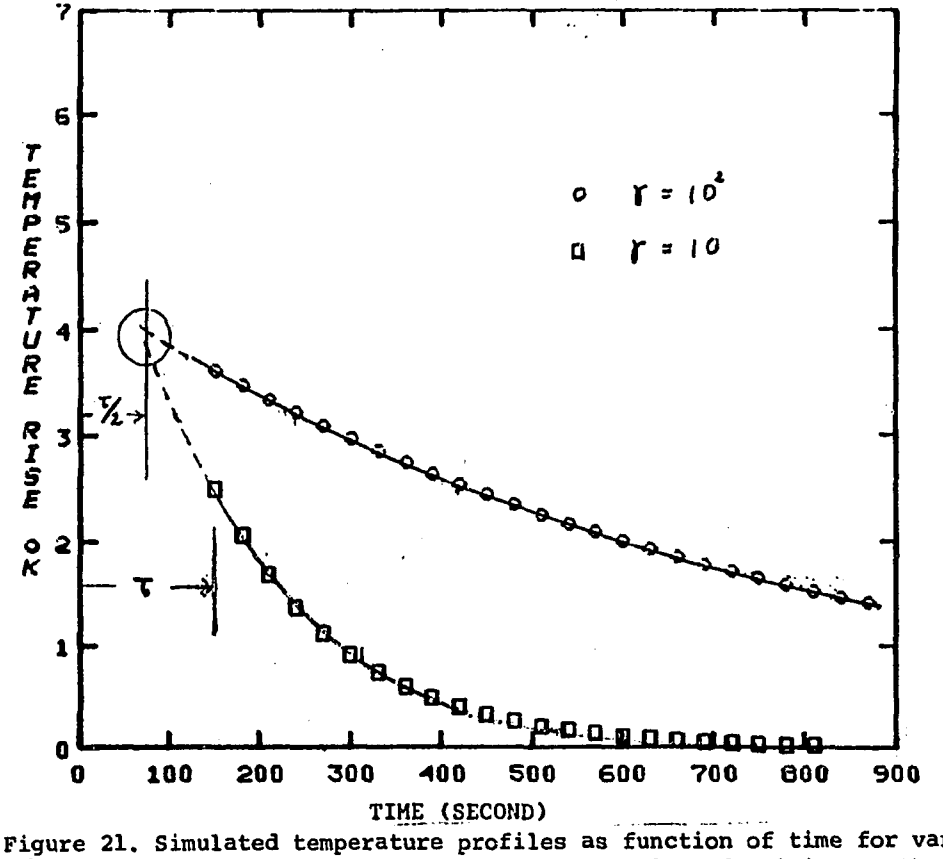

Figure 21. Simulated temperature profiles as function of time for various ratios (γ) of the calorimeter thermal conductivity to the heat exchange coefficient between calorimeter and surroundings.

3.3 Sample Characterization

3.3.1 Chemical Analysis of Samples

The carbon, hydrogen and nitrogen contents of the samples were determined by using a Perkin Elmer's Model 240B Elememtal Analyzer. The ash content of the sample was determined by weighing the combustion boat before and after analysis. The performance of this system for the analysis of coal has been reported in the literature.[22]

3.3.2 X-ray Diffractometry

X-ray diffractometry has been proved to be a powerful tool in characterizing coals. In this study, the X-ray diffraction spectra were obtained with Norelco's Model 12045/B diffractometer using Nickel filtered CuK_{α} radiation.

The samples used in the diffraction study were in the form of flat slabs prepared by spreading 1 gram of -250 mesh coal/char into a rectangular sample holder of interior dimension 3.5 cm by 1.1 cm using Elmer's glue as a binder, then dried at 105°C for about one hour.

Diffraction patterns were obtained by placing the sample in the reflection position and scanning over the angular range 2θ = 17 to 150 degree at a rate of 1 degree/minute with time constant of 0.5 seconds and chart speed of 30 in/hr.

3.3.3 Pore Size and Particle Size Analyses

In order to characterize the physical state of the powdered sample, one coal sample (PSOC-246) was analyzed commercially using the Coulter Counter Model T&TA particle size analyzer, and other samples were analyzed using an Aminco's porosimeter.

For reference purposes, a copper sample (-250 mesh size) was also measured to determine the approximate breakthrough pressure to fill the inter-particle void space. It is to be emphasized that no attempt will be made to explain quantitatively the pore size and pore size distribution of our samples, and what is reflected in our analysis should be the contribution to the void volume by the inter- and intra-particle voids. The analysis by porosimetry is made graphically on standard forms provided by the Aminco Corporation.

4. RESULTS AND DISCUSSION

4.1 Sample Characterization

4.1.1 Chemical Composition Analysis

Table 4 shows CHN and ash content obtained with the Perkin-Elmer Elemental Analyzer 240B on the coal and char samples used in this study. Also included are the H/C atomic ratios.

These composition data will be used to normalize the heat capacity of coal chars in later section. It is observed that the ashes remaining after the combustion analysis exhibit different colors characteristic of the coal type. This indicates the difference in the nature of the original mineral matter and the resulting ash amongst the coals studied. As shown in the composition analysis of the demineralized samples (see Table 4), the greater decrease in the atomic H/C ratio of the lignite char as compared to that of the bituminous chars when heat-treated to 1100°C reflects the very different nature of the C-H bonding in the remaining structures for these two types of coals.

4.1.2 Pore Size and Particle Size Analyses

The particle size analysis of an undemineralized lignite (UNDM PSOC-246) is shown in Figure 22. This is a typical

Table 4. CHN and Ash Analyses of Coal/Char Samples.

Sample	Weight per cent				Atomic Ratio
	C	H	N	Ash	H/C
POCO Graphite	99.35	0.78	0.07	nil	0.09
UNDM PSOC-265	70.14	4.02	1.1	15.1	0.68
UNDM PSOC-265-700-1	73.27	0.73	1.15	20.2	0.11
DM PSOC-265	81.83	4.41	1.51	2.02	0.64
DM PSOC-265-700-1	88.41	0.85	1.36	2.82	0.11
DM PSOC-265-1100-1	95.46	0.68	0.81	2.7	0.08
UNDM PSOC-22	63.58	4.03	1.18	12.32	0.75
UNDM PSOC-22-700-1	74.07	0.83	1.17	18.38	0.13
DM PSOC-22(undried)	73.57	4.3	1.37	0.66	0.69
DM PSOC-22(dried)	73.68	4.37	1.29	0.6	0.7
DM PSOC-22-700-1	88.44	1.33	1.45	0.87	0.17
DM PSOC-22-1100-1	94.19	0.64	1.31	1.07	0.08

Table 4. (conti.)

Sample	C	H	N	Ash	H/C
UNDM PSOC-246	59.26	3.96	0.99	6.86	0.79
UNDM PSOC-246-700-1	78.65	0.74	1.3	12	0.11
DM PSOC-246	64.7	4.05	1.25	0.47	0.74
DM PSOC-246-700-1	90.17	1.02	1.46	nil	0.13
DM PSOC-246-1100-1	99.51	0.29	1.4	nil	0.03

COULTER COUNTER® Model T&TA — PARTICLE SIZE ANALYSIS — .15 – 200 μ, # PERCENT — COULTER ELECTRONICS INC, 590 W 20 ST., HIALEAH, FLA. 33010

ORGANIZATION: City College of New York
OPERATOR: M.B.
EQUIPMENT: TA II, M3

$k = d\sqrt[3]{\frac{\pi}{6}}$ $\quad \frac{A2}{A1} = \left(\frac{d2}{d1}\right)^2$ when W2 = W1 FOR MODEL T $\quad \frac{A2}{A1} = \left(\frac{d1}{d2}\right)^2$ when W2 = W1 FOR MODEL TA

SAMPLE	ELECTROLYTE	DISPERSANT	APER. SIZE	SERIAL		PART DIA.	W	± tA	A	SAMPLE SETTINGS DIA.	W	± tA	A
PSOC - 246	Isoton	IB, 15 sec ultra	280	42969	Microspheres	19	8	3.2	153	20	8	3.2	14[illegible]
		sonics	70	24447	Microspheres	5	9	3.2	241	6	9	3.2	12[illegible]

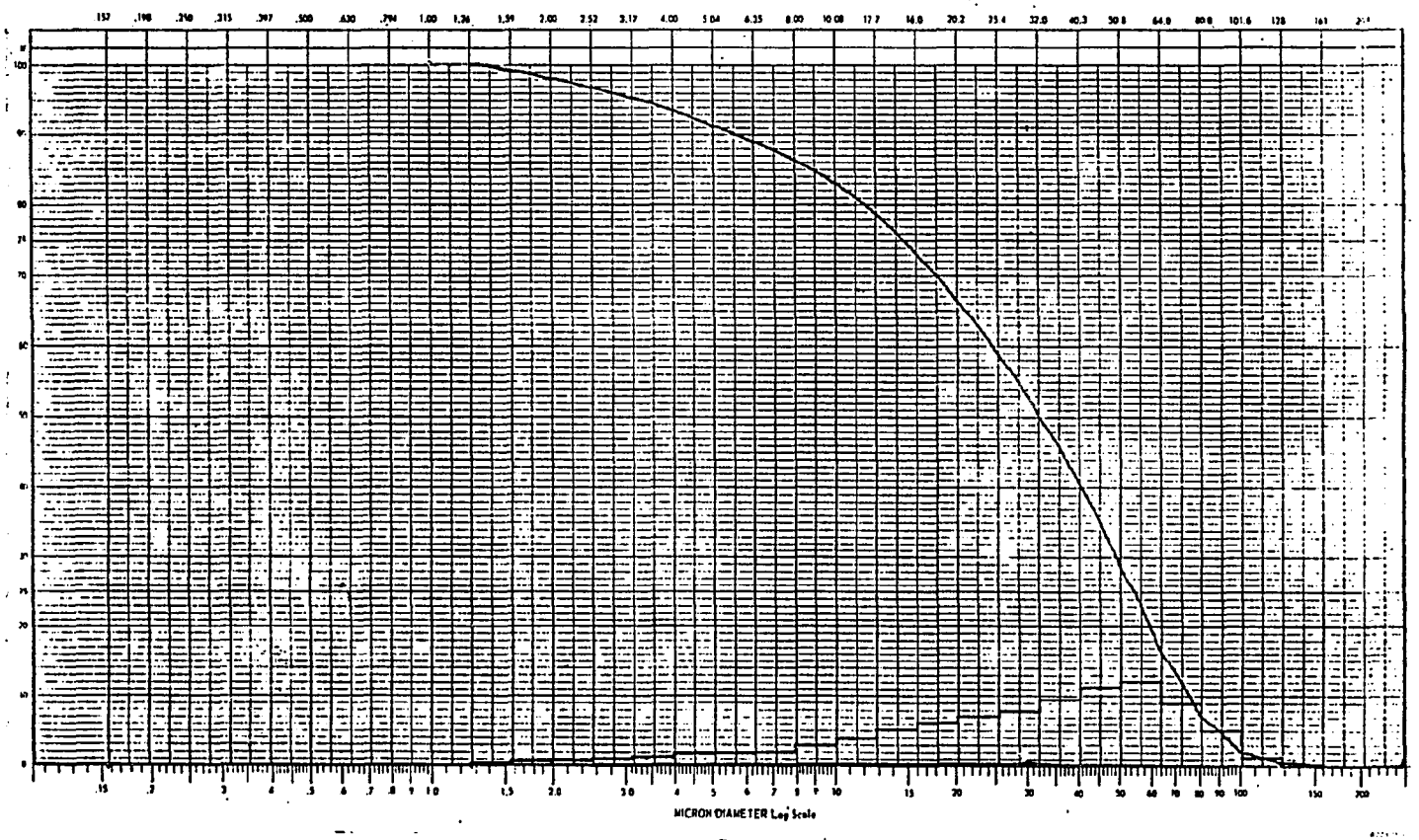

Figure 22. Particle size analysis of UNDM PSOC-246 coal.

particle size distribution curve for our coal samples all prepared by the same size-reduction procedures. The median of the measured diameter is 32.75 μm, far greater than the microcrystalline units existing in the coal structure. When the samples are well compacted into the calorimeter, the reduced void space will help in the even distribution of the heat energy added. The size reduction also helps the demineralization procedure and provides more representative samples for analyses (e.g. around 1 mg sample was used for Perkin-Elmer's Elemental Analyzer).

Some coals and chars were studied using the mercury porosimeter. The power of this tool is quite limited by the nature of samples and particle sizes. When the particles are finer than 200 μm and cover a wide size distribution, it is difficult to differentiate between inter- or intra-particle voids when investigating the macropore structure of the sample.

Figures 23 to 25 show the pore size distribution curves of some demineralized and undemineralized lignite and bituminous coals (DM and UNDM PSOC-246, 22, 265). There is a significant increase in pore volume for the samples after demineralization process. But in Figures 26 and 27, which show the pore size distribution curves of two additional coals (PSOC-282, 241), a slight decrease in pore volume was found for the samples after demineralization process.

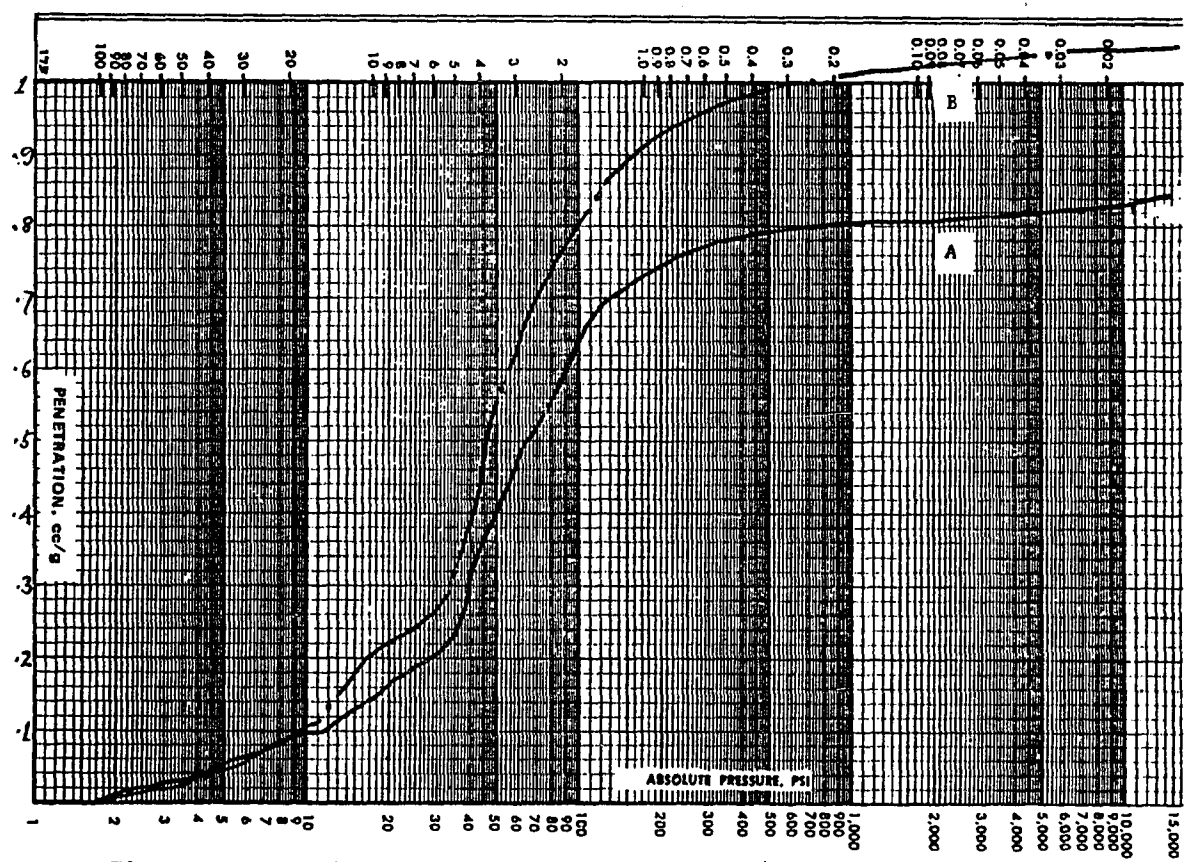

Figure 23. Porosimeter data of UNDM PSOC-265 (A), and DM PSOC-265 (B).

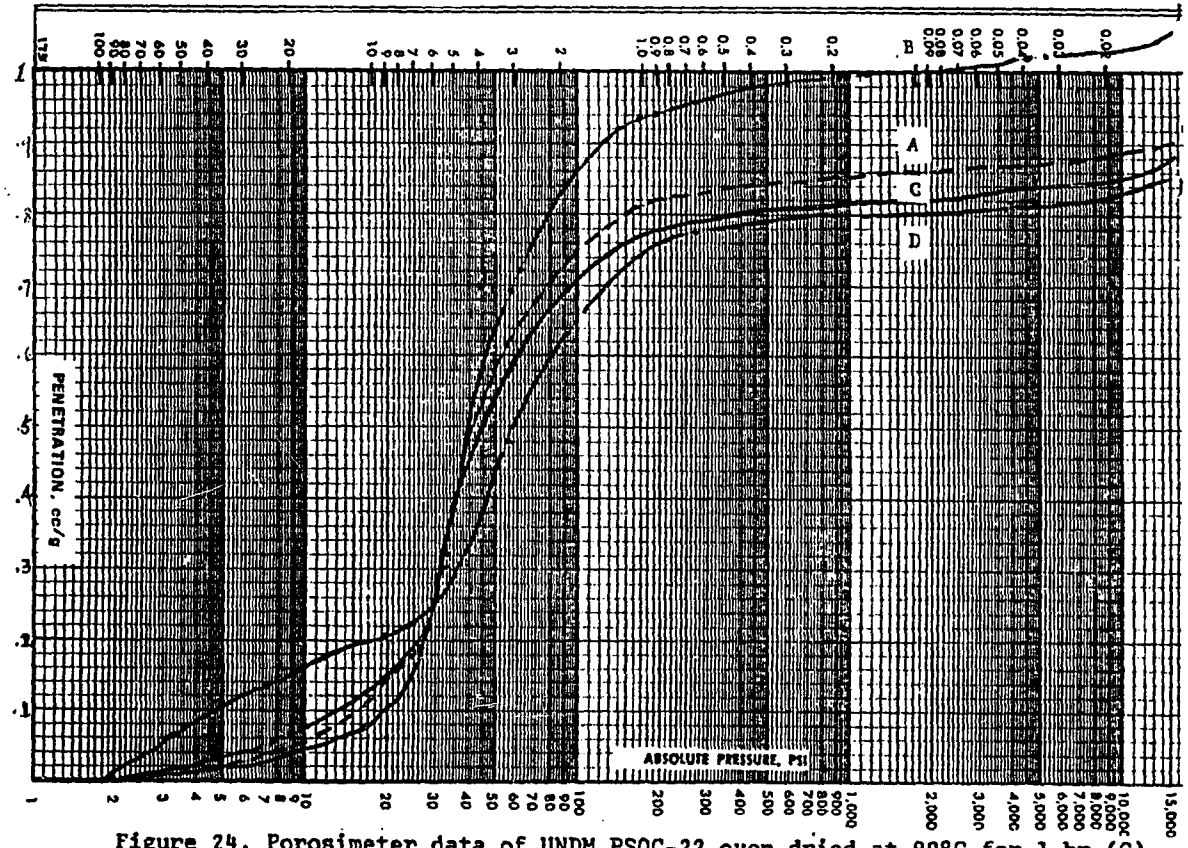

Figure 24. Porosimeter data of UNDM PSOC-22 oven dried at 90°C for 1 hr (C), at 105°C for 1 hr (A), UNDM PSOC-22-900-1 (D), and DM PSOC-22 (B).

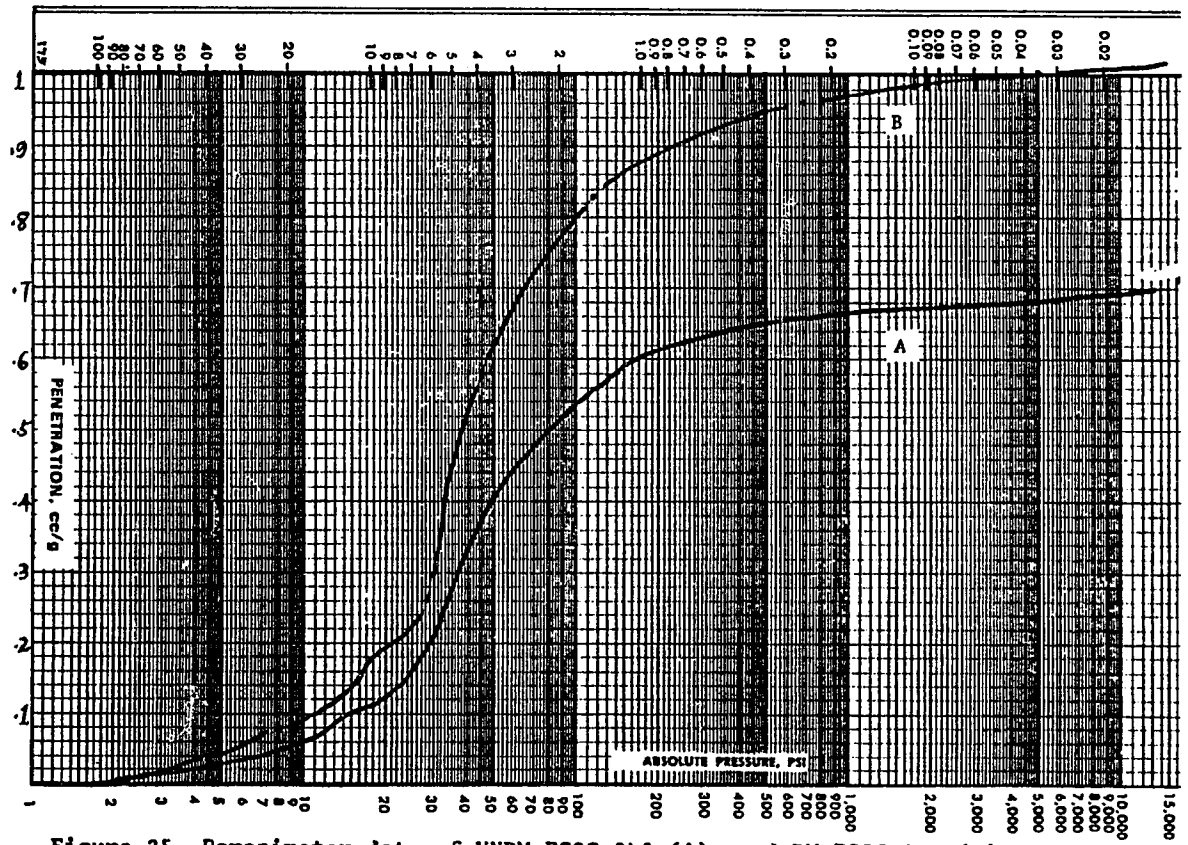

Figure 25. Porosimeter data of UNDM PSOC-246 (A), and DM PSOC-246 (B).

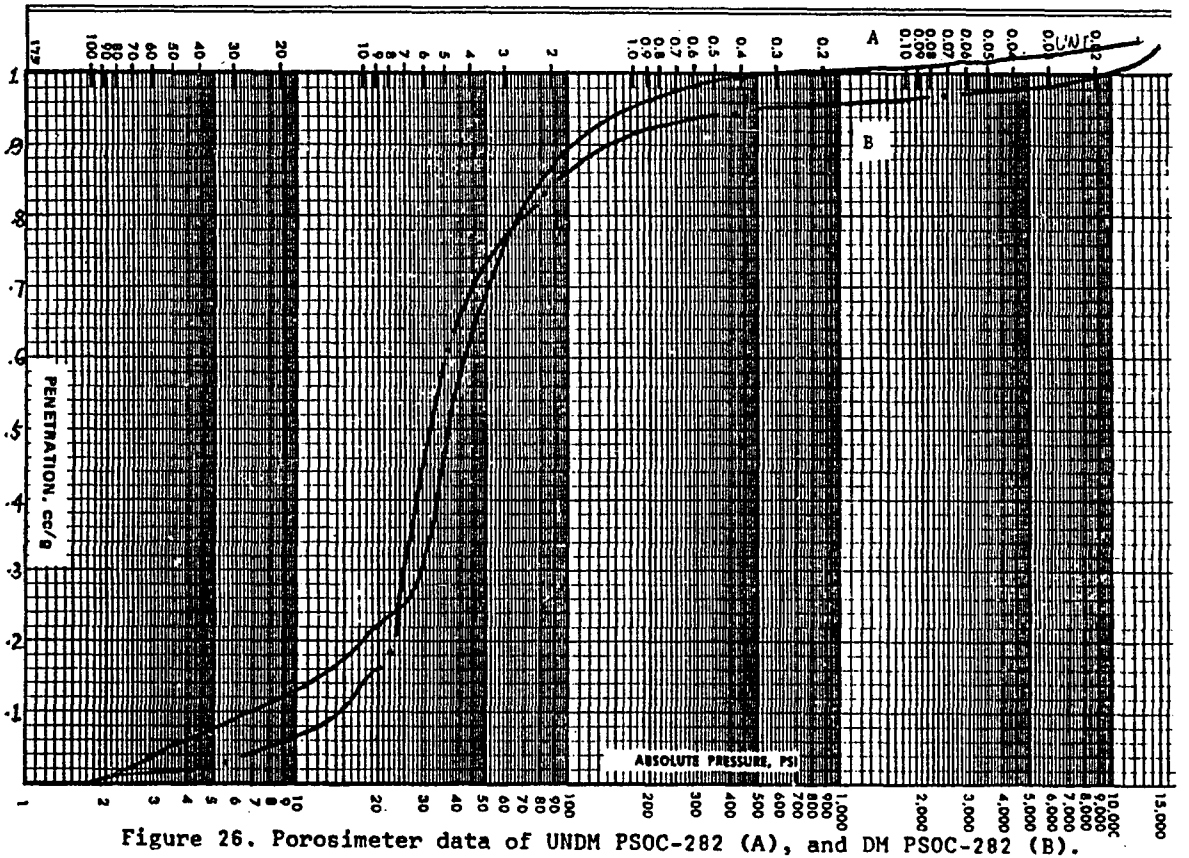

Figure 26. Porosimeter data of UNDM PSOC-282 (A), and DM PSOC-282 (B).

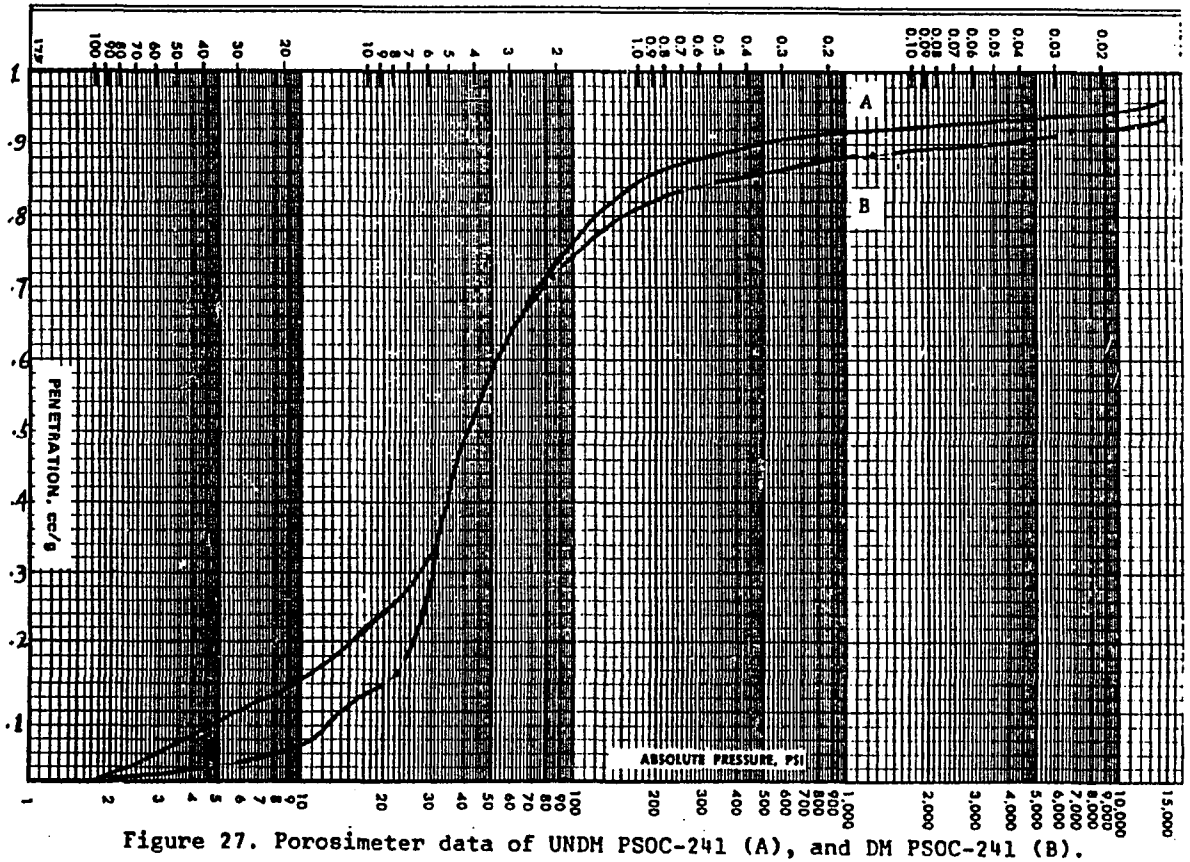

Figure 27. Porosimeter data of UNDM PSOC-241 (A), and DM PSOC-241 (B).

These indicate that, after demineralization process, the change on the pore structure of coal depends on the original coal type. Because we do not have enough information about the physical and chemical state of the mineral matter of the original coals, it is difficult to explain whether this result is due to the effect of demineralization on the organic matrix or it is only due to the mineral matter removal.

It is of interest to know the variation of the pore structure of coals after pyrolysis. For this purpose, one char (UNDM PSOC-22-900-1) was prepared from an undemineralized bituminous coal (PSOC-22) heat treated at 900°C for one hour. Figure 24 shows the reduction in the total pore volume of this char and also the change in the macropore size distribution, as compared to the original coal.

4.1.3 X-ray Analysis

The similarity of the X-ray scattering curves for coal to those of microcrystalline graphite suggested the application of the standard methods for interpreting the X-ray patterns of coals.

The diffuseness of the X-ray pattern of coals has been attributed to particles in which the arrangement of carbon atoms is that of graphite, but with extremely small size of elemental crystallites. An explanation, accepted even today,

is that coal possesses a "turbostratic structure" (Figure 28) which means that coal contains stacked aromatic layers which are roughly parallel and equidistant, but with each layer having a completely random orientation in the plane and about the plane normals.

This interpretation is based on the assumption that coal is an amorphous substance with high aromaticity. The ordering of carbon atoms in the aromatic rings and the parallel packing of these ring systems determine the X-ray scattering curve at medium and large angles, and the aromatic systems are associated with the absorption maxima indexed as (10) and (11), whereas the parallel ordering of the aromatic layers is associated with the (00ℓ) reflections of which the most intense is (002).

The crystalline dimensions revealed by X-ray diffraction of chars produced from low rank American coals (non-caking bituminous and sub-bituminous) have been studied by Inouye et al. [24] Their samples were prepared under similar process conditions as ours, and the lattice parameters ((10), (002)) calculated from the X-ray data did not show any substantial changes or trends for crystallite growth for all the samples examed as indicated in the Figure 29. They concluded that the properties of chars are mostly influenced by factors such as the state of the agglomeration of crystallites and possibly three dimensional networks developed in chars carbonized at

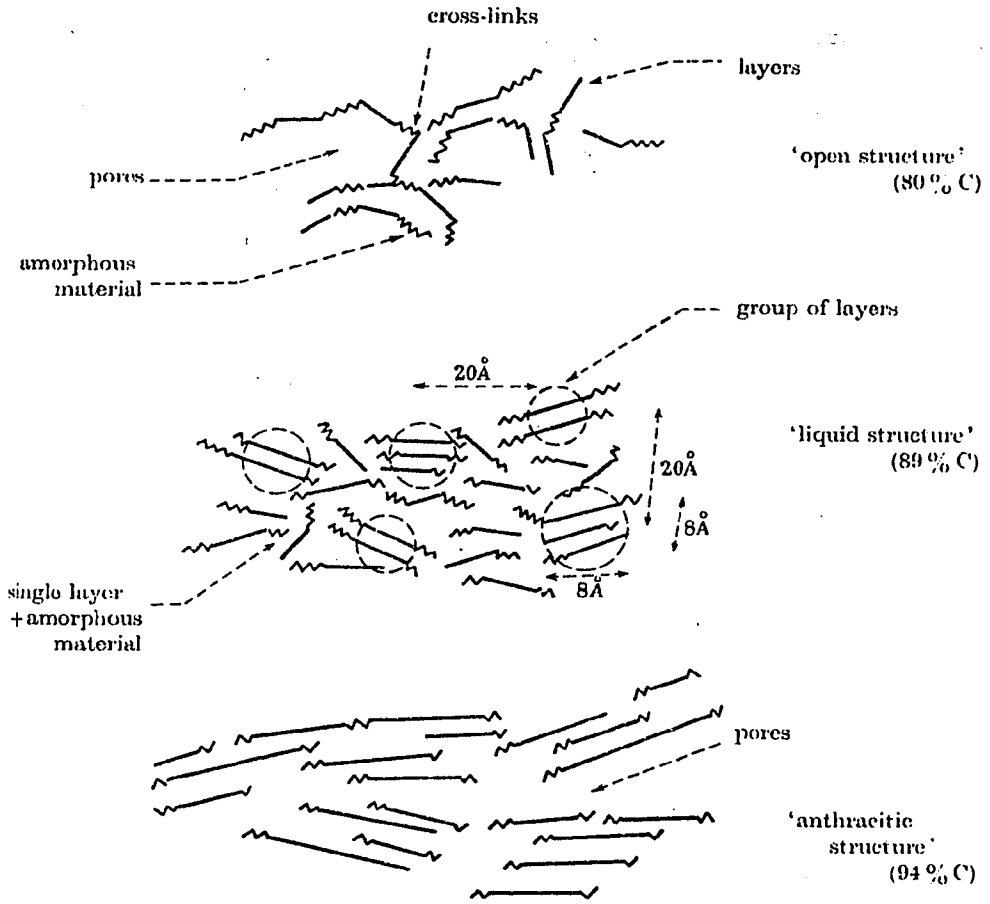

Figure 28. Turbostratic structure of coals as proposed by Hirsch's X-ray study.(23)

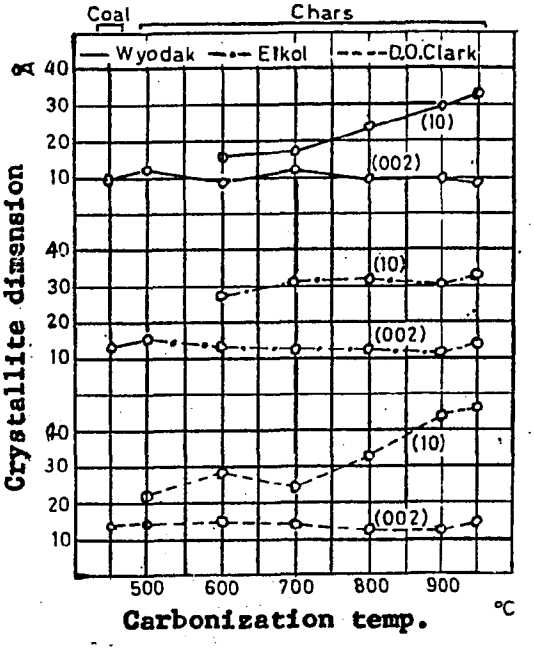

Figure 29. Inouye's X-ray study on low rank American coals with estimated crystallite dimensions plotted against carbonization temperature.

temperatures higher than 800°C.

Here, we wish to emphasize the difficulties involved in correlating physical properties of low rank coal chars with X-ray structural information. Graphite-like structure is not necessarily the end product for low rank coals at the pyrolysis temperatures used in our work.

Summary of X-ray Observation

X-ray diffraction data on our samples is summarized in Table 5. It shows that: (1) All the original coals possess the (002), (10) peaks, and at least one of the (110), or the (114) peak, except for PSOC-282 which has no (10) peak. (2) All demineralized (DM) coals possess (10), (110) and (114) peaks, and these peaks remain after heat treatment at 900°C for one hour.

Heat Treatment Effect on the Coals As-received

Our X-ray data showed the presence of the (002) peak in all the coals in the as-received state. On pyrolysis, this peak increased in intensity. The intensity of the peak increased both with increasing pyrolysis temperature and increasing soak time.

Effect of Acid Treatment on Coals

We observed that when coals were treated with HCl, the

Table 5. Summary of X-ray Analysis of Coal/Char Samples.

Sample No.		2θ°		(002)			(10)		(110)		(114)			
		21	25	26.5	32	38	44	65	77	82	98	112	116	137
PSOC-265	Parent	†	†	†		†	†	†	†		†			
	500°C/1hr	x		x							x			
	DM					Δ	Δ	Δ	Δ	Δ	Δ	Δ	Δ	Δ
	900°C/24hr			*			*		*		*		*	
PSOC-282	Parent			†							†		†	
	DM						Δ	Δ	Δ		Δ		Δ	
PSOC-22	Parent	†		†			†	†	†		†	†	†	
	900°C/1hr	x		x	x		x							
	DM					Δ	Δ	Δ	Δ	Δ	Δ	Δ	Δ	
	900°C/1hr					*	*	*	*		*		*	
PSOC-241	Parent			†		†	†	†	†	†	†	†	†	†
	DM					Δ	Δ	Δ	Δ	Δ	Δ	Δ	Δ	Δ
	500°C/01hr						*		*		*		*	
PSOC-246	Parent			†			†	†	†		†	†	†	
	900°C/1hr	x		x	x		x		x		x		x	
	DM					Δ	Δ	Δ	Δ			Δ	Δ	
	900°C/1hr						*		*		*		*	

intensity of the (002) peak increased. After treatment with hydrofluoric acid, the X-ray reflection indexed as (002) in the original coals was no longer present. This may be explained by the expansion of the unit cell by the intercalation of fluoride ions between layers of the aromatic units or other structures originally giving the (002) reflection. The retention of the high angle lines and the appearance of a new peak argues for structural rearrangement. Chemical analysis did detect small ammount of fluorine remaining in demineralized coals even after carefully washing the HF treated samples to apparant acid neutrality.

Heat Treatment Effect on Demineralized Coals

X-ray evidence shows that the (002) peak is still missing after pyrolyzing the demineralized coals at 500°C for one hour. For one char sample (DM PSOC-265-900-24), which was prepared from a demineralized bituminous coal (PSOC-265) heat treated at 900°C for 24 hours, the (002) peak was again observed. But the intensity of this peak is not as strong as in the original coal. We believe this shows that the weakly bonded fluoride was driven off and the (002) reflection was recovered during the thermal annealing of the remaining char structure.

4.2 The Heat Capacity of Coal Chars

4.2.1 Verification of Experimental Technique

Heat capacities of the addenda with or without sample were run several times to check the reproducibility of the measuring technique. Figure 18 in Section 3.2.3 shows the graphically smoothed heat capacity curve of the addenda, which was used to check the reproducibility and the subsequent analysis for the coal/char heat capacity.

In order to check the validity of our experimental techniques and data reduction schemes, we measured the heat capacity of a standard copper sample (of purity 99.99%). The results are consistent within 1% as compared with the published standards.[25] This, by itself, is not quite an adequate test, because of the order of magnitude difference both in the thermal conductivity and heat capacity between a char and a metal. But after we were satisfied that our technique was adequate and reproducible, we measured the heat capacity of a standard reference graphite (POCO AXM-5Q-1). This sample was supplied by Dr. Jerome Hust of the National Bureau of Standards' Boulder Laboratories. Data for this graphite was further analyzed to justify the reproducibility amongst different runs. Table 6 gives the measured data of three separate runs. Also indicated in the same table are the deviations of each measured point from the value calculated by the least-square fitting equation. The

Table 6. Analysis of POCO-graphite Heat Capacity Data

Run No.	T(K)	C_{meas}(Joule/gm,K)	C_{calc}(Joule/gm,K)	Dev=C_{calc}-C_{meas}	% Dev.
1	82.80	0.1172	0.1189	0.0017	1.4
	89.96	0.1558	0.1339	-0.0219	16.6
	95.38	0.1473	0.1395	-0.0078	5.6
	111.24	0.1802	0.1834	0.0032	1.8
	118.31	0.2016	0.2016	0	0
	188.02	0.4600	0.4279	-0.0321	7.5
	221.25	0.5498	0.5687	0.0189	3.3
	228.75	0.5593	0.6036	0.0043	0.7
	235.04	0.6183	0.6338	0.0155	2.4
	271.08	0.8175	0.8235	-0.0213	2.6
2	116.14	0.1829	0.1959	0.013	6.6
	125.52	0.2227	0.2209	-0.0018	0.8

Table 6. (conti.)

	133.89	0.2395	0.2445	0.005	2.1
	142.70	0.2654	0.2707	0.0053	2.0
	152.06	0.2880	0.3000	0.0120	4.0
	160.45	0.3077	0.3277	0.02	6.1
	168.02	0.3640	0.3538	-0.0102	2.9
	175.24	0.3696	0.3797	0.0101	2.6
	181.50	0.4232	0.4044	-0.0188	4.6
	188.81	0.4053	0.4310	0.0297	6.0
3	172.88	0.3500	0.3711	0.0211	5.7
	180.78	0.4192	0.4002	-0.0190	4.8
	187.52	0.4492	0.4318	-0.0174	4.0
	194.25	0.4594	0.4526	-0.0068	1.5
	209.14	0.5015	0.5148	0.0133	2.6
	215.71	0.5730	0.5436	-0.0294	5.4
	232.12	0.6387	0.6197	-0.0190	3.1
	238.36	0.6587	0.6501	-0.0086	1.3

Table 6. (conti.)

245.67	0.6703	0.6868	0.0165	2.4
260.80	0.7600	0.7664	0.0064	0.8
269.05	0.8342	0.8120	-0.0222	2.7
274.1	0.8180	0.8407	0.0227	2.7
279.56	0.8751	0.8724	-0.0027	0.3
285.04	0.8899	0.9048	0.0149	1.7
289.42	0.9554	0.9313	-0.0241	2.6

average deviation was found to be 3.6%. This is consistent with the estimation of the total error for the coal char heat capacity measurement as explained in section 3.2.5. Figure 30 shows the scattering of all the data points around the fitting curve. The approximately 10% difference in the heat capacity of this sample as compared with that of the natural graphite was observed. This is believed to be contributed by the residual heat capacity of this synthetic graphite as compared with that of the crystalline natural graphite. The same order of magnitude difference in the heat capacity of a synthetic CS graphite as compared with that of a natural ceylon graphite was also observed by De Sorbo[26] over the temperature range 120 to 300 °K.

4.2.2 The Heat Capacity Data

The heat capacity data are summarized in Table 7. About twenty data points can be generated for each separate run, over the whole temperature range. The data are reported on the experimental per gram dry basis (C_g^s). Data are also plotted in Figures 31 to 46 in the same units. Data have been least-square curve fitted by the appropriate equations as shown in Table 14 in the Appendix.

4.2.3 The Heat Capacity of Coals

Figure 31 shows heat capacity data for the Virginia

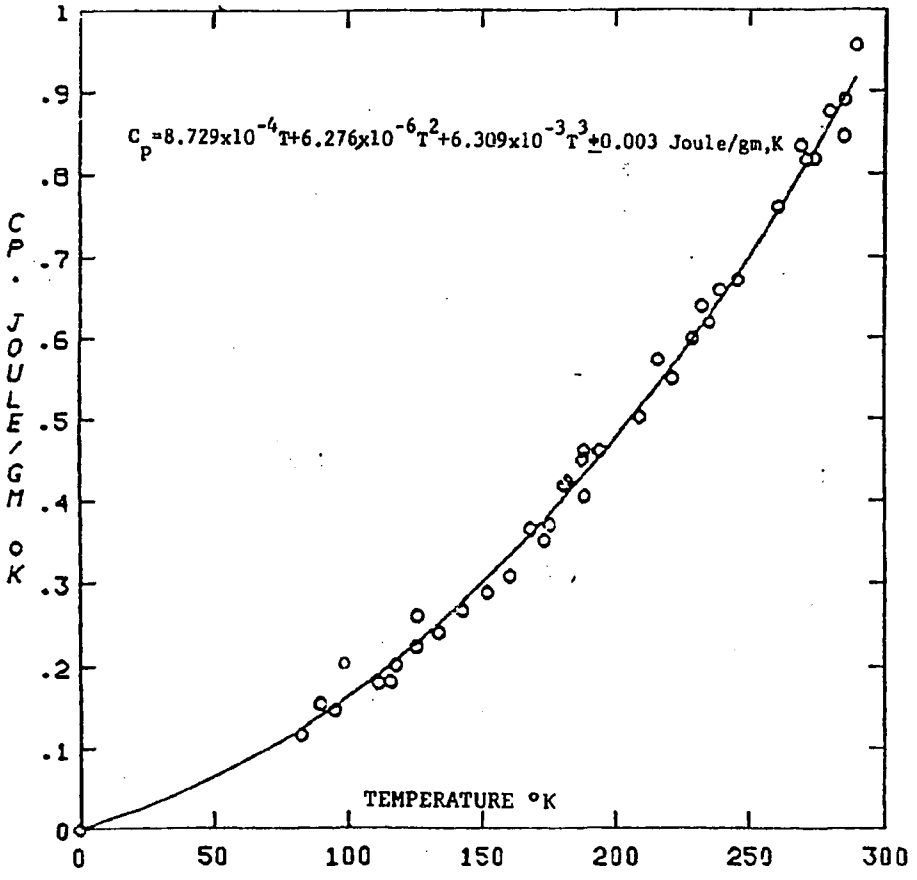

Figure 30. Heat Capacity of POCO-graphite.

Table 7. Heat Capacity Data of Coal/Char Samples.

UNDM PSOC-265

T(°K)	C_p(Joule/gm,°K)	T	C_p
93.96	0.096	203.08	0.181
100.64	0.112	212.32	0.182
117.9	0.103	240.68	0.219
146.22	0.117	252.15	0.243
161.9	0.122	262.75	0.223
192.57	0.179		

DM PSOC-265

91.9	0.253	185.8	0.37
106.48	0.264	201.43	0.399
117.3	0.295	224.98	0.411
135.35	0.347	234.6	0.432
145.06	0.337	242.82	0.478
160.33	0.333	251.38	0.456
166.46	0.368		

Table 7. (conti.)

UNDM PSOC-265-700-1

T(°K)	C_p(Joule/gm,°K)	T	C_p
93.97	0.11	180.84	0.15
117.52	0.09	188.42	0.151
125.95	0.117	195.7	0.154
133.76	0.11	222.8	0.185
140.62	0.131	235.6	0.164
162.24	0.135	280.2	0.245

DM PSOC-265-700-1

106.1	0.086	168.82	0.139
114.2	0.084	176	0.13
128.01	0.1	201.65	0.132
152.4	0.095	213.12	0.136
160.96	0.113	263	0.136

DM PSOC-265-1100-0.1

92.72	0.222	201.89	0.381
108.28	0.207	213.36	0.416
116.1	0.216	224.14	0.419
122.96	0.215	233.85	0.412
129.2	0.259	255.32	0.532
149.84	0.23	263.92	0.526
159.74	0.271	270.85	0.562
169.02	0.282		

Table 7. (conti.)

DM PSOC-265-1100-1

T(°K)	C_p (Joule/gm,°K)	T	C_p
88.93	0.145	170.22	0.221
94.76	0.145	180.55	0.234
120.5	0.146	228.81	0.27
130.2	0.172	238.2	0.316
138.93	0.175	247.6	0.315
146.64	0.196	255.86	0.318
157.86	0.192	262.9	0.327

DM PSOC-265-1100-24

103.83	0.213	204.3	0.808
109.34	0.236	213.42	0.851
128.35	0.305	223.47	0.875
137.26	0.364	233.69	1.018
159.1	0.445	242.86	1.105
183.02	0.623	251.97	1.028
194.44	0.767	269.84	1.359

Table 7. (conti.)

UNDM PSOC-22

T(°K)	C_p(Joule/gm,°K)	T	C_p
88	1.832	179.7	1.222
101.1	1.711	188.7	1.18
109.6	1.422	197.8	1.082
126.7	1.246	215.5	1.018
140.8	1.246	225.8	1.029
154.8	1.268	235.4	1.14
162	1.402	258	1.276
170.7	1.32		

DM PSOC-22

110.15	0.252	196.8	0.569
116.12	0.266	221.84	0.687
142.3	0.355	233.65	0.677
149.9	0.393	258.8	0.838
169.84	0.499	270.68	0.844
188.6	0.57		

DM PSOC-22 (undried)*

94.4	0.806	198.85	0.85
118.3	0.823	222.62	0.953
125.3	0.828	231.18	1.201
148.8	0.885	238.4	1.382
191.2	0.833	256.6	1.596

* Sample contains 10.8 wt% of moisture before measurement.

Table 7. (conti.)

UNDM PSOC-22-700-1

T(°K)	C_p (Joule/gm,°K)	T	C_p
90.66	0.092	173.39	0.251
97.58	0.155	196.54	0.287
113.54	0.134	216.88	0.407
130.98	0.174	243.87	0.497
165.61	0.235		

DM PSOC-22-700-1

100.8	0.164	188.96	0.263
126.5	0.176	195.4	0.294
135.7	0.162	217.86	0.314
144.9	0.162	224.1	0.334
153.6	0.201	239.9	0.407
160.9	0.221	247.39	0.373
175.95	0.247	254.5	0.45
182.6	0.262	260.78	0.427

Table 7. (conti.)

DM PSOC-22-900-1

T(°K)	C_p (Joule/gm,°K)	T	C_p
95.7	0.178	154.75	0.279
105.41	0.219	164.94	0.341
113.84	0.236	174.78	0.337
121.06	0.238	245.2	0.404
127.39	0.276	251.62	0.43
133.42	0.278	256.62	0.466
142.9	0.28	263.9	0.471

DM PSOC-22-1100-1

82	0.136	175.14	0.276
108.6	0.181	206.9	0.299
118.16	0.173	237.25	0.354
128.4	0.195	252.1	0.372
148.6	0.237	260	0.376
158.3	0.237		

Table 7. (conti.)

UNDM PSOC-246

T(°K)	C_p (Joule/gm,°K)	T	C_p
86.3	0.496	183.68	1.266
108.2	0.669	194.54	1.337
115.3	0.702	226.78	1.448
123.12	0.814	234.21	1.564
131.95	0.955	243.16	1.682
140.52	0.91	263.32	1.603
148.16	1.052	271.07	1.772
171.9	1.129		

DM PSOC-246

101.08	0.29	187.35	0.789
115.32	0.304	200.8	0.78
132.87	0.476	237.75	0.851
141.1	0.523	248.14	0.939
148.64	0.511	257.28	1.117
170.51	0.67	265.11	1.14
179.93	0.737	272.66	1.152

Table 7. (conti.)

UNDM PSOC-246-700-1

T(°K)	C_p(Joule/gm,°K)	T	C_p
93.32	0.197	178.69	0.225
106.53	0.183	215.28	0.306
149.2	0.192	226.01	0.279
157.96	0.195	249.85	0.376
165.43	0.195	270.16	0.368
172.58	0.203		

DM PSOC-246-700-1

101.68	0.274	188.32	0.348
107.66	0.256	197.92	0.43
145.35	0.209	220.8	0.5
155.81	0.26	243.23	0.519
165	0.252	253.16	0.686

DM PSOC-246-1100-1

105.7	0.756	225.5	1.253
119.54	0.847	234.52	1.316
129.4	0.988	245.03	1.398
148.1	0.978	255.92	1.531
173.54	1.107	266.35	1.446
201.95	1.113	276.58	1.422
215.48	1.184	285.2	1.414

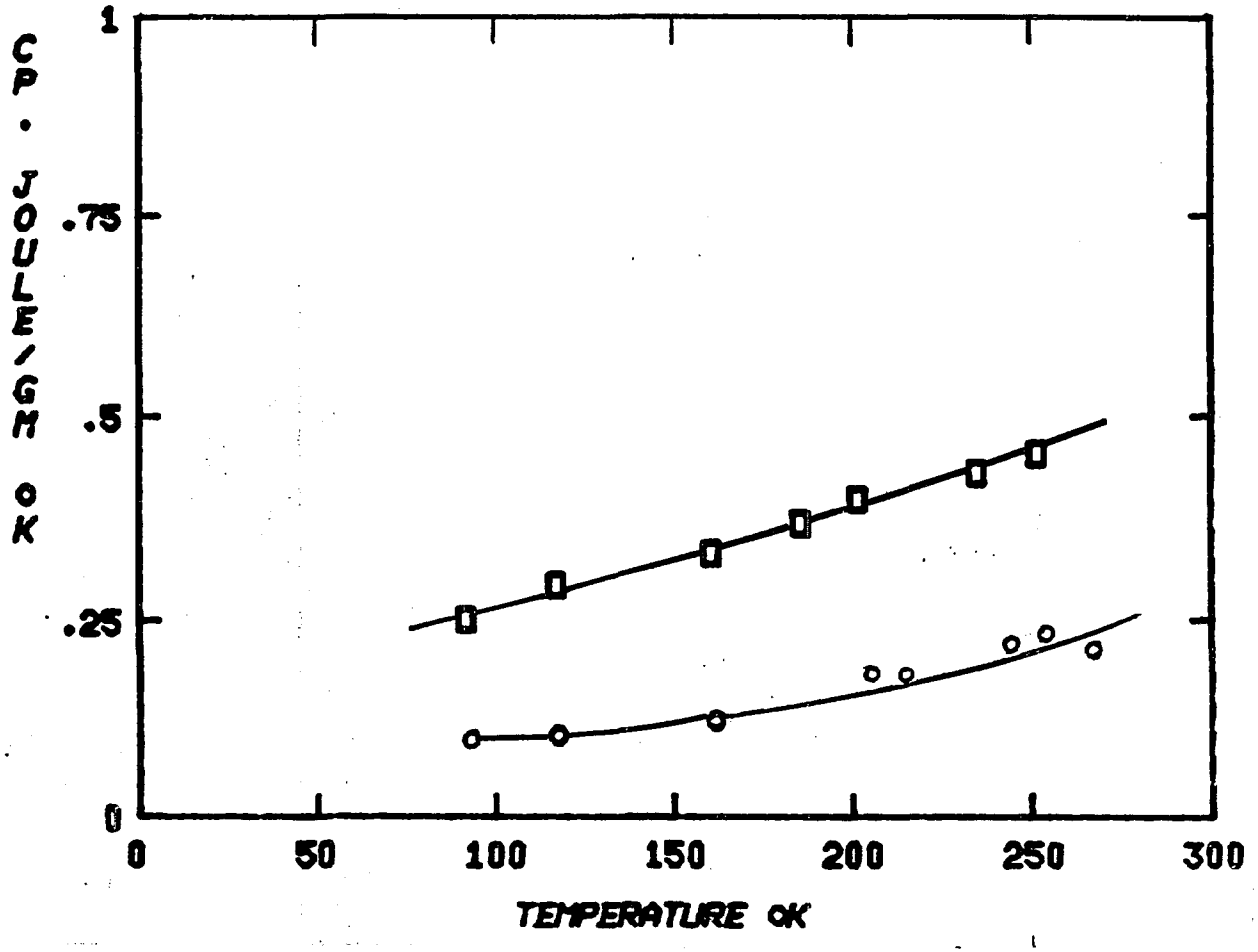

Figure 31. Heat capacities of UNDM PSOC-265 (o), and DM PSOC-265 (□).

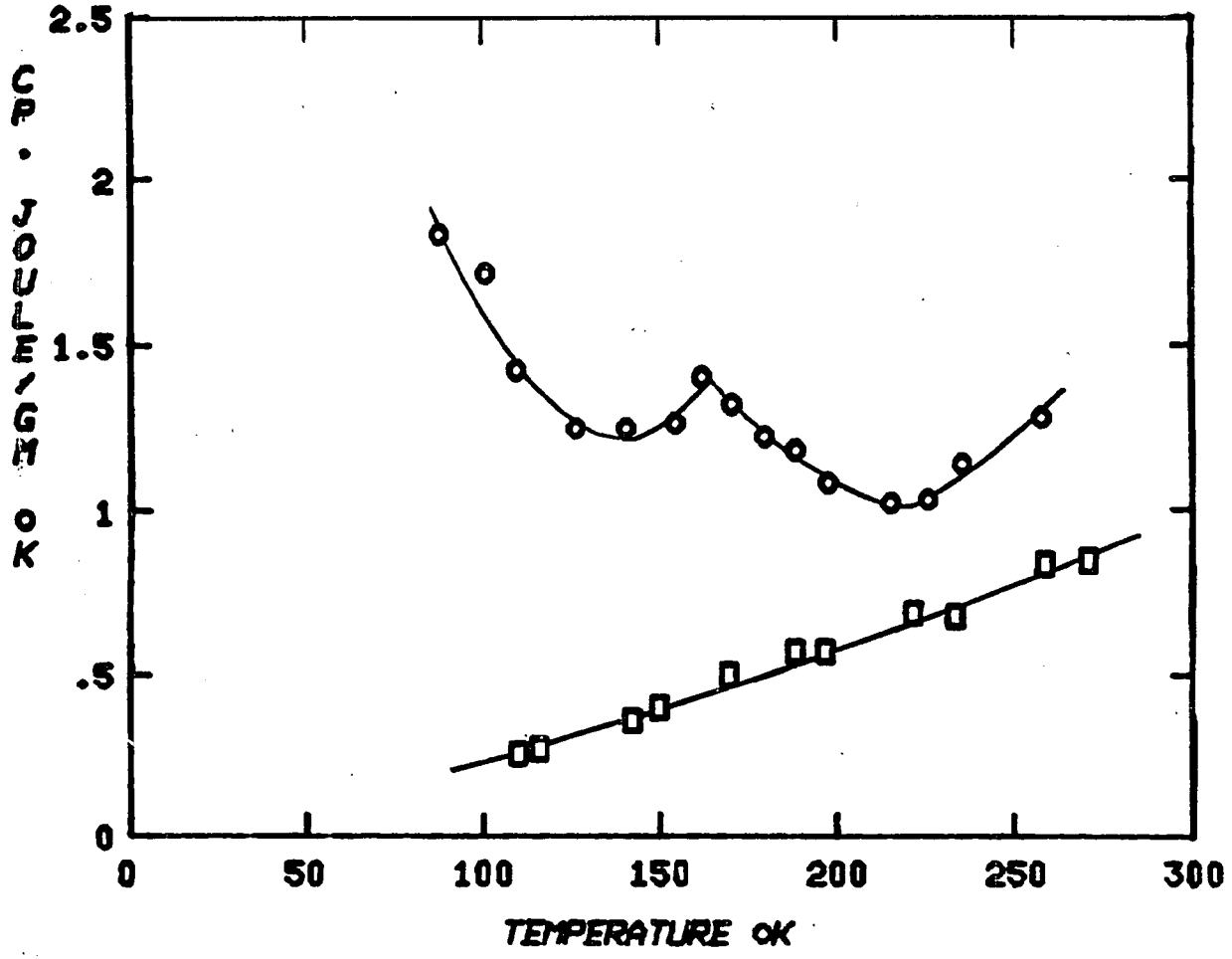

Figure 32. Heat capacities of UNDM PSOC-22 (O), and DM PSOC-22 (□).

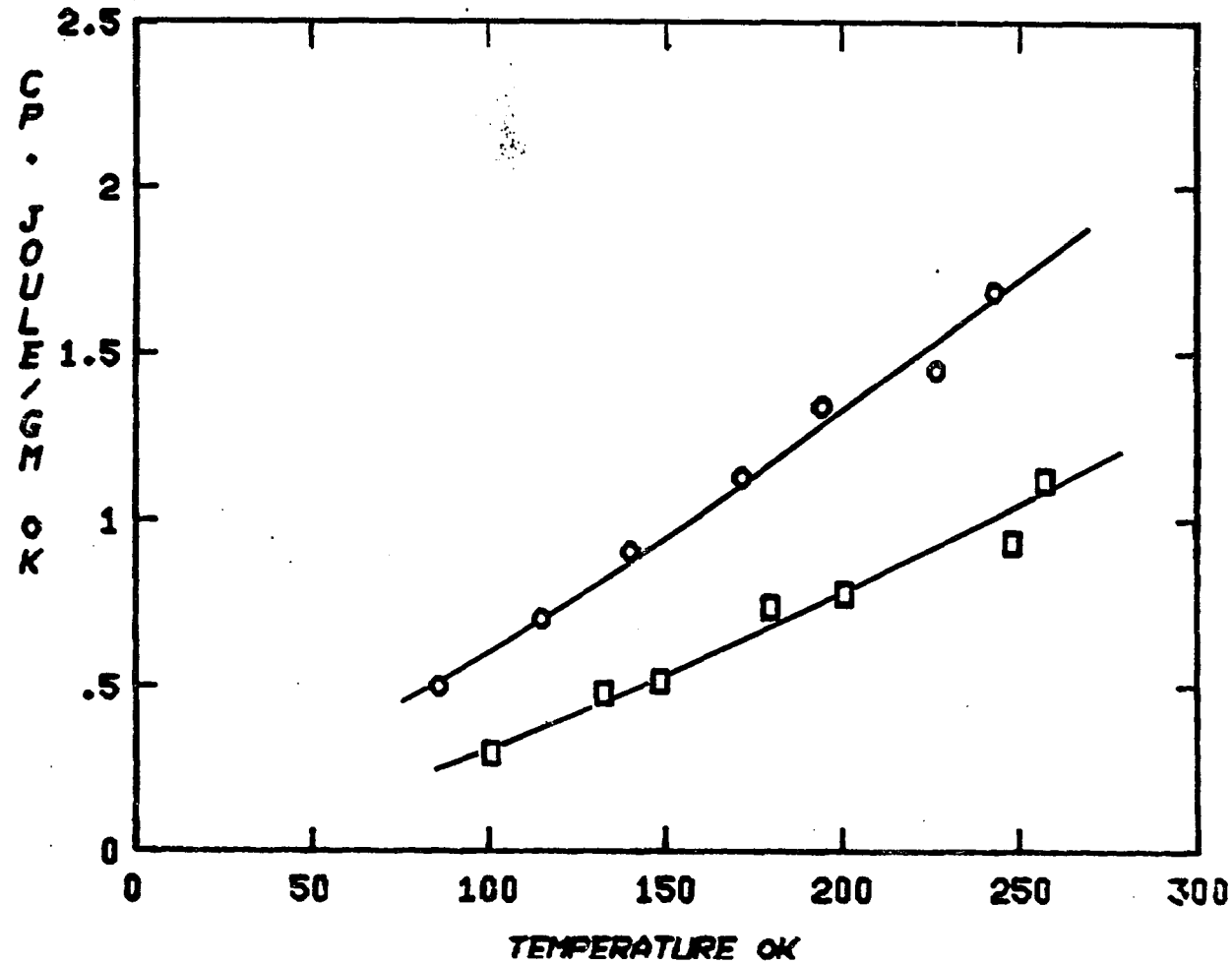

Figure 33. Heat capacities of UNDM PSOC-246 (o), and DM PSOC-246 (□).

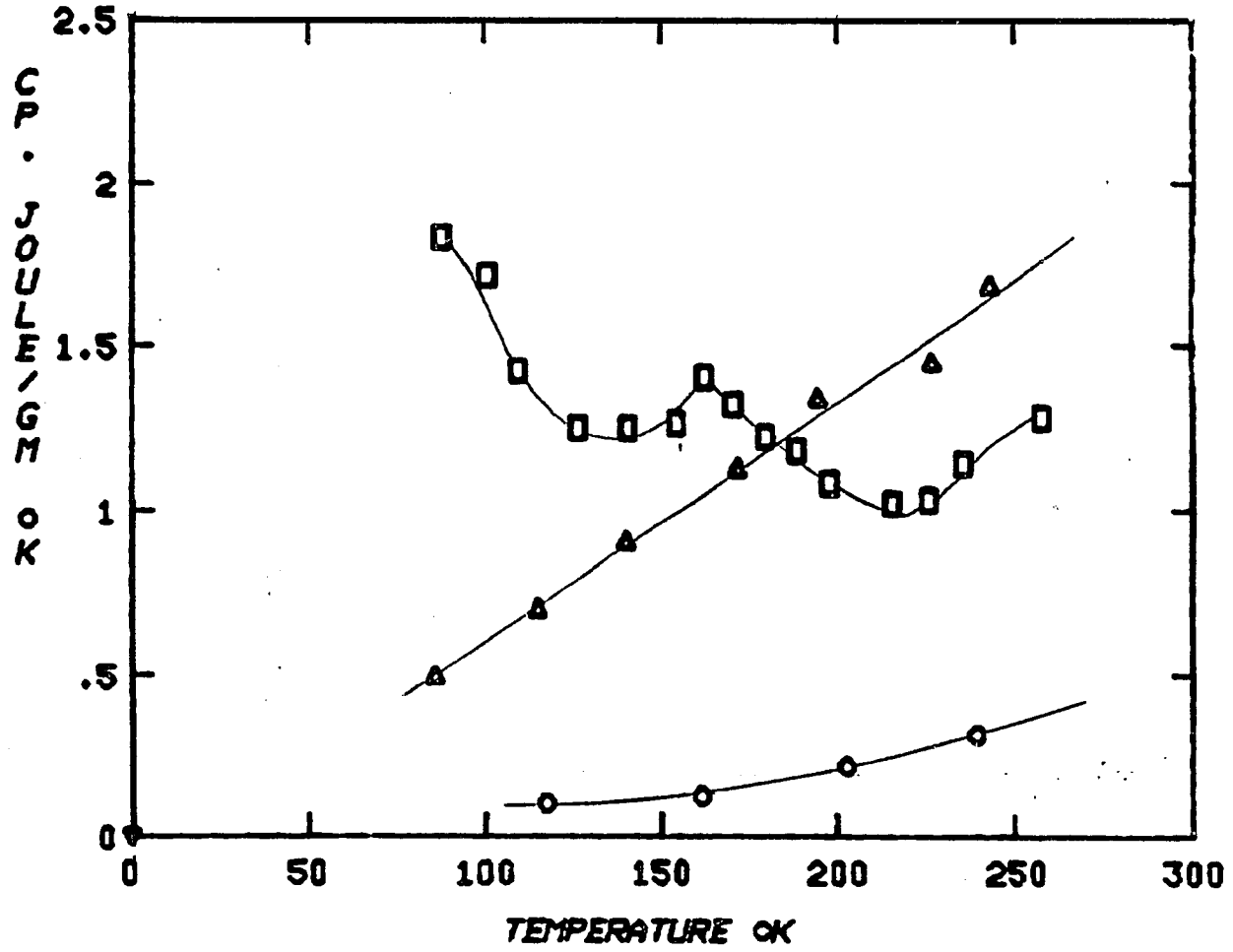

Figure 34. Heat capacities of UNDM PSOC-265(○), UNDM PSOC-22 (□), and UNDM PSOC-246 (△).

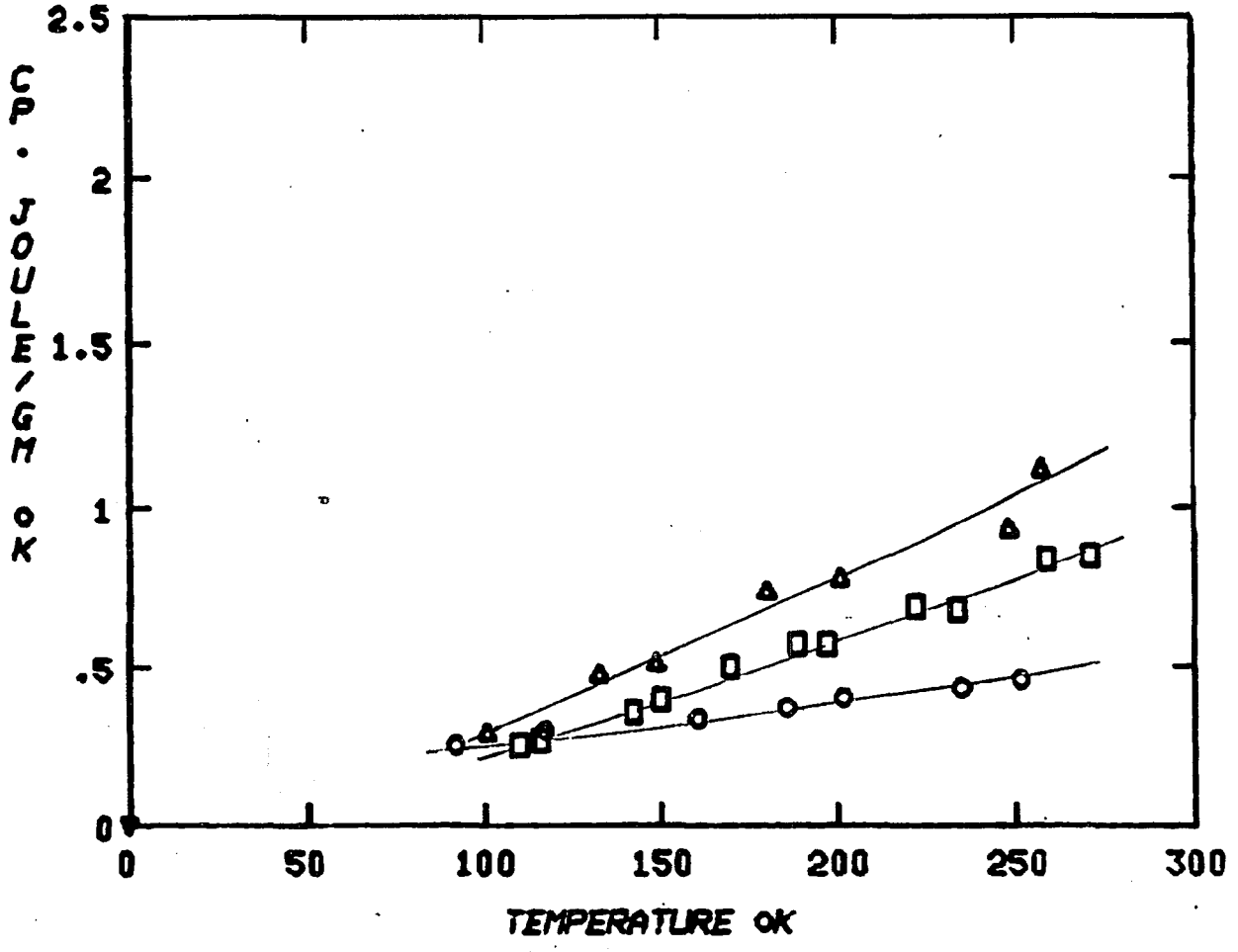

Figure 35. Heat capacities of DM PSOC-265 (o), DM PSOC-22 (□), and DM PSOC-246(Δ).

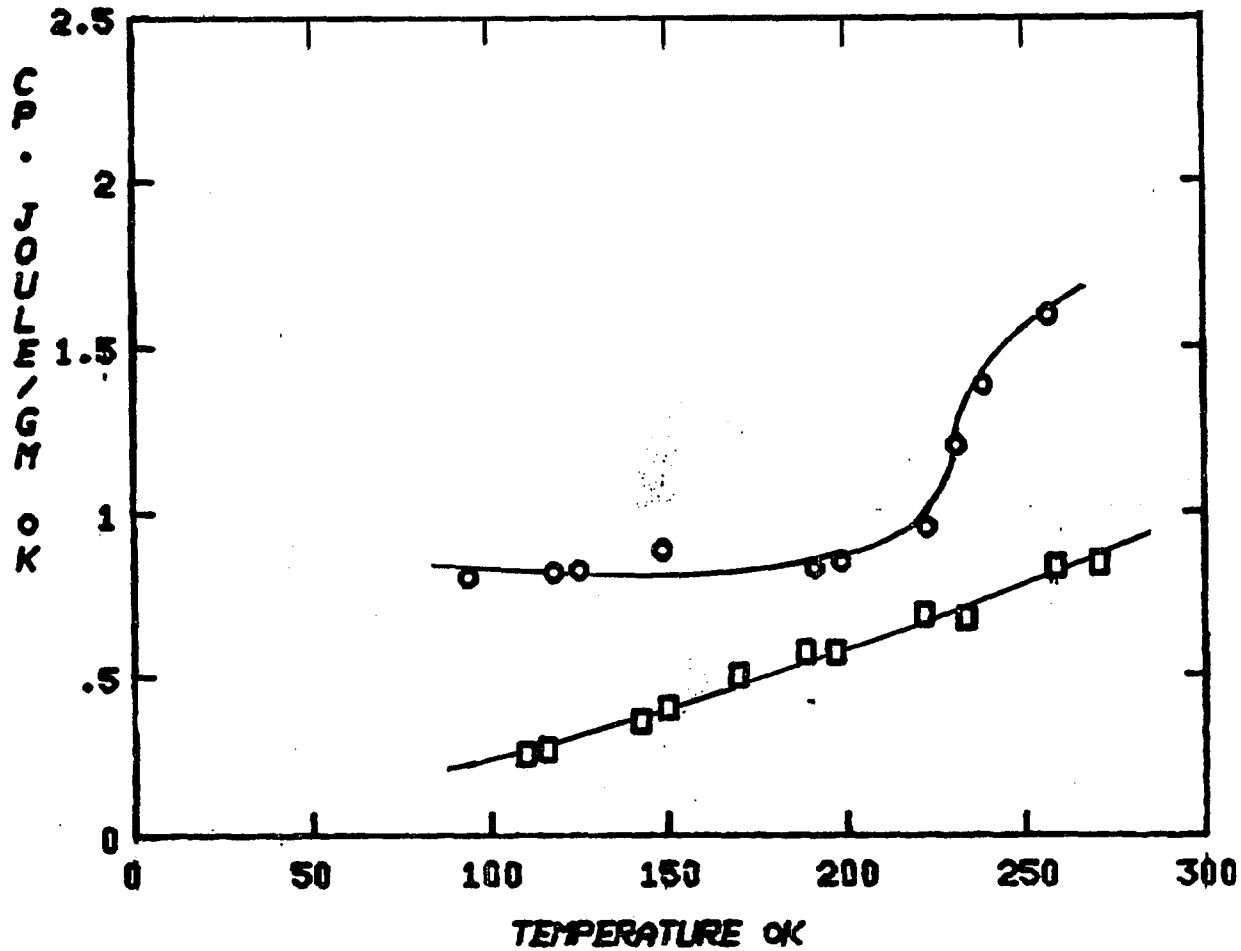

Figure 36. Heat capacities of DM PSOC-22 before vacuum dried (o), and after vacuum dried (□).

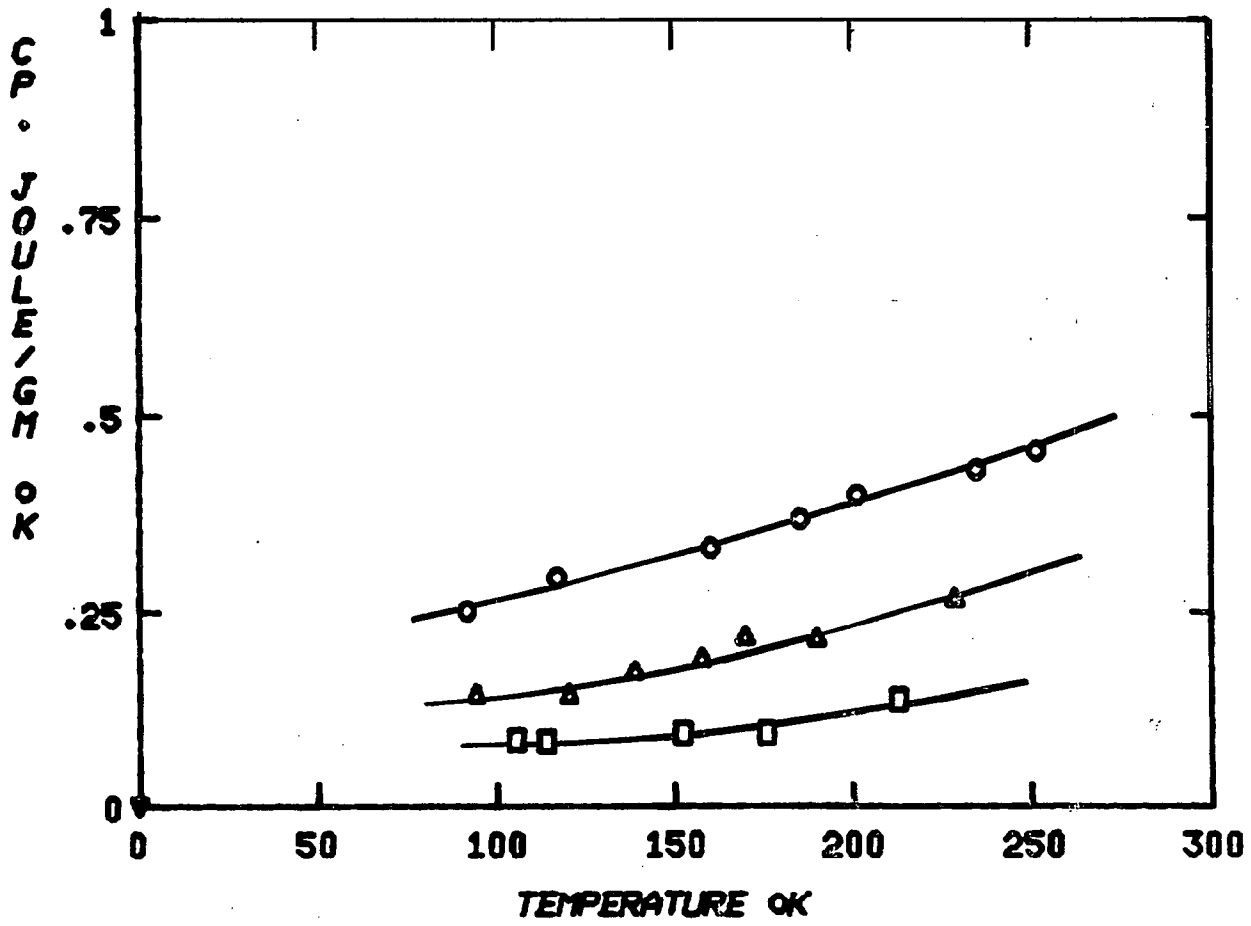

Figure 37. Heat capacities of DM PSOC-265 (o), DM PSOC-265-700-1 (□), and DM PSOC-265-1100-1 (Δ).

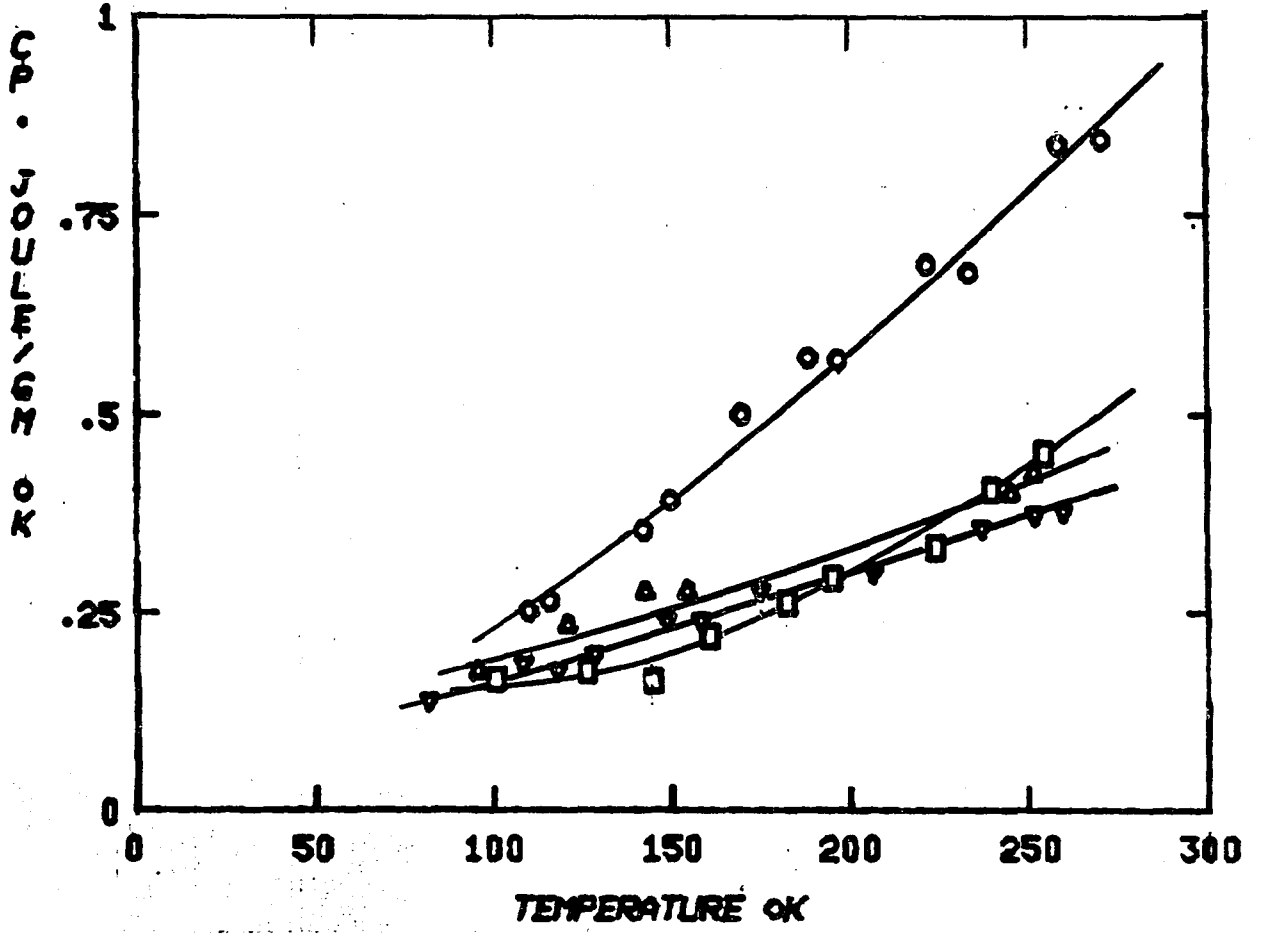

Figure 38. Heat capacities of DM PSOC-22 (o), DM PSOC-22-700-1 (□), DM PSOC-22-900-1 (Δ), and DM PSOC-22-1100-1 (▽).

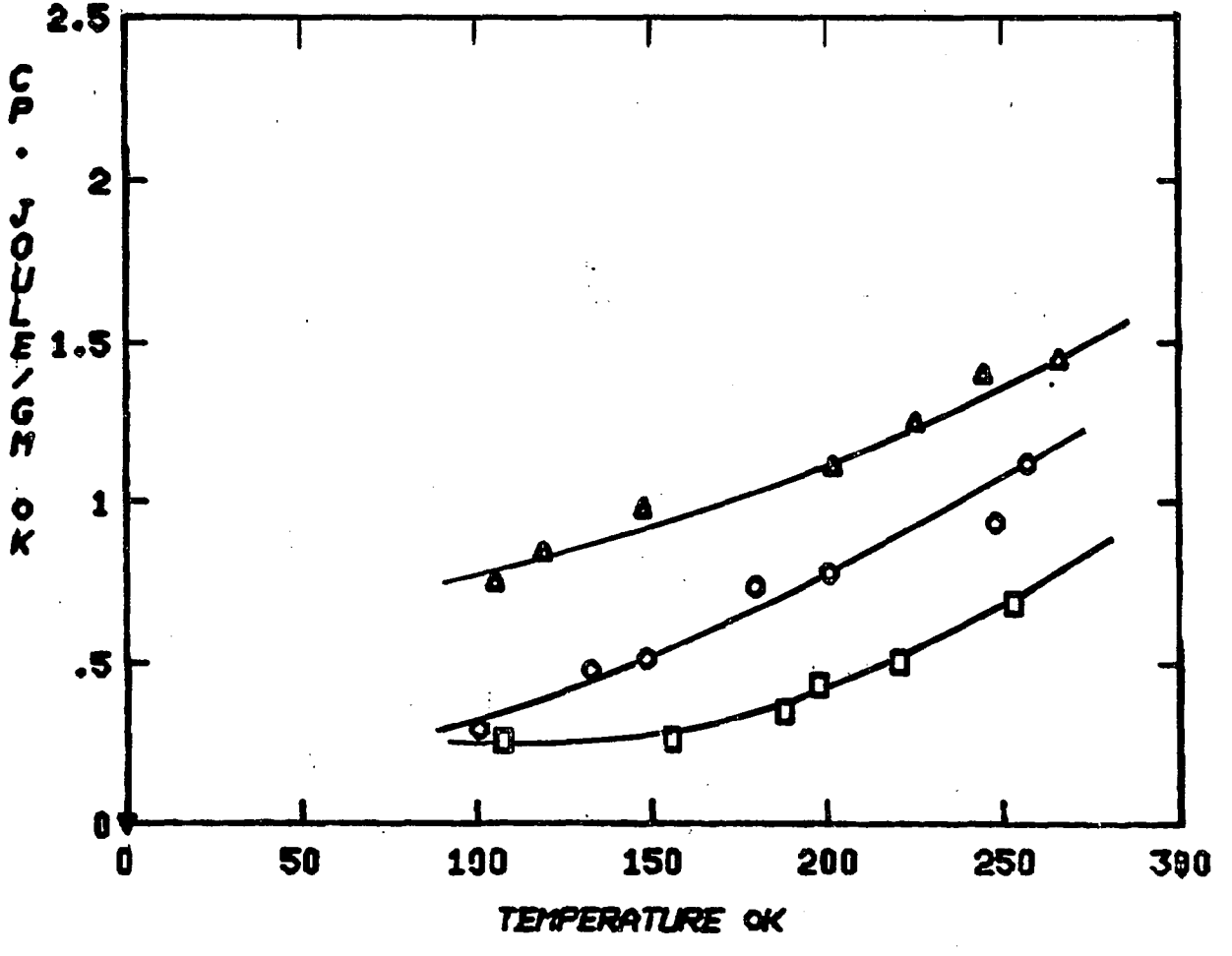

Figure 39. Heat capacities of DM PSOC-246 (o), DM PSOC-246-700-1 (□), and DM PSOC-246-1100-1 (Δ).

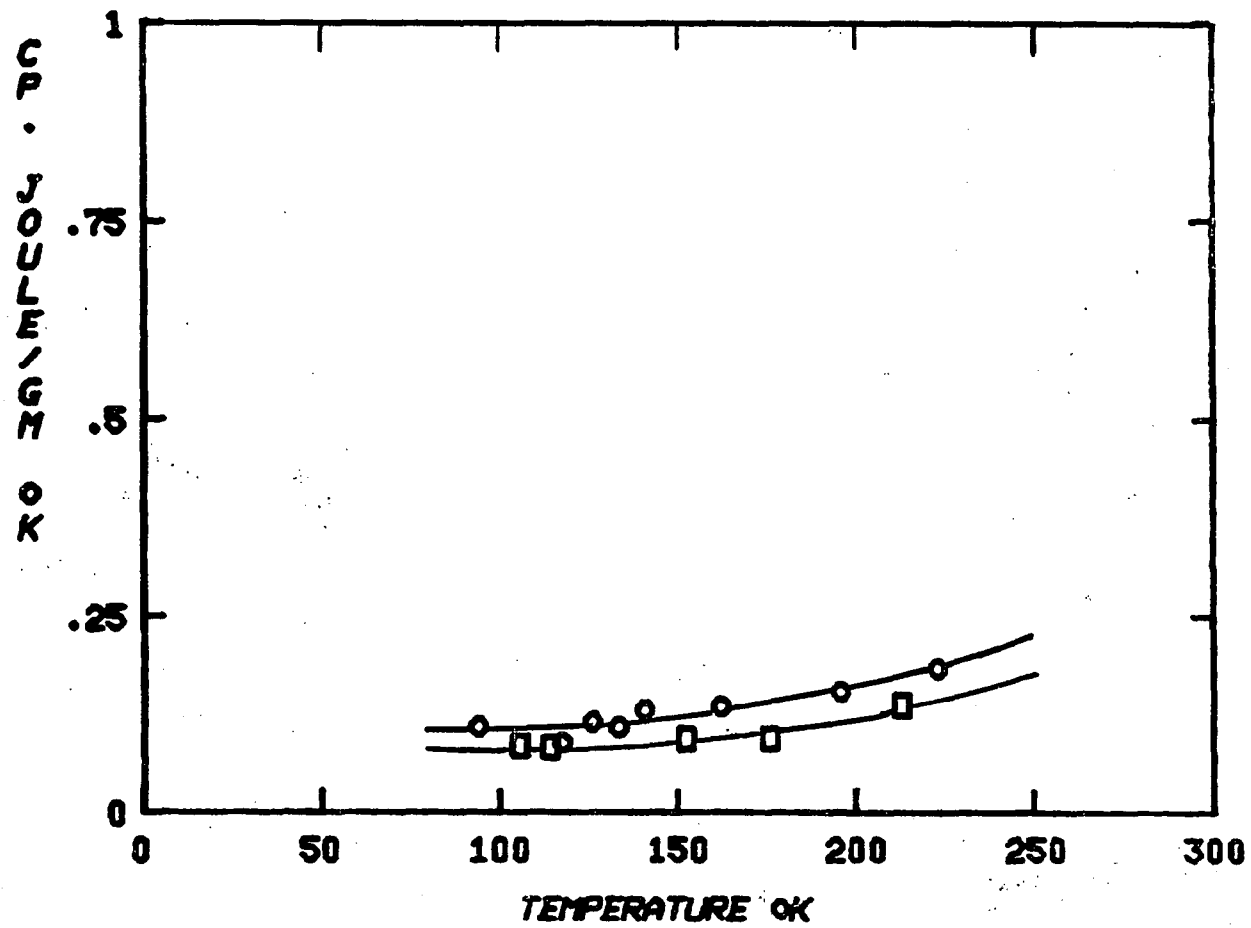

Figure 40. Heat capacities of UNDM PSOC-265-700-1 (o), and DM PSOC-265-700-1 (□).

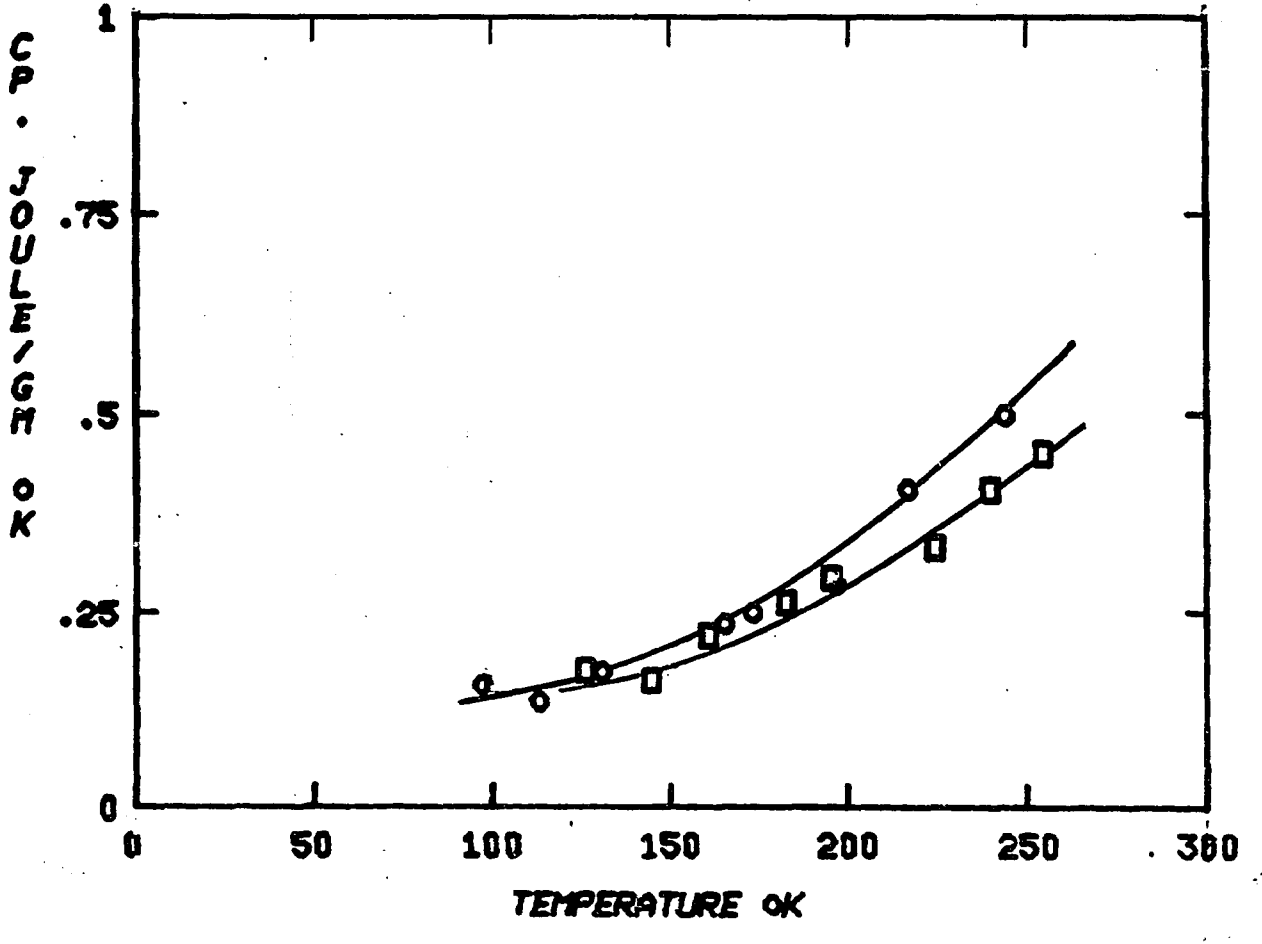

Figure 41. Heat capacities of UNDM PSOC-22-700-1 (○), and DM PSOC-22-700-1 (□).

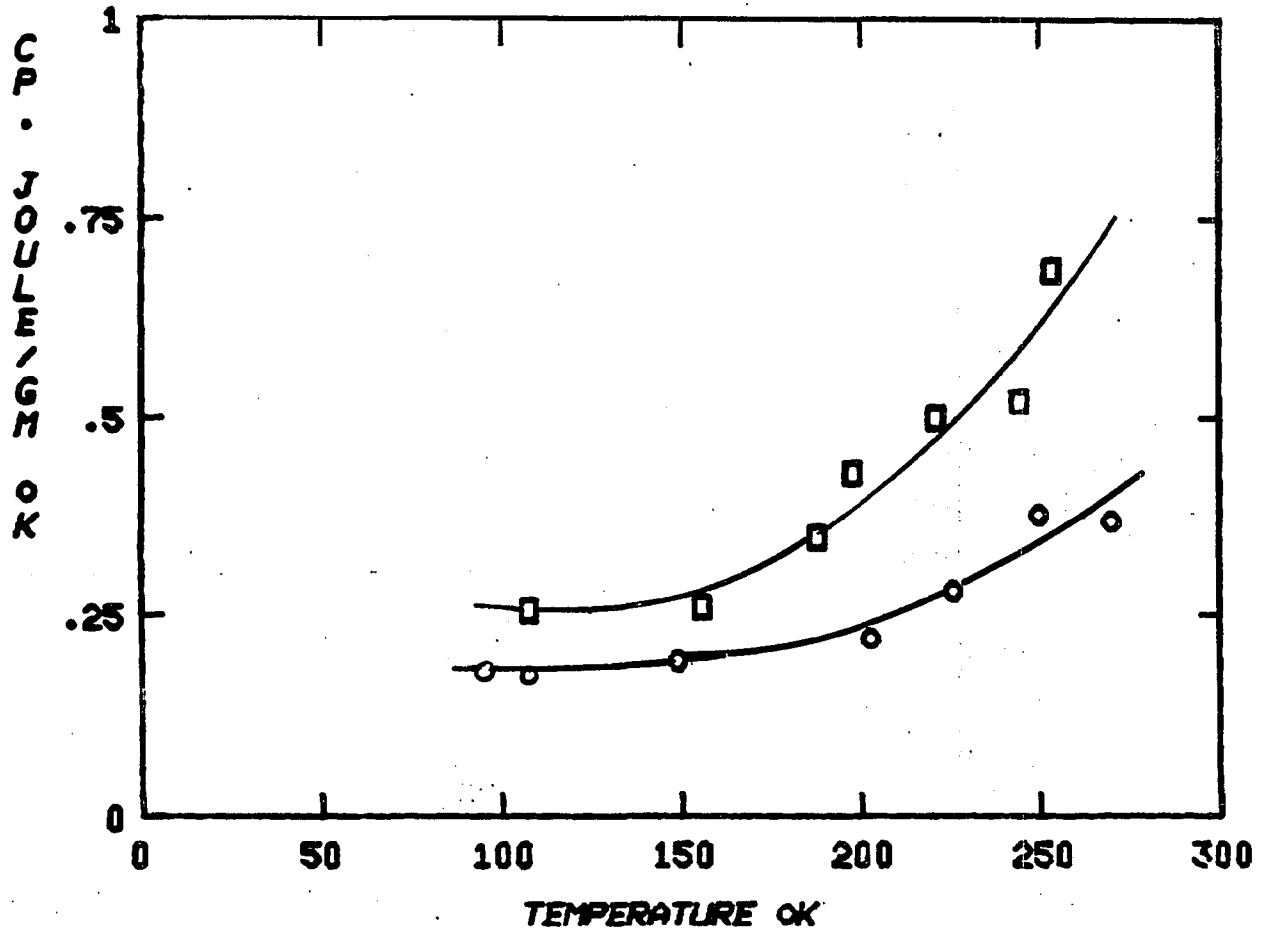

Figure 42. Heat capacities of UNDM PSOC-246-700-1(o), and DM PSOC-246-700-1(□).

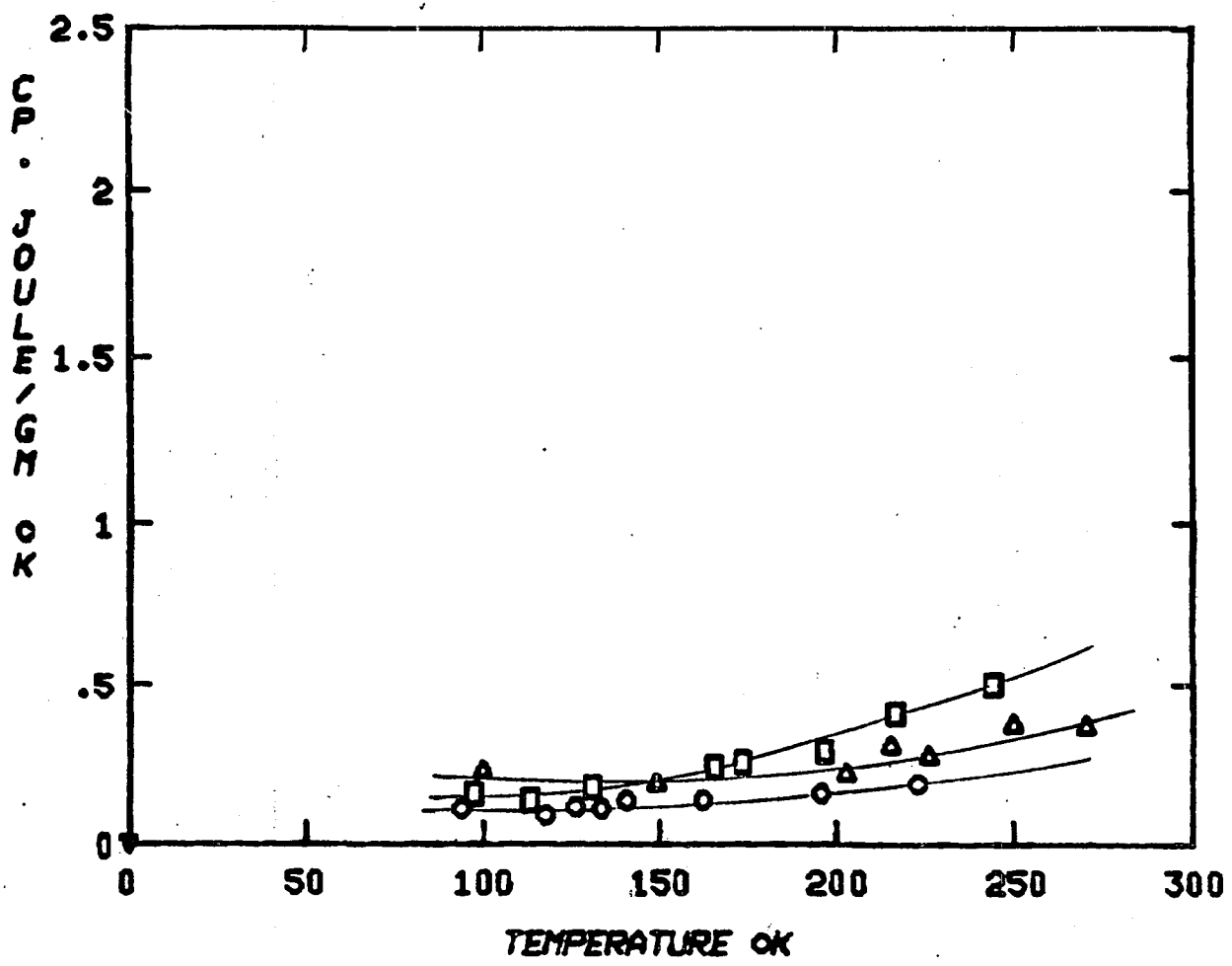

Figure 43. Heat capacities of UNDM PSOC-265-700-1 (o), UNDM PSOC-22-700-1 (□), and UNDM PSOC-246-700-1 (Δ).

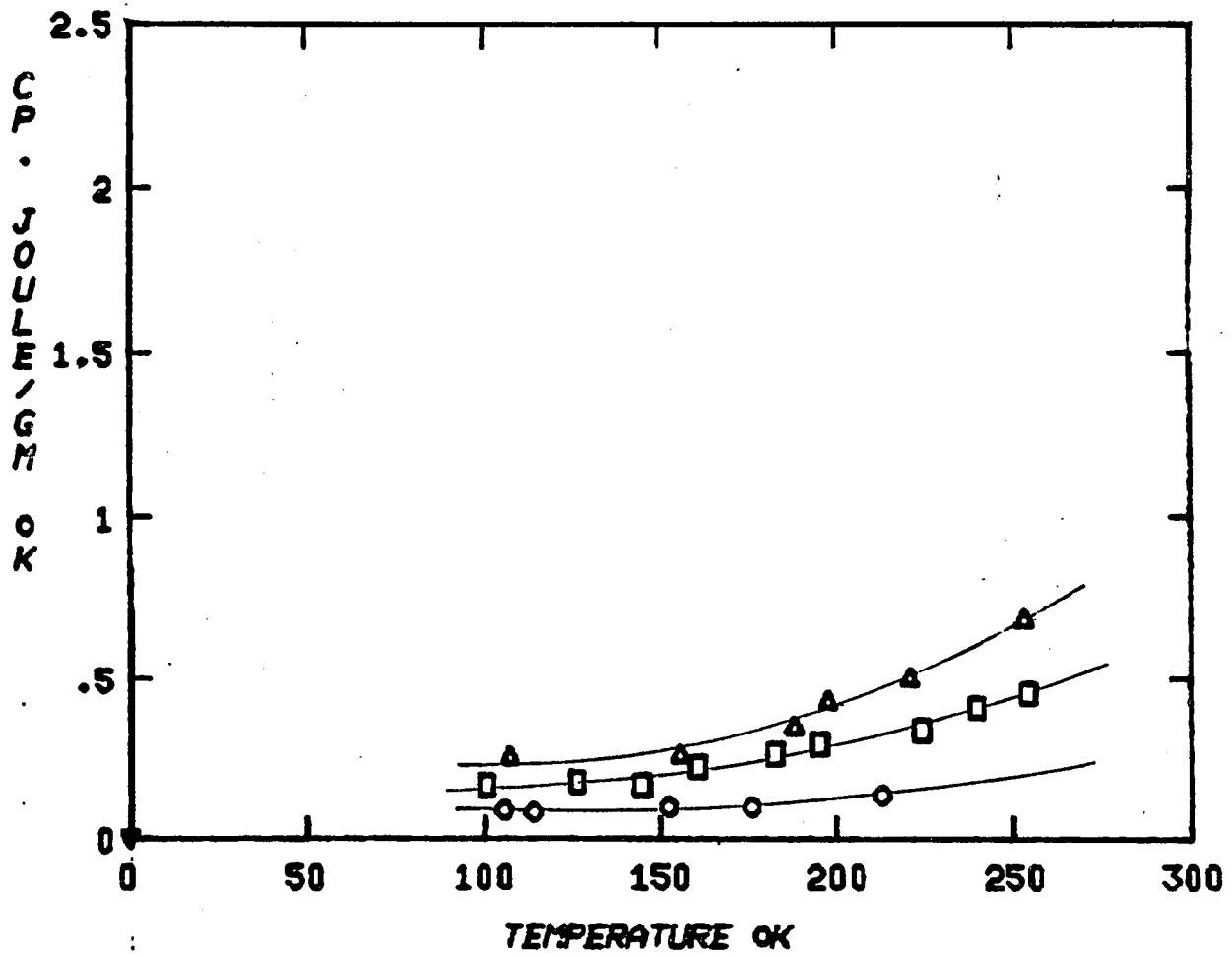

Figure 44. Heat capacities of DM PSOC-265-700-1 (o), DM PSOC-22-700-1 (□), and DM PSOC-246-700-1 (△).

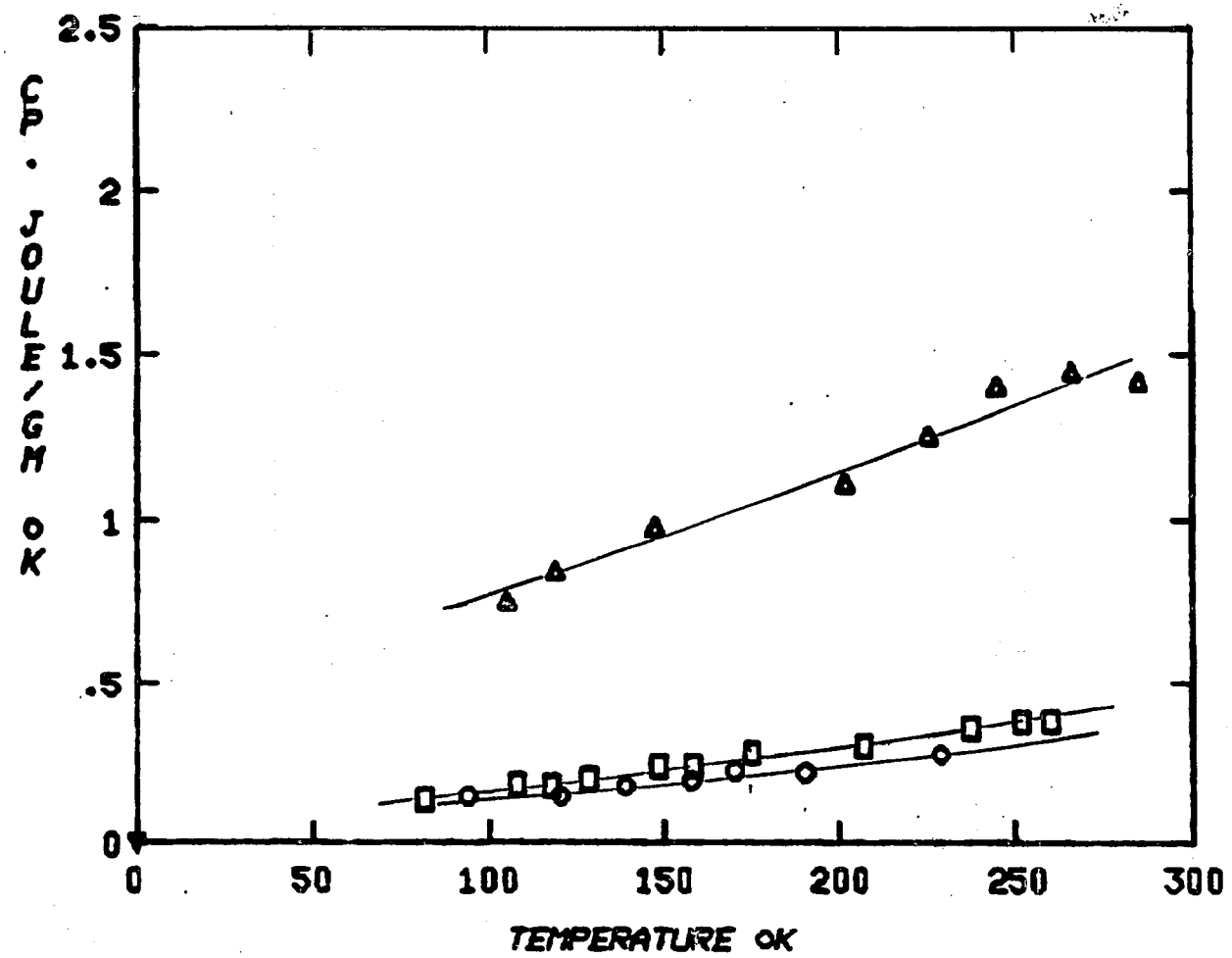

Figure 45. Heat capacities of DM PSOC-265-1100-1 (o), DM PSOC-22-1100-1 (□), and DM PSOC-246-1100-1 (Δ).

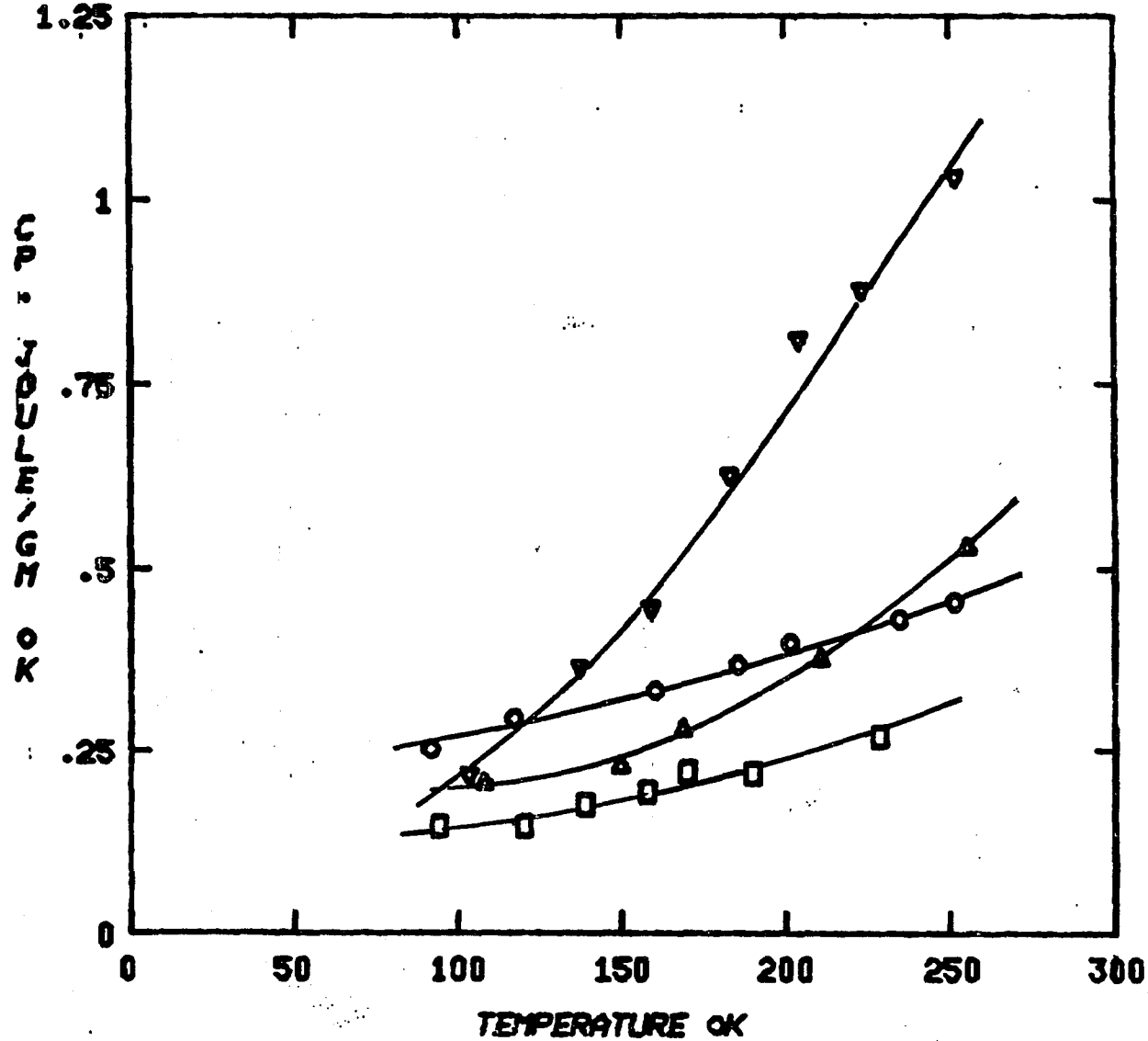

Figure 46. Heat capacities of DM PSOC-265 (o), DM PSOC-265-1100-0.1 (Δ), DM PSOC-265-1100-1 (□), and DM PSOC-265-1100-24 (▽).

coal. If the heat capacities of the organic and inorganic components of the coal were simply additive quantities, then one would expect that the heat capacity of the demineralized sample, normalized to some suitable reference quantity, would be less than that of a sample containing both the organic and the inorganic matter. Thus, the data clearly indicates that the demineralization process, involving warm acids (50°C) also alters the hydrocarbon structure of the coal. The situation is even more complicated for the Illinois No. 6 coal. As seen in Figure 32, the as-received sample data indicates the existence of several ordering type phase transitions. The transitions do not appear in the demineralized sample. Heat capacity data on some high rank coals are shown in Figures 1 and 2 (see Section 2.3).

X-ray diffraction data on these samples has been summarized in Table 5 (see Section 4.1.3). In the demineralized sample, the X-ray absorption peak (002) associated with the interplanar spacing of rings in graphite structures has disappeared. This indicates that at the least the long range crystalline order has been severely reduced by the acid treatment. The retention of the high angle lines and the appearance of a new peak argues for structural rearrangement. Thus, the present information is insufficient to check the conventionally employed assumption that coal heat capacities may be calculated from a quantitative analysis of the composition.

Adsorbed water and free moisture both significantly affect the heat capacities of coals. This problem was investigated by Mraw.[27] In Figure 36 we show the effect of "water" on demineralized Illinois No. 6 coal. The results are in excellent qualitative agreement with Mraw's work.

4.2.4 The Heat Capacity of Chars

In Figures 37 to 39 we present the heat capacity data on chars prepared from demineralized coals. The significant influence of the pyrolysis temperature and of the parentage on the heat capacities is clearly evident. Comparable data on very high rank coal derived chars has been shown in Figure 3 (see Section 2.3). Figures 40 to 49 show the influence of inorganic matter on the chars.

In the case of the chars prepared from the two bituminous coals, the heat capacities of the organic component and of the associated mineral matter do seem to be additive. Therefore, a relation of the form-

$$C_g^s = (1-w_a)\, C_g^o + w_a C_g^a \qquad (11)$$

can be used to separate the contributions to the total sample heat capacity. Here w_a represents the weight fraction mineral matter in the form of ash in the sample, as determined from the compositional analysis. C_g^s, C_g^o and C_g^a are the sample,

organic component and mineral matter (ash) heat capacities on a per gram basis at a given temperature. In estimating the ash heat capacity, it is assumed that: 1) in the demineralization procedure the relative composition of the residual mineral matter remaining with the organic matter is unchanged; and 2) the pyrolysis temperature does not affect the mineral matter composition. The result of the data separation was found to be adequately expressible in the form -

$$\frac{C_g^a}{C_g^o} = a + bT^3 \qquad (12)$$

where a and b are constants, whose values depend on the parentage of the sample and T is the temperature. For the Virginia coal based chars a = 1.5 and b = 1.6×10^{-7}. For the Illinois coal based chars a = 1.0 and b = 9×10^{-8}.

The compositional analysis of the char samples gives us besides the overall mineral content also the atomic ratios - H/C, N/C, and $\frac{O + S}{C}$. Thus, using the elemental analysis and equations 11 and 12 we can express the char heat capacities on a mineral matter free basis as -

$$C_g^o = [1 + w_a(a-1) + w_a bT^3]^{-1} \cdot C_g^s \qquad (13)$$

and

$$C_m = \frac{12 \cdot C_g^o \cdot (1 - w_a)}{w_c\left(1 + \frac{H}{C} + \frac{N}{C} + \frac{O + S}{C}\right)} \qquad (14)$$

where C_m is the heat capacity per mole of char atoms on a mineral matter free basis, and w_c is the weight fraction of carbon in the char sample.

The coefficient of C_g^s in equation 13 gives the fraction of the total sample heat capacity contributed by the hydrocarbon portion of the char. Thus at 300°K a 1% mineral matter content accounts for 5% of the total heat capacity in a Virginia char and 2.5% in an Illinois char. Note that this contribution is nonlinear in mineral content.

4.2.5 Correlation of The Char Heat Capacity with Pyrolysis Temperature and Composition

In Figure 47 we present the experimental data on the chars, normalized by the use of equation 14. One would like to find a representation in which the heat capacity could be correlated with the parameters describing the conditions of pyrolysis and the parentage of the char. The simplest realistic physical model for the temperature dependence of the heat capacity of a nonconductive solid comes from the Debye theory. To see if this leads toward a useful correlation, the effective Debye temperatures, θ, were calculated and plotted as a function of T in Figure 48. This plot is very instructive in as much as that it shows: 1) the chars do qualitatively behave like graphite; 2) one would have to handle the chars separately from cokes; and 3) there is a

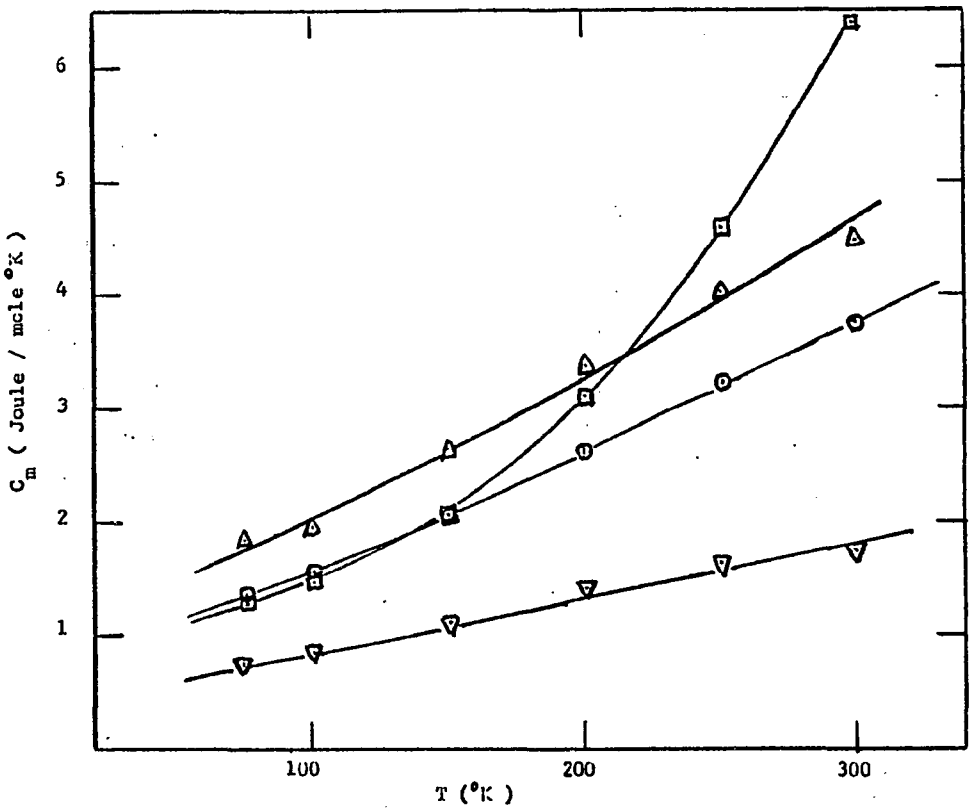

Figure 47. Heat capacities of PSOC-265-700-1 (▽), PSOC-265-1100-1 (o), PSOC-22-700-1 (□), and PSOC-22-1100-1 (△) vs temperature on the per mole atom ash-free basis.

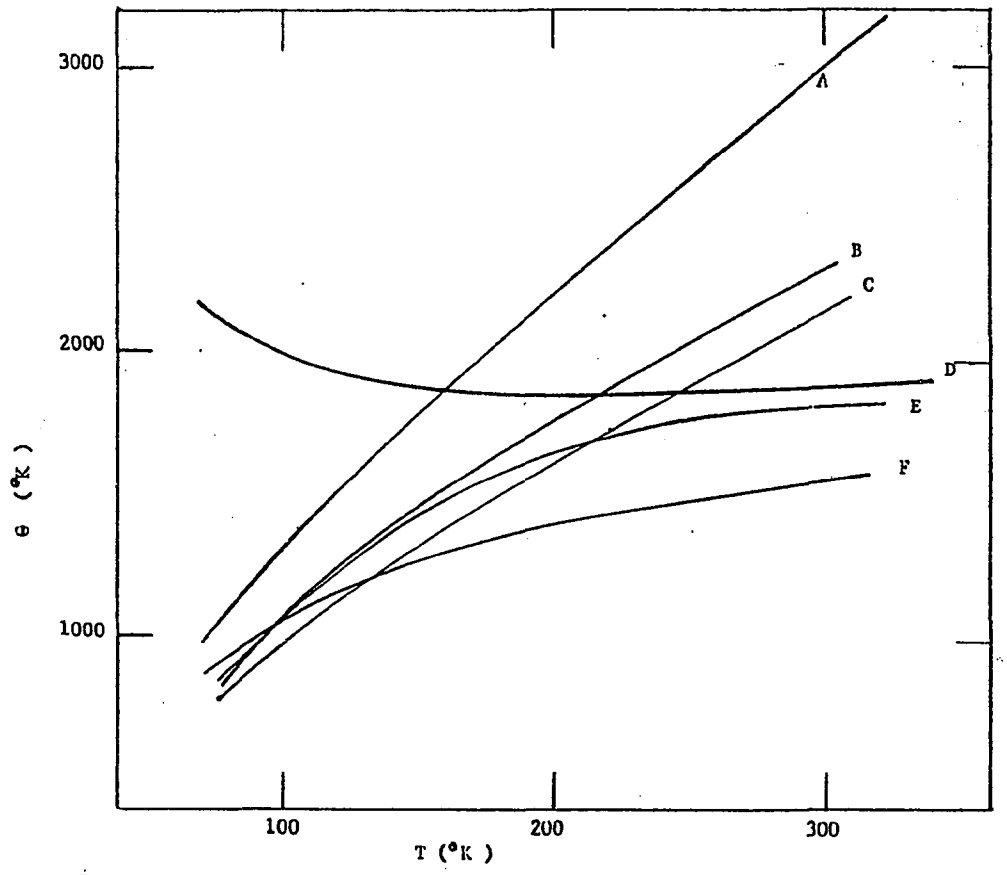

Figure 48. Debye's characteristic temperatures of graphite (F), diamond (D), PSOC-265-700-1 (A), PSOC-265-1100-1 (B), PSOC-22-700-1 (E), and PSOC-22-1100-1 (C) vs temperature.

possibility to find correlation for θ in terms of a reduced temperature and char composition.

The kind of bonds in the coal which are broken during the pyrolysis depend on the temperature. At lower temperature, mainly carbon-carbon bonds are broken, and the small fragments escape in the form of gaseous products. On the average two to three hydrogens are removed for each carbon leaving the condensed phase. Temperatures in the excess of $1000^{\circ}K$ are needed to break carbon hydrogen bonds, and to further dehydrogenate the char. Temperature also controls the rearrangement of the condensed phase structure, since mass diffusion is exponentially dependent on temperature. However, in the establishment of the char structure, it is difficult to separate the effect of "soak time" from temperature. The instantaneous (metastable) structure is a function of some product of the pyrolysis temperature, T_p, and the soak time. Holding the char for a longer time at lower T_p is equivalent to a shorter time at higher T_p. We look for the dependence of θ at T_p by correlating the heat capacity data for chars held at a given T_p for the same length of soak time (1 hr.). In Figure 49 we have replotted the Debye temperatures of the chars as a function of T/T_p. Comparing Figures 48 and 49, we see that this approach has merit. The effective Debye temperature can be expressed as a function of T/T_p.

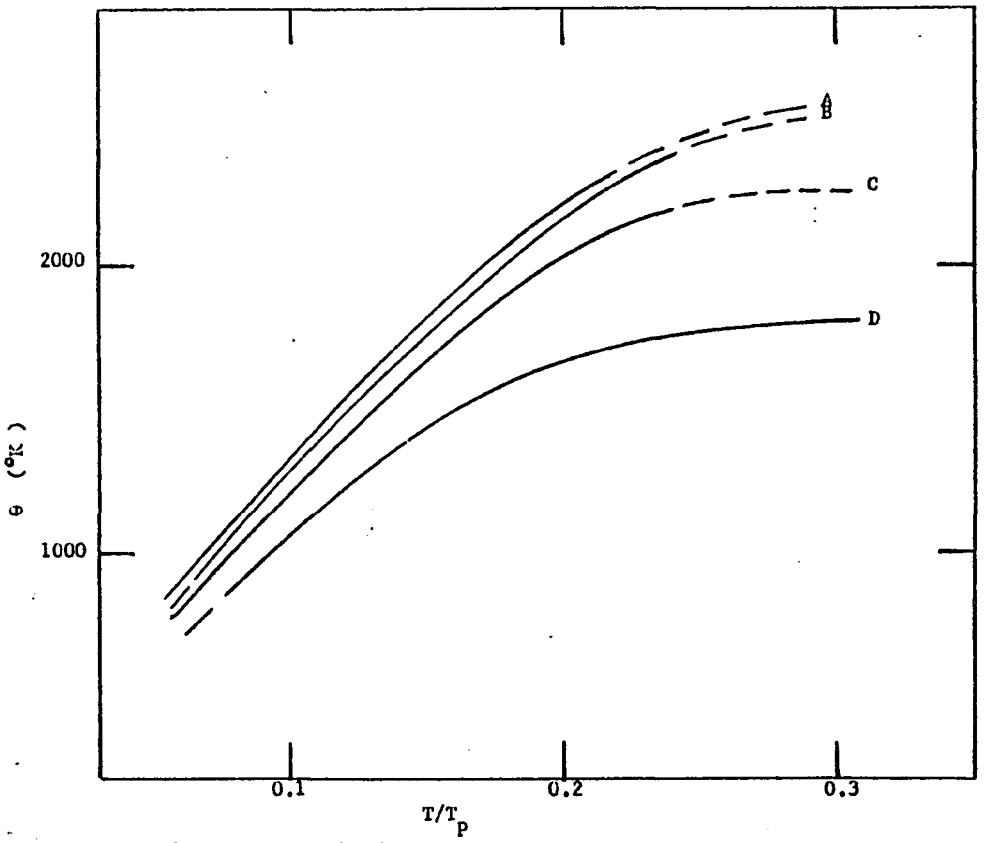

Figure 49. Debye's characteristic temperatures of PSOC-265-700-1 (B), PSOC-265-1100-1 (A), PSOC-22-700-1 (D), and PSOC-22-1100-1 (C) vs T/T_p.

We still have the char composition as a variable at our disposal. Normally, a solid material composed of identical units (atoms or molecules) can be modeled as a three-dimensional array of masses interacting with some specific force constant. This perfect lattice can be disturbed by the random introduction of a second kind of unit. This disturbance modifies the frequency spectrum by adding some Eistein modes to the top of distribution. This modifies the effective Debye temperature to the form -

$$\theta(T/T_p) = \theta_o(T/T_p)e^{f(c)} \tag{15}$$

where $\theta_o(T/T_p)$ is the effective Debye temperature in absence of disturbing atoms, and f(c) is some function of the concentration, c, of the disturbing atoms, and an interaction (which may be temperature dependent) parameter. To the lowest order f(c) should depend on c as c(1-c) because the most likely interaction will be between a disturbing specie and a normal specie unit. By trial and error, we found f(c) to be expressible as

$$f(c) = \frac{I(T/T_p)}{c(1-c)} \tag{16}$$

The interaction constants $I(T/T_p)$ were found as the slopes of the plots of $\ln\theta(T/T_p)$ against $[c(1-c)]^{-1}$. $I(T/T_p)$ is a linear function of T/T_p

$$I = I_o + \alpha (T/T_p) \qquad (17)$$

where $I_o = 0.0135$, and $\alpha \approx 0.04$ for the Virginia chars and $I_o = 0.005$ and $\alpha = 0.19$ for the Illinois chars. $\theta_o(T/T_p)$ was calculated from equation 15. A plot of θ_o versus T/T_p is shown in Figure 50.

The order of magnitude of the θ_o's for the Illinois char is comparable to that of graphite. This does not imply, however, that a very high pyrolysis temperature would lead to a nearly perfect graphite-like structure.

4.2.6 Thermodynamic Functions

In Table 8 are listed the values of the thermodynamic functions of the Illinois and Virginia coal chars calculated by the fitting equations of the heat capacity data and the following equations:

$$H_T - H_{75°K} = \int_{75°K}^{T} C_m dT \qquad (18)$$

$$S_T - S_{75°K} = \int_{75°K}^{T} \frac{C_m}{T} dT \qquad (19)$$

$$G_T - G_{75°K} = (H_T - H_{75°K}) - T\cdot(S_T - S_{75°K}) \qquad (20)$$

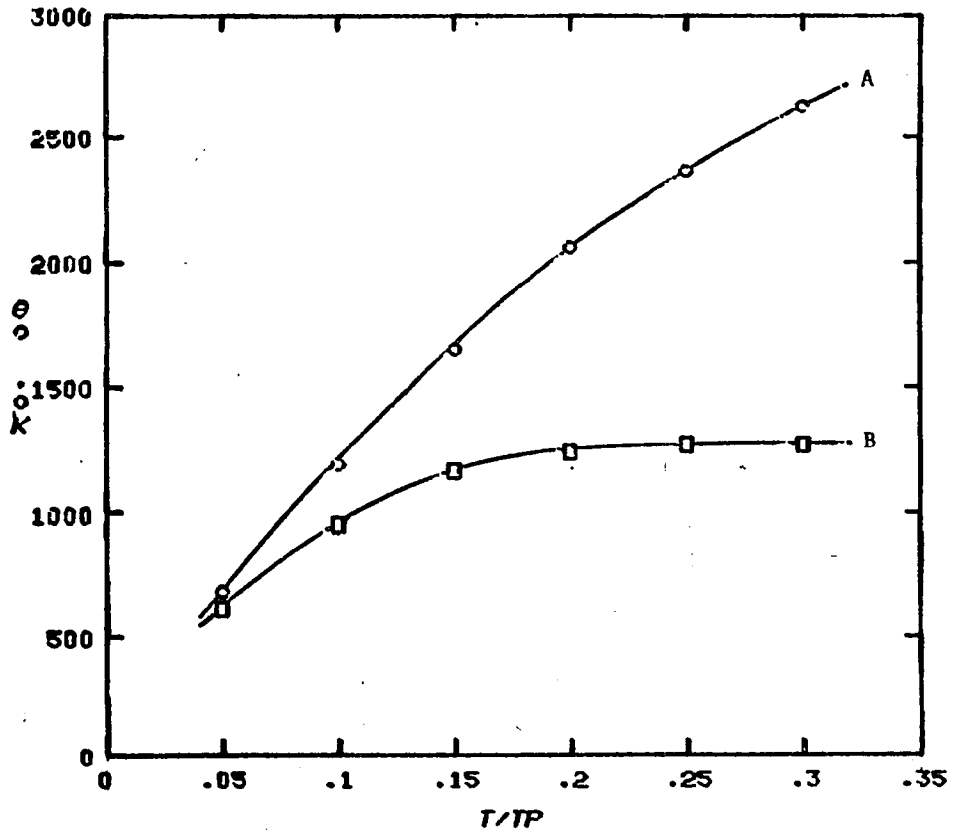

Figure 50. θ_e of PSOC-265 Char (A) and PSOC-22 Char (B) vs T/T_P

Table 8. Thermodynamic Functions of Coal Chars.

PSOC-265-700-1

T (°K)	C_m (Joule/mole°K)	$H-H_{75}$ (Joule/mole)	$S-S_{75}$ (Joule/mole°K)	$-(G-G_{75})$ (Joule/mole)
80	0.7456	3.671	0.0474	0.119
100	0.8451	19.556	0.224	2.864
150	1.132	68.841	0.620	24.149
200	1.4198	132.774	0.986	64.384
250	1.6412	209.715	1.328	122.346
300	1.729	294.665	1.638	196.663

PSOC-265-1100-1

80	1.4006	6.911	0.089	0.224
100	1.5639	36.512	0.419	5.366
150	2.0668	126.808	1.144	44.815
200	2.2461	244.265	1.817	118.957
250	3.2283	391.467	2.471	226.218
300	3.7398	566.117	3.106	365.734

Table 8. (conti.) PSOC-22-700-1

T	C_m	$H-H_{75}$	$S-S_{75}$	$-(G-G_{75})$
80	1.3512	6.704	0.0865	0.215
100	1.4726	34.832	0.4	5.153
150	2.069	121.598	1.095	42.712
200	3.1033	249.031	1.822	115.272
250	4.5997	439.829	2.686	226.856
300	6.5825	717.105	3.672	384.572
		PSOC-22-1100-1		
80	1.8495	9.164	0.118	0.298
100	2.0158	47.727	0.548	7.057
150	2.6195	162.712	1.472	58.094
200	3.3509	311.807	2.325	153.158
250	4.0338	496.991	3.148	290.116
300	4.4922	711.442	3.929	467.296

5. APPLICATION OF THE DATA; A SIMPLE MODEL FOR CHAR-GASIFICATION

Thermodynamics may be applied to the gasification of coal chars in order to calculate the limiting performance of individual processes and to guide the practical design and scale up of reactor systems. For these purposes, the thermochemical properties of the coal char gasification system must be used to estimate the heat effects and equilibrium or pseudoequilibrium behavior of the process. The following example uses the thermochemical properties of a 900°C Synthane -process char of empirical formula $CH_{0.199}O_{0.016}N_{0.008}S_{0.006}$ to estimate "equilibrium" for a steam-oxygen gasification process. The chemical analysis, heat of combustion and heat capacity data above room temperature of this char has been reported in literature.[2] Since our PSOC-22 char has the same coal origin as the gasifier char, our data for the PSOC-22 char will be used to extend the thermodynamic functions to low temperatures.

The following chemical reactions are considered as a model for the char reaction to form methane in a hydrogen atmosphere:

$$CH_{0.199}O_{0.016}N_{0.008}S_{0.006(s)} + 1.9225H_{2(g)}$$
$$= CH_{4(g)} + 0.016H_2O_{(g)} + 0.004N_{2(g)} + 0.006H_2S_{(g)} \qquad (21)$$

$$CH_{0.199}O_{0.016}N_{0.008}S_{0.006(s)} + 1.8745H_{2(g)}$$

$$=0.984CH_{4(g)}+0.016CO_{(g)}+0.004N_{2(g)}+0.006H_2S_{(g)} \quad (22)$$

$$CH_{0.199}O_{0.016}N_{0.008}S_{0.006(s)} + 1.8905H_{2(g)}$$

$$=0.992CH_{4(g)}+0.008CO_{2(g)}+0.004N_{2(g)}+0.006H_2S_{(g)} \quad (23)$$

$$CH_{0.199}O_{0.016}N_{0.008}S_{0.006(s)} + 1.9345H_{2(g)}$$

$$=CH_{4(g)}+0.016H_2O_{(g)}+0.008NH_{3(g)}+0.006H_2S_{(g)} \quad (24)$$

$$CH_{0.199}O_{0.016}N_{0.008}S_{0.006(s)} + 1.8865H_{2(g)}$$

$$=0.984CH_{4(g)}+0.016CO_{(g)}+0.008NH_{3(g)}+0.006H_2S_{(g)} \quad (25)$$

$$CH_{0.199}O_{0.016}N_{0.008}S_{0.006(s)} + 1.9025H_{2(g)}$$

$$=0.992CH_{4(g)}+0.008CO_{2(g)}+0.008NH_{3(g)}+0.006H_2S_{(g)} \quad (26)$$

where we define a mole of char to be that amount of char that contains one mole of carbon atoms. At a given temperature, the equilibrium constants for the above reactions can be calculated if we know the standard heat of formation, standard entropy and heat capacity as a function of temperature for the char. The standard heat of formation of the char, $(\Delta H^{\circ}_{f298})_{char}$, can be calculated from the measured heat of combustion by considering the following combustion reaction:

$$CH_{0.199}O_{0.016}N_{0.008}S_{0.006(s)} + 1.039O_{2(g)}$$

$$=CO_{2(g)}+0.004N_{2(g)}+0.006H_2S_{(g)}+0.0935H_2O_{(g)} \quad (27)$$

Where the standard heat of combustion, ΔH°_{c298}, equals -97658.18 $\pm$ 152 cal/mole char.[2] The JANAF thermochemical tables were used for the other compounds to calculate the standard heat of formation for this char. In this case $(\Delta H^{\circ}_{f298})_{char}$ equals -1825.82$\pm$152 cal/mole char.

The heat capacity of the ash-containing char can be expressed by the following equation:

$$C^{s}_{g}(T) = 1.1109 + 0.000684T - 4.98x10^{4}T^{-2} \quad \text{Joule/gm°K} \quad (28)$$

Which is accurate to $\pm$ 2% over the temperature range of 273-1200°K($\pm$ 1% error is introduced by the curve fitting method and $\pm$ 1% by experimental measurements.). Using Kirov's correlation for the heat capacity of ash[28], the heat capacity of the ash-free char can be expressed in the following form:

$$C^{ch}(T) = 16.919 + 0.0092T - 9x10^{5}T^{-2} \pm 3\% \text{ Joule/mole char°K} \quad (29)$$

By assuming that the Debye Θ_o of the char is the same as that of the PSOC-22 char, the heat capacity correlation model presented in this study is used to generate the heat capacity of the ash-free char over the temperature range of 75 to 300°K. Below 75°K, the heat capacity of the ash-free char is calculated

by the Debye's T^3 law. The heat capacity estimated as such is reliable within $\pm$ 3% above room temperature and $\pm$ 5% below room temperature.

The thermochemical data described above are listed in Table 9. These data and the JANAF thermochemical tables are used to estimate the heat of reaction for equations (21) to (26) separately at standard conditions. Tables 10 and 11 give the values of the standard heat of reaction for these reactions and the values for the thermodynamic quantities required in the equilibrium constant evaluation.

At a given reaction temperature τ, the equilibrium constant Ki is calculated by the following equation:

$$
\begin{aligned}
-R\tau \ell n Ki &= \Delta G^{\circ}_{Ri}(\tau) \\
&= \Delta H^{\circ}_{Ri}(\tau) - \Delta S^{\circ}_{Ri}(\tau) \\
&= \Delta H^{\circ}_{Ri}(298) + \left[\sum_{\text{products}} \left(n_i \int_{298}^{\tau} C^{\circ}_{pi} dT \right) - \sum_{\text{reactants}} \left(n_i \int_{298}^{\tau} C^{\circ}_{pi} dT \right) \right] \\
&\quad - \left[\sum_{\text{products}} n_i S^{\circ}_i(\tau) - \sum_{\text{reactants}} n_i S^{\circ}_i(\tau) \right] \qquad (30)
\end{aligned}
$$

where the symbols have their usual meaning. $S^{\circ}_{char}(\tau)$ is given by $S_o + \int_o^{\tau} \frac{C^{ch}}{T} dT$. S_o is the residual entropy of char at 0°K.

As a first approximation we set $S_o = 0$. Table 12 gives the calculated equilibrium constant Ki at selected temperatures

Table 9. Thermochemical Data of Ash-free Char Required in the Equilibrium Constant Evaluation.

Temperature Range		ΔH° Values cal/mole char
$\Delta H^\circ(298\text{-}1000^\circ K)$	$\int C\,dT$	3333.41 ± 100.00
$\Delta H^\circ(298\text{-}1200^\circ K)$	$\int C\,dT$	4590.05 ± 137.70
		ΔS° Values cal/mole char °K
$\Delta S^\circ(0\text{-}75^\circ K)$	Debye's Extrapolation	0.079 ± 0.004
$\Delta S^\circ(75\text{-}300^\circ K)$	$\int (C/T)\,dT$	1.083 ± 0.054
$\Delta S^\circ(300\text{-}1000^\circ K)$	$\int (C/T)\,dT$	5.334 ± 0.16
$\Delta S^\circ(300\text{-}1200^\circ K)$	$\int (C/T)\,dT$	6.453 ± 0.194
$\Delta S^\circ(0\text{-}1000^\circ K)$		6.496 ± 0.218
$\Delta S^\circ(0\text{-}1200^\circ K)$		7.615 ± 0.252

Table 10. Thermochemical Data Required in the Equilibrium Constant Evaluation (from JANAF tables).

Reaction Temperature	1000 °K		1200 °K	
Substance	$H°(T)-H°_{298}$ cal/mole	$S°(T)$ cal/mole°K	$H°(T)-H°_{298}$ cal/mole	$S°(T)$ cal/mole°K
$H_{2(g)}$	4944	39.702	6404	41.033
$CH_{4(g)}$	9125	59.141	12732	62.424
$H_2O_{(g)}$	6209	55.592	8240	57.441
$CO_{(g)}$	5183	56.028	6794	57.496
$CO_{2(g)}$	7984	64.344	10632	66.756
$N_{2(g)}$	5129	54.507	6718	55.955
$NH_{3(g)}$	7787	58.851	10592	61.404
$H_2S_{(g)}$	6687	60.342	8943	62.396

Table 11. Calculated Values for the Standard Heat of Reaction of Char.

	Reaction 1	Reaction 2	Reaction 3
$\Delta H^{\circ}_{Ri,298}$ cal/mole char	-17016.84±152	-16228.5±152	-16701.37±152
	Reaction 4	Reaction 5	Reaction 6
	-17104.6±152	-16316.26±152	-16789.63±152

Table 12.Calculated Equilibrium Constant Ki at Selected Reaction Temperatures (case S_0=0 e.u.)

Reaction Temperature	1000 °K	1200 °K
K_1	0.438	0.0775
K_2	0.4635	0.0878
K_3	0.450	0.0823
K_4	0.412	0.0724
K_5	0.434	0.082
K_6	0.424	0.0768

1000 and 1200°K. The equilibrium constants thus calculated are incorporated into Squires'[29] pseudoequilibrium plot as shown in the Figure 51. In this figure, line A represents steam gasification of a bituminous and a subbituminous coal; line B represents atmospheric-pressure gasification of anthracite, cokes, and chars that were previously soaked in nitrogen for many hours at gasification temperature; line C is for a bituminous char, also soaked in nitrogen, at 9.3 atmospheres; line D is for anthracite at 12 to 17 atmospheres.

In figure 51 the equilibrium constants Ki have been plotted for reactions (21) through (26) while the experimental data are plotted in terms of the ratio $p_{CH_4}/p_{H_2}^2$. Assuming the ideal gas law, these are related by

$$Ki = \prod p_j^{\nu_j}$$

$$= A \cdot \left(p_{CH_4}/p_{H_2}^2 \right) \qquad (31)$$

where p_j is the partial pressure, ν_j is the stoichiometric coefficient (negative for the reactants) of species j in the equilibrium mixture, and A is a parameter containing the appropriate partial pressure terms. Under given gasification conditions, the equilibrium yields of each component can be found and A can be calculated. Results for gasification in pure hydrogen atmosphere are

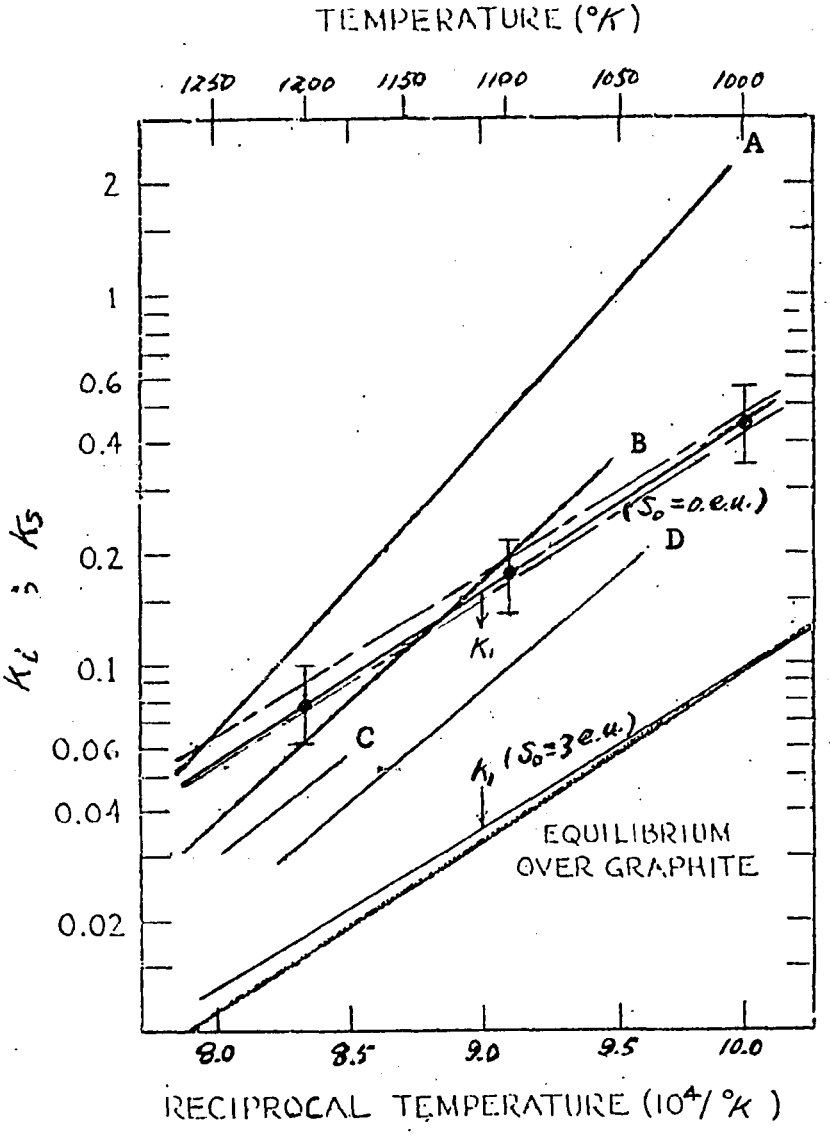

Figure 51. Methane "Equilibrium" Constant Ki of Sample Char and Pseudoequilibrium Constant Ks from Squires.
Lines A-D from Squires(1961,Part I,Fig.1) were used where Ks is defined as $P_{CH_4} / P_{H_2}^2$ with P_{CH_4}, P_{H_2} measured from gasifier effluent; Ki is calculated by hypothetical hydrogenation reactions with end product gases of nitrogen in the form of N_2 or NH_3 and oxygen in the form of H_2O, CO or CO_2, respectively. For S_o=0, all Ki lines fall in the region bounded by the dotted lines.

shown in Table 13. For these cases A = 1 within ± 25% below 20 atmospheres. Therefore, as a rough approximation, we may equate $p_{CH_4}/p_{H_2}^2$ to Ki over the temperature range 1000 to 1200°K.

The error in Ki introduced by the estimation of the thermodynamic quantities of the char is around ± 25%. The major error is contributed by estimating the thermal entropy of the char, which is around ± 12%. The thermal enthalpy and heat of combustion terms give another ± 13% error. The uncertainty in the high temperature heat capacity data is the major source for these errors. Error introdued by extrapolation of the heat capacity to low temperatures is comparatively small in this case (about ±3%). Our results indicate that the equilibrium constant Ki for the methane formation by the char in a hydrogen atmosphere is higher than equilibrium over graphite in the temperature range of 1000 to 1200°K. The values of Ki are close to each other for a fixed reaction temperature. The model formulated this way can be used to estimate the methane formation equilibrium or pseudoequilibrium conditions in conversion processes of a more complicated nature.

In above calculations, the residual (zero-point) entropy for the char is assumed as zero. Our present knowledge of char structure is inadequate to permit any direct estimates

Table 13. Deviation of $P_{CH_4}/P_{H_2}^2$ from Ki in terms of A (Constant Pressure Operation).

Equation (21) : $A = P_{H_2}^{0.0775} P_{H_2O}^{0.016} P_{N_2}^{0.004} P_{H_2S}^{0.006}$								
Total Pressure (atm.)	1	5	10	20	30	40	50	60
(1) At 1000°K								
% Deviation of A from 1	-16	-3	3	9	12	15	17	18
(2) At 1200°K								
% Deviation of A from 1	-17	-1	6	13	17	20	23	25
Equation (22) : $A = P_{CH_4}^{-0.016} P_{H_2}^{0.1255} P_{CO}^{0.016} P_{N_2}^{0.004} P_{H_2S}^{0.006}$								
Total pressure (atm.)	1	5	10	20	30	40	50	60
(1) At 1000°K								
% Deviation of A from 1	-16	0	7	14	18	21	23	25
(2) At 1200°K								
% Deviation of A from 1	-14	5	14	23	28	32	34	37

Table 13. (conti.)

Equation (23) : $A = P_{CH_4}^{-0.008} P_{H_2}^{0.1095} P_{CO_2}^{0.008} P_{N_2}^{0.004} P_{H_2S}^{0.006}$								
Total Pressure (atm.)	1	5	10	20	30	40	50	60
(1) At 1000°K								
% Deviation of A from 1	-12	6	14	22	26	29	32	34
(2) At 1200°K								
% Deviation of A from 1	-13	1	8	14	18	20	22	24

of residual entropy. Typical values of residual entropy for disordered amorphous structures are 1-5 entropy units (cal/mole model unit,°K).[30] It is interesting to note that on assumption of a value of 3 e.u. for S_o will bring the Ki lines down to near the equilibrium line over graphite. If accurate "equilibrium" data for the gasification of chars were available, we could estimate the residual entropy of chars as the number of entropy units which has to be added to the thermal entropy of chars in order to match the Ki line to the experimentally determined "equilibrium" line. Of course these results would have to be verified using other char reactions in the same way (e.g. char with water, oxygen, or carbon dioxide). It is important to note that the S_o = 0 e.u. line will give an estimate for the upper limit for the methane formation by the char reaction with hydrogen. In this case, it is about six times higher as compared with equilibrium over graphite.

6. CONCLUSIONS

(1) Our sample characterizations indicate that physical and chemical alterations of the coal structure occur during demineralization. The heat capacity data for the original and demineralized coal samples show that the acid-washing method of demineralization modifies the hydrocarbon portion of coal in addition to removing the inorganic matter. The extent of modification seems to depend on the type of coal involved.

(2) The heat capacities of the coals studied are correlated with coal rank on a dry inorganic matter free basis. The magnitudes of the heat capacities of these coals indicates the significance of coal rank in evaluation of the standard state thermodynamic functions of coals.

(3) Both the pyrolysis temperature (700 to 1100°K) and soak time (0.1 to 24 hrs) have to be considered as important parameters in characterizing the heat capacity behavior of coal chars.

(4) Our data show that the heat capacity of coal chars behaves similarly to that of pure carbons, and has the same order of magnitude as that of pure carbons.

(5) A correlation model, which is based on Debye's heat capacity theory, is presented in this study to estimate the heat capacity of the organic phase of chars at different pyrolysis temperatures. This model applies to chars prepared from two bituminous coals at different pyrolysis temperatures but with same length of soak time.

(6) This correlation model has been used to extend the heat capacity data of a gasifier char to lower temperatures. "Equilibrium" constants for methane formation from this char by hydrogenation gives an upper limit about six times higher than equilibrium over graphite in the temperature range of 1000 to 1200°K.

7. RECOMMENDATIONS FOR FUTURE RESEARCH

From the author's point of view, the study of the heat capacity of coal chars should now move in the following directions:

(1) More samples have to be investigated to test and improve our heat capacity correlation model. From the data collected so far, it is expected that the heat capacity of chars prepared from higher rank coals can be properly characterized by our correlation based on a modification of Debye's theory.

(2) Since the physical properties of coal char are very much process related, the extension of the present work to other process conditions is of great importance.

(3) Incorporation of an ash composition study into the present program will prove to be valuable in estimating the heat capacity contribution of ash to the total heat capacity of coal chars.

(4) Extension of the heat capacity measurements to both lower and higher temperature is important. The lower temperature data are required in estimating the standard state absolute entropy value of coal char. Besides its importance in thermodynamics, high temperature heat capacities have direct application in estimating the process heat effects. Literature data at high temperatures are obsolete, scattered, incon-

sistent and usually without careful sample characterization. The high temperature research program should include experimental calorimetric development, sample data base generation, and process variable correlation. It should be emphasized that the meaning of the heat capacity itself has to be clearly defined in the high temperature study.

(5) More structural information on coal chars are required in the formulation of a heat capacity theory for these materials. The heat capacity of amorphous structures is still a challenging subject needing further investigation.

(6) Since our present knowledge of char structure is inadequate to permit any direct estimates of residual entropy, experimental equilibrium data on char reactions with hydrogen, water, oxygen and carbon dioxide are required for its determination.

8. REFERENCES

(1) Kasatochkin, V.I., Usenbaev, K., Zhadanov, V.M., Sabyraliev, K., Rasalbaev, M. and Zhumalieva, K., Dokl. Akad, Nauk, S.S.S.R. 216, 93(1974).

(2) Internal Report of The Thermodynamics Research Group, Bartlesville Energy Research Center, DOE, "Thermal Data on Gasifier Streams from Synthane Test" (1973).

(3) Delhaes, P. and Hishiyama, Y., Carbon, 8, 31, (1970); Kamiya, K., Mrozowski, S., and Vagh, A. S. Carbon, 10, 267(1972).

(4) Horton, M. D., Fast Pyrolysis, in "Pulverized-Coal Combustion and Gasification", Smoot, L.D. and Pratt, D. T., Ed., Plenum Press, New York, p. 133 (1979).

(5) Johnson, J.D., Kinetics of Coal Gasification, Wiley, New York, p. 59 (1979).

(6) Johnson, J.D., Kinetics of Coal Gasification, Wiley, New York, p. 96 (1979); Skinner, F.O. and Smoot, L.O., Heterogeneous Reactions of Char and Carbon, in "Pulverized-Coal Combustion and Gasification", Smoot, L.O. and Pratt, D.T., Ed., Plenum Press, New York, p. 149 (1979).

(7) Debye, P.,Ann. Physik, 39, 789 (1912).

(8) Born, M. and Von Karman, T., Phys. Z., 13, 297 (1912).

(9) Gaede, W., Physik, Z., 4, 105 (1902).

(10) Nernst, W., Sitzber.kgl.preuss, Akad. Wiss., 12, 13, 261 (1910); Chem. Abstr., 4, 2397 (1910); Eucken, A., Physik, Z., 10, 586 (1909).

(11) Southard, J.C., and Andrews, D.H., J. Franklin Inst. 209, 349 (1930).

(12) Kelly, B.J. and Taylor, R., The Thermal Properties of Graphite, in "Chemistry and Physics of Carbon", Walker, P.L. Jr. and Thrower, P.A., Ed., Vol. 10, Marcell Dekker, New York, p. 1 (1973).

(13) De Sorbo, W., J. Chem. Phys., 21, 876 (1953); De Sorbo, W., and Tyler, W.W., J. Chem. Phys., 21, 1660 (1953); De Sorbo, W., J. Chem. Phys. 23, 1970 (1955); De Sorbo, W., J. Amer. Chem. Soc. 77, 4713 (1955); De Sorbo, W.,

and Tyler, W.W., J. Chem. Phys. 26, 244 (1957); De Sorbo, W., and Nichols, G.E., J. Phys. Chem. Solids, 6, 352 (1958).

(14) Radmacher, W. and Mohrhauer, P., Brennst Chemie, 36, 236 (1955).

(15) Bishop, M. and Ward, D.L., Fuel, 37, 191 (1958).

(16) Raj, S., personal communication (1977).

(17) Isaacs, L.L. and Panosh, R.L., Argonne National Laboratories' Communication Article ANL-MS-1270 (1970).

(18) Anderson, A.C., Rev. Sci. Instrum. 39, 605 (1968).

(19) Westrum, E.F. Jr., Furukawa, G.T. and McCullough, J.P., Adiabatic Low-Temperature Calorimetry, in "Experimental Thermodynamics", McCullough, J.P. and Scott, D.W., Ed., Vol. 1, Plenum Press, New York, p. 185 (1968).

(20) White, G.K., Experimental Techniques in Low Temperature Physics, Oxford University Press, p. 58 (1979).

(21) Vasileff, H.D., J. Appl. Phys., 23, 979 (1952).

(22) Culmo, R.F., CHN Analysis of Coals With The Perkin-Elmer Model 240 Elemental Analyzer, Perkin-Elmer Corp., (1977).

(23) Hirsch, P.B., Proc. R. Soc. A 226, 143 (1954); Hirsch, P.B., Trans. R. Soc. A252, 68 (1960).

(24) Inouye, K., Rice, N. and Prostel, E., Fuel, 39, 81 (1960).

(25) Furukawa, G.T., Shaba, W.G. and Reilly, M.L., NSROS-NBS-18, U. S. GPO, Washington, D. C. (1968).

(26) De Sorbo, W., J. Amer. Chem. Soc., 77, 4713 (1955).

(27) Mraw, S.C., Naas-O'Rourke, D.F., Science, Vol. 205, 31 (1979).

(28) Kirov, N.Y., Br. Coal. Util. Res. Assoc. Mon. Bull., 29, 33 (1965).

(29) Squires, A.M., Trans. Inst. Chem. Engrs., 39, 3 (1961); Squires, A.M., Science, 191, 689 (1976).

(30) Gutzow, G., Z. Phys. Chem. 221, 153 (1962); Gutsov, G., Properties, Structure, and Physical-chemical Effects, in "The Structure of Glass", Porai-Koshits, E.A., Ed., Vol. 6, Consultants Burear, New York, (1966).

9. APPENDIX

9.1 Data Reduction Scheme

Data reduction of the heat capacity of coal chars is illustrated in the following data reduction scheme:

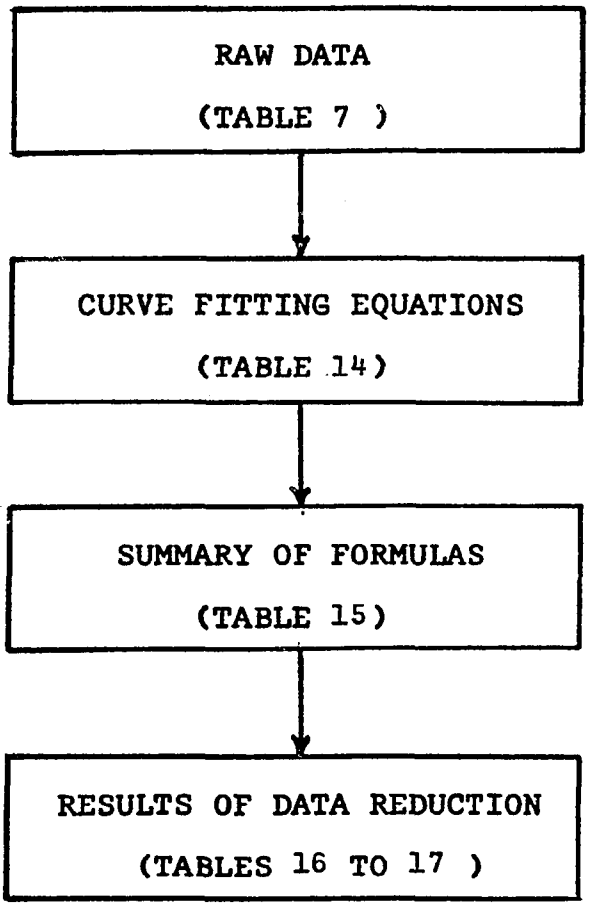

Table 14. Polynomial curve-fitting equations for the measured heat capacity data.

POCO Graphite :	$C_g^s = 0.251 + 1.953\times10^{-8}\ T^3 - 4\times10^{-11}\ T^4$
UNDM PSOC-265-700 :	$C_{gac}^s = 1.493 + 1.03\times10^{-5}\ T^2 + 9.191\times10^{-8}\ T^3$
DM PSOC-265-700 :	$C_{gac}^s = 0.7299 + 4.253\times10^{-5}\ T^2 - 8.129\times10^{-8}\ T^3$
DM PSOC-265-1100 :	$C_{gac}^s = 1.276 + 5.88\times10^{-5}\ T^2 - 8.048\times10^{-8}\ T^3$
UNDM PSOC-22-700 :	$C_{gac}^s = 1.917 + 3.271\times10^{-7}\ T^3 + 4.203\times10^{-10}\ T^4$
DM PSOC-22-700 :	$C_{gac}^s = 1.529 + 3.877\times10^{-7}\ T^3 - 4.342\times10^{-10}\ T^4$
DM PSOC-22-1100 :	$C_{gac}^s = 1.509 + 8.922\times10^{-5}\ T^2 - 1.562\times10^{-7}\ T^3$

Table 15. Summary of Equations used in Data Reduction.

$$C_g^s = (1 - w_a)\, C_g^o + w_a\, C_g^a$$

$$C_g^a / C_g^o = a + b\, T^3$$

$$C_g^o = (1 + w_a (a - 1) + w_a\, b\, T^3)^{-1}\, C_g^s$$

$$C_m = \frac{12\, C_g^o (1 - w_a)}{w_c \left(1 + H/C + N/C + \frac{O+S}{C}\right)}$$

$$C_{gac}^o = 12\, C_g^o (1 - w_a) / w_c$$

$$C = 3\, n\, R\, D(\theta_D / T)$$

$$\theta (T/T_p) = \theta_o (T/T_p)\, e^{f(c)}$$

$$f(c) = I(T/T_p) / c(1-c)$$

$$I = I_o + \alpha (T/T_p)$$

Table 16. Results of Data Reduction.

POCO-graphite				
T (°K)	C_m	$C_m/3R$	θ/T	θ (°K)
75	1.468	0.0591	10.9	818
100	1.908	0.0768	10.0	1000
150	3.239	0.1304	8.15	1223
200	5.370	0.2161	6.63	1326
250	7.964	0.3205	5.45	1363
300	10.452	0.4207	4.57	1371

Table 16. (conti.)

DM PSOC-265-700

T(°K)	C^s_{gac}	C^s_g	C^a_g	C^o_g	C^o_{gac}	C_m	T/T_p	$C_m/3R$	θ/T	θ (°K)
75	0.9348	0.0689	0.2266	0.1223	0.844	0.723	0.077	0.0291	13.9	1042.5
100	1.0739	0.0791	0.2133	0.1399	0.987	0.845	0.103	0.0340	13.2	1320
150	1.4124	0.1041	0.2170	0.1842	1.322	1.132	0.154	0.0455	11.9	1785
200	1.7808	0.1312	0.2989	0.2357	1.658	1.420	0.206	0.0571	11.05	2110
250	2.1178	0.1560	0.5038	0.2880	1.916	1.641	0.257	0.0662	10.5	2625
300	2.3628	0.1741	0.8742	0.3350	2.019	1.729	0.308	0.0696	10.3	3090

Table 16. (conti.)

DM PSOC-265-1100

T(°K)	C^{s}_{gac}	C^{s}_{g}	C^{a}_{g}	C^{o}_{g}	C^{o}_{gac}	C_{m}	T/T_{p}	$C_{m}/3R$	θ/T	θ(°K)
75	1.5729	0.1251	0.2266	0.1223	1.496	1.366	0.055	0.055	11.2	840
100	1.711	0.1419	0.2133	0.1399	1.711	1.563	0.073	0.063	10.7	1070
150	2.3274	0.1851	0.2170	0.1842	2.253	2.058	0.109	0.083	9.7	1455
200	2.9842	0.2374	0.2989	0.2357	2.883	2.663	0.146	0.106	8.85	1770
250	3.6935	0.2938	0.5038	0.2880	3.522	3.216	0.182	0.129	8.2	2050
300	4.395	0.3496	0.8742	0.3350	4.098	3.742	0.218	0.151	7.7	2310

Table 16. (conti.)

DM PSOC-22-700

T (°K)	C^s_{gac}	C^s_g	C^a_g	C^o_g	C^o_{gac}	C_m	T/T_p	$C_m/3R$	θ/T	θ (°K)
75	1.6789	0.1237	0.1497	0.1235	1.647	1.326	0.077	0.0534	11.3	847.5
100	1.8733	0.1381	0.1579	0.1379	1.839	1.481	0.103	0.0596	10.85	1085
150	2.6177	0.1929	0.2342	0.1925	2.568	2.068	0.154	0.0832	9.7	1455
200	3.9359	0.2901	0.4707	0.2885	3.848	3.095	0.206	0.1297	8.32	1664
250	5.8907	0.4341	1.0099	0.4290	5.722	4.608	0.257	0.1854	7.08	1770
300	8.4799	0.6250	2.0358	0.6126	8.170	6.580	0.308	0.2648	6.02	1806

Table 16. (conti.)

DM PSOC-22-1100

$T(^{\circ}K)$	C^{s}_{gac}	C^{s}_{g}	C^{a}_{g}	C^{o}_{g}	C^{o}_{gac}	C_{m}	T/T_{p}	$C_{m/3R}$	θ/T	θ ($^{\circ}K$)
75	2.077	0.163	0.1497	0.1614	2.034	1.834	0.055	0.0738	10.1	757.5
100	2.245	0.176	0.1579	0.1745	2.199	1.983	0.073	0.0798	9.8	980
150	2.989	0.235	0.2342	0.2321	2.925	2.638	0.109	0.1061	8.85	1327.5
200	3.828	0.300	0.4707	0.2954	3.723	3.357	0.146	0.1351	8.05	1610
250	4.645	0.370	1.0099	0.3537	4.458	4.020	0.182	0.1617	7.5	1875
300	5.321	0.418	2.0358	0.3957	4.987	4.497	0.218	0.1810	7.17	2151

Table 17. Calculated Values of Θ_o vs T/T_p for PSOC-265 Char and PSOC-22 Char.

T/T_p	PSOC-265 char (°K)	PSOC-22 char (°K)
0.05	685	615
0.1	1190	950
0.15	1651	1165
0.20	2061	1240
0.25	2362	1270
0.30	2621	1270